NASA TECHNICAL REPORT

APPROXIMATE METHOD FOR CALCULATING TRANSONIC FLOW ABOUT LIFTING WING-BODY CONFIGURATIONS

Richard W. Barnwell

Langley Research Center
Hampton, Va. 23665

1. Report No. NASA TR R-452	2. Government Accession No.	3. Recipient's Catalog No.
4. Title and Subtitle APPROXIMATE METHOD FOR CALCULATING TRANSONIC FLOW ABOUT LIFTING WING-BODY CONFIGURATIONS		5. Report Date April 1976
		6. Performing Organization Code
7. Author(s) Richard W. Barnwell		8. Performing Organization Report No. L-10482
9. Performing Organization Name and Address NASA Langley Research Center Hampton, Va. 23665		10. Work Unit No. 505-06-11-02
		11. Contract or Grant No.
12. Sponsoring Agency Name and Address National Aeronautics and Space Administration Washington, D.C. 20546		13. Type of Report and Period Covered Technical Report
		14. Sponsoring Agency Code

15. Supplementary Notes

16. Abstract

The three-dimensional problem of transonic flow about lifting wing-body configurations is reduced to a two-variable computational problem with the method of matched asymptotic expansions. The computational problem is solved with the method of relaxation. The method accounts for leading-edge separation, the presence of shock waves, and the presence of solid, slotted, or porous tunnel walls. The Mach number range of the method extends from zero to the supersonic value at which the wing leading edge becomes sonic. A modified form of the transonic area rule which accounts for the effect of lift is developed. This effect is explained from simple physical considerations.

17. Key Words (Suggested by Author(s)) Transonic flow Wing-body configurations Lifting wing bodies	18. Distribution Statement Unclassified — Unlimited Subject Category 01

19. Security Classif. (of this report) Unclassified	20. Security Classif. (of this page) Unclassified	21. No. of Pages 109	22. Price* $5.25

CONTENTS

APPROXIMATE METHOD FOR CALCULATING TRANSONIC FLOW
ABOUT LIFTING WING-BODY CONFIGURATIONS

Richard W. Barnwell
Langley Research Center

SUMMARY

The three-dimensional problem of transonic flow about lifting wing-body configurations is reduced to a two-variable computational problem with the method of matched asymptotic expansions. The computational problem is solved with the method of relaxation. The method accounts for leading-edge separation, the presence of shock waves, and the presence of solid, slotted, or porous tunnel walls. The Mach number range of the method extends from zero to the supersonic value at which the wing leading edge becomes sonic. A modified form of the transonic area rule which accounts for the effect of lift is developed. This effect is explained from simple physical considerations.

INTRODUCTION

It is well known that there are approximate methods for calculating transonic flow about lifting swept-wing configurations with span-length ratios of order one and small reduced span-length ratios (the reduced span is the product of the span and the factor $\sqrt{\left|1 - M_\infty^2\right|}$ where M_∞ is the free-stream Mach number) if the angle of attack is sufficiently small. A recent example of such a method is that of Stahara and Spreiter (ref. 1). These methods are based on the analysis of Heaslet and Spreiter (ref. 2) which shows that if the angle of attack is less than the wing thickness ratio, the problem of transonic flow over a wing can be separated into noninteracting thickness and cross-flow problems. The analysis also shows that at these small angles of attack, the effect of lift on the flow in the outer region is negligible and that the determination of the shock-wave strength and location is part of the thickness problem. It should be noted that these results are consistent with those of Oswatitsch and Keune (ref. 3), who have proved that at transonic speeds the flow in the outer region of a nonlifting wing is mathematically equivalent to that about the axisymmetric body with the same cross-sectional area distribution (the equivalent body), and Whitcomb (ref. 4), who has demonstrated experimentally that the transonic wave drag of a nonlifting wing-body is almost the same as that on the equivalent body. The basic solution to the cross-flow problem is the slender-wing solution of

Jones (ref. 5). This solution has been generalized for lifting wing-body configurations by Spreiter (ref. 6) and Ward (ref. 7). It should be noted that slender-wing theory is applicable to wings with span-length ratios of order one only for Mach numbers very close to one and not throughout the entire transonic range.

Panel methods based on the linearized potential equation have been applied to lifting configurations in the high subsonic and low supersonic flow regimes where transonic phenomena are present. However, these methods cannot be applied throughout the entire transonic range because of the obvious inability of linear methods to resolve the shock waves associated with transonic flow properly.

At the present time three-dimensional finite-difference methods are being developed for application to the problem of transonic flow about lifting wing-body configurations. These methods, which are formulated in terms of the velocity potential, employ the successive line overrelaxation procedure introduced by Murman and Cole (ref. 8). Bailey and Ballhaus (ref. 9) and Schmidt, Rohlfs, and Vanino (ref. 10) have obtained solutions for infinite-cylinder swept-wing combinations and Klunker and Newman (ref. 11) have treated infinite-cylinder rectangular-wing combinations. It is probable that methods of this type will be generalized so that configurations with finite-length bodies can be treated. It should be noted that these methods require large amounts of computing time and computer storage since the problem being calculated is three dimensional. Also, these methods have not been developed to the point where the phenomenon of leading-edge separation can be treated.

The purpose of this paper is to present an approximate method for calculating transonic flow about lifting configurations with span-length ratios of order one and small reduced-span—length ratios which are at angles of attack large enough to insure that the effects of lift and thickness are comparable in the outer region. The approximations used in the method are based on the analyses of Barnwell (refs. 12 and 13) and Cheng and Hafez (refs. 14 and 15), which show that in this angle-of-attack range the thickness problem is dependent on the lift solution. These analyses are used to reduce the three-dimensional problem of transonic flow about a lifting swept-wing configuration to a two-variable computational problem which is solved with a finite-difference method of the type introduced by Murman and Cole (ref. 8). It should be noted that a preliminary version of the present method was presented in reference 16, and that some results obtained with the final version are given in reference 17. A description of the computer program for the present method and a user's manual are given in reference 18.

SYMBOLS

Where applicable, values are given in both SI and U.S. Customary Units.

A coefficient of quasiconical lift potential (see eq. (26))

A_k, B_k, C_k coefficients in finite-difference formula (F7) given by equations (F8)

A_1, A_2 wing-geometry parameters

$\bar{A}_0, \bar{A}_1, \bar{A}_2, \ldots, \bar{A}_N$ coefficients of Fourier series (eq. (D19))

a constant of proportionality in equation (B21) for angle of attack

a_w, b_w slot width and slot spacing

$\bar{a}_w, \bar{c}_w$ slot-width parameter and slot-thickness parameter

B coefficient of proportionality in equation (74) for effective cross-sectional area of lifting configuration

B_w coefficient of wall-induced contribution to velocity potential (see eq. (34))

B_1, B_2 wing-geometry parameters

b wing semispan

b_1, b_2 apparent semispans in quasiconical model (see fig. 39)

C body geometry parameter

C_L lift coefficient

C_p pressure coefficient

C_w coefficient of wall-induced contribution to velocity potential (see eq. (35))

$c(y)$ chord at span station y

c_1, c_2 distances depicted in figure 39

$E(k)$ complete elliptic integral of second kind with modulus k

$F(x, r, \omega)$ forcing function in equation (F2)

$F_e(x)$ nondimensional radius of equivalent body

$f(x)$ nondimensional dipole strength distribution

$f_v(x)$ contribution to $f(x)$ due to vortex (see eq. (27))

$G(x, r, \omega)$ function in equation (F3)

$G_1(x), G_3(x)$ arbitrary functions in equations (B26) and (B28)

$g(x)$ lift function defined by equation (D13)

$g_\delta(x), g_{2,2}(x), g_{2,1}(x)$ functions of x in inner potentials ϕ_δ, $\phi_{2,2}$, and $\phi_{2,1}$

$H(x)$ source-strength function defined by equation (B17)

$\overline{H}(\sigma, \tau)$ function defined by equation (D18)

K constant of proportionality relating M_∞ and δ (see eqs. (B5) and (B6))

$K(k)$ complete elliptic integral of first kind with modulus k

k wing-geometry parameter defined by equation (C12)

k_1, k_2 wing-geometry parameters

$\bar{k}(x)$ lift function defined by equation (D12)

$L(x)$ total lift on portion of configuration between nose and longitudinal location x given by equation (64)

$L_0(x)$ lift on portion of configuration between nose and longitudinal location x due to nonlinear effects

4

$L_1(x)$ lift on portion of configuration between nose and longitudinal location x due to linear effects

ℓ longitudinal length scale, configuration length unless otherwise noted

M local Mach number

M_n Mach number of component of upstream flow normal to shock

M_∞ free-stream Mach number

$m(x,y)$ $= \frac{1}{2}\left(m_+ - m_-\right)$

$m_p\left(x, y/y_2\right)$ nondimensional function in equation (B31)

$m_\pm(x,y)$ function in equation (B12) for potential near configuration

n exponent in equations for equivalent body radius (see appendix A)

P coefficient in equation (33) for porous-wall boundary condition

R function defined by equation (14) or (E1)

R_0 coefficient of equation (D29) given by equation (D30)

R_1 coefficient of equation (D40) given by equation (D41) unless otherwise noted

r radial coordinate

$\bar{r}$ outer radial variable νr

$r_b(x)$ radius of equivalent body

r_0 value of r at which body boundary condition is applied

$S(x)$ Mirels' S function for wings with swept trailing edges

S_{eff} effective cross-sectional area of lifting wing body (see eq. (74))

S_{ref} reference area for lift coefficient

t maximum radius of equivalent body

U_{∞} free-stream velocity

u,v,w perturbation velocity components in axial, radial, and cross-flow directions, respectively

$\bar{u}$ x-component of perturbation velocity on surface of wing alone

$u_{\alpha}(x)$ average velocity at points near axis given by equations (57)

V_a $= \dfrac{\partial \phi_a}{\partial y} - i \dfrac{\partial \phi_a}{\partial z}$

$W(x,X)$ complex potential

W_v complex potential for flow due to vortices

$\bar{w}$ downwash for wing alone

X complex variable in cross-flow plane, $y + iz$

X_v value of X where vortex core is located

x longitudinal coordinate

x_c quantity used in expression for equivalent body (see appendix A)

x_0 value of x where wing leading edge intersects body surface

x_1, x_2, x_3 values of x used in description of wing planform (see appendix A)

x_I, x_{II}, x_{III} values of x where different segments of wing planform intersect

$Y(x,X)$ complex function defined by equation (C4)

$Y_v(x)$ value of Y at vortex-core location

y	spanwise variable
$y_v(x)$	spanwise location of vortex core in physical plane
$y_2(x), y_1(x)$	functions giving location of wing leading and trailing edges, respectively
$y_I(x), y_{II}(x), y_{III}(x)$	straight-line segments used to construct planform (see appendix A)
y_{I0}, y_{II0}	values of y where different segments of wing planform intersect
Z	complex function defined by equation (C9)
z	vertical coordinate
z_v	value of z where vortex core is located
α	angle of attack
β	$= \sqrt{\left| 1 - M_\infty^2 \right|}$
$\bar{\beta}(\sigma)$	function defined by equation (D16)
γ	ratio of specific heats
$\gamma_v(x)$	vortex core strength
Δ	parameter used to specify wing planform shape (see appendix A)
ΔF	forcing function due to wall effects given by equation (44)
$\Delta x_1, \Delta x_2, \Delta x_3$	mesh spacings given by equations (F4)
$\Delta \phi_\alpha'$	difference in the values ϕ_α' above and below wing
δ	equivalent-body thickness ratio, t/ℓ
$\epsilon_1, \epsilon_2, \epsilon_3$	gage functions of outer expansion (eq. (B3)) given by equations (B5) and (B22)
η	spanwise coordinate in Z-plane given by equation (25)

η_2, η_1 values of η for leading and trailing edges, respectively, given by equations (C11)

θ polar angle of body-oriented coordinate system

κ coefficient in equation (29) for slotted-wall boundary condition

Λ coefficient of derivative $\partial^2 \varphi / \partial x^2$ in equation (42) given by equation (43)

λ quantity defined by equation (49) or (50)

$\lambda_v(x)$ spanwise location of vortex core in Y-plane, see equation (C20)

ν radial stretching parameter in outer region

ξ vertical coordinate in Z-plane

σ, τ angular coordinates given by equations (D15)

$\tau_v(x)$ vertical location of vortex core in Y-plane, see equation (C20)

Φ_v part of ϕ_α due to vortex, see equation (D33)

Φ_0 second-order part of potential φ in inner region, see equation (45)

Φ_1, Φ_2, Φ_3 potentials in outer expansion (eq. (B3)) for φ

φ perturbation velocity potential

$\varphi_0, \varphi_1, \varphi_2$ coefficients of Fourier components of φ (see eq. (10))

ϕ potential defined by equation (D11)

ϕ_a attached-flow portion of ϕ_α (see eq. (D33))

ϕ_α linear lift potential

$\phi_1, \phi_{2,2}, \phi_{2,1}, \phi_2$ potentials in inner expansion (eq. (B7)) for φ

8

ψ_1, ψ_2 solutions to the two-dimensional Laplace equation in cross-flow plane

ω polar angle of wind-oriented coordinate system

∇_2^2 two-dimensional Laplace operator in cross-flow plane (see eq. (4))

Superscripts:

C   complementary solution

P   particular solution

*   complex conjugate

Subscripts:

b   backward difference expression

c   centered difference expression

j   index for x-coordinate

k   index for r-coordinate

ℓ lower surface of wing

ℓe   leading edge of wing

max   maximum value

min   minimum value

t   trailing edge

u   upper surface of wing

Primes denote differentiation with respect to x.

PROBLEM DESCRIPTION

The configurations which are considered in this report are characterized by the parameters

$$\left.\begin{array}{l} \dfrac{b}{\ell} = O(1) \\[2em] \delta = \dfrac{t}{\ell} \ll 1 \\[2em] \alpha \ll 1 \end{array}\right\} \tag{1}$$

where b, ℓ, and t are the wing semispan, longitudinal length scale (configuration length unless otherwise noted), and maximum equivalent-body radius, and δ and α are the thickness ratio and the angle of attack in radians. The free-stream Mach number M_∞ is restricted to the range from zero to low supersonic. In this report it is demonstrated that flow can be calculated about lifting configurations in free air and in solid-, slotted-, and porous-wall wind tunnels.

Wind-oriented cylindrical polar and Cartesian coordinate systems are used in this report. These coordinate systems are shown in figure 1. Wind orientation is chosen in order to simplify the governing equation and to facilitate the enforcement of boundary conditions at the wind-tunnel walls. The origin is at the configuration nose, the positive x-axis is in the free-stream direction, the positive y-axis is to starboard in the horizontal plane, and the positive z-axis is in the upward vertical direction.
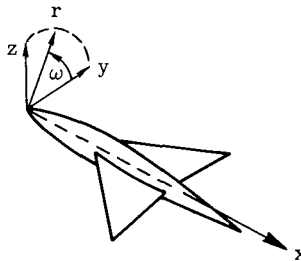
Figure 1.- Wind-oriented coordinate systems.

In this report, wing-body combinations are approximated by flat-plate wings and equivalent axisymmetric bodies. It is assumed that the wing plane passes through the axis of the body so that the angles of attack of the body and wing are the same. The

10

geometry of an approximate wing-body combination is shown in figure 2. The equivalent-body surface is specified by the equation

$$r_b(x) = tF_e(x) \tag{2}$$

where $F_e(x)$ is the nondimensional thickness distribution of the equivalent body. The leading and trailing edges of the wing planform are designated by the functions $y_2(x)$ and $y_1(x)$, respectively. The functions $F_e(x)$, $y_2(x)$, and $y_1(x)$ which are used in this report are discussed in appendix A.
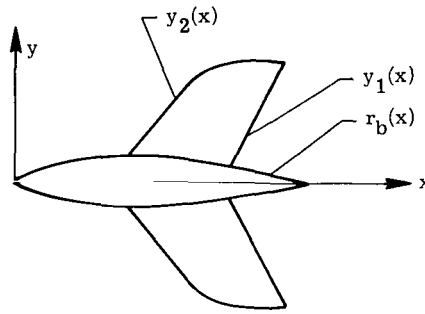

Figure 2.- Geometry of configuration.

It is assumed that the flow fields under consideration are isentropic. This assumption is not strictly valid when shock waves are present in the flow field. However, it can be shown (ref. 19) that the largest term which is affected by the nonisentropic condition is of the order $\left(1 - M_n^2\right)^3$ where M_n is the Mach number of the component of the upstream flow normal to the shock. Terms of this order are negligible in the present approximation; therefore, the isentropic assumption is valid.

Since the flow is assumed to be isentropic, the problem is formulated in terms of the perturbation velocity potential φ. The governing equation for φ is

$$
\begin{aligned}
\left(1 - M_\infty^2\right)\frac{\partial^2 \varphi}{\partial x^2} + \nabla_2^2 \varphi &= M_\infty^2 \Bigg\{ (\gamma + 1)\frac{\partial \varphi}{\partial x}\frac{\partial^2 \varphi}{\partial x^2} + 2\frac{\partial \varphi}{\partial r}\frac{\partial^2 \varphi}{\partial x \partial r} + \frac{2}{r^2}\frac{\partial \varphi}{\partial \omega}\frac{\partial^2 \varphi}{\partial x \partial \omega} + (\gamma - 1)\frac{\partial \varphi}{\partial x}\nabla_2^2 \varphi \\
&+ \left(\frac{\partial \varphi}{\partial r}\right)^2\frac{\partial^2 \varphi}{\partial r^2} + \frac{1}{r^4}\left(\frac{\partial \varphi}{\partial \omega}\right)^2\frac{\partial^2 \varphi}{\partial \omega^2} + 2\frac{\partial \varphi}{\partial x}\frac{\partial \varphi}{\partial r}\frac{\partial^2 \varphi}{\partial x \partial r} + \frac{2}{r^2}\frac{\partial \varphi}{\partial x}\frac{\partial \varphi}{\partial \omega}\frac{\partial^2 \varphi}{\partial x \partial \omega} + \frac{2}{r^2}\frac{\partial \varphi}{\partial r}\frac{\partial \varphi}{\partial \omega}\frac{\partial^2 \varphi}{\partial r \partial \omega} \\
&+ \left(\frac{\partial \varphi}{\partial x}\right)^2\frac{\partial^2 \varphi}{\partial x^2} + \frac{\gamma - 1}{2}\left[\left(\frac{\partial \varphi}{\partial x}\right)^2 + \left(\frac{\partial \varphi}{\partial r}\right)^2 + \frac{1}{r^2}\left(\frac{\partial \varphi}{\partial \omega}\right)^2\right]\left(\frac{\partial^2 \varphi}{\partial x^2} + \nabla_2^2 \varphi\right) \Bigg\}
\end{aligned}
\tag{3}
$$

11

where $\nabla_2{}^2$ is the Laplace operator in planes normal to the x-axis and is written as

$$\nabla_2{}^2 = \frac{\partial^2}{\partial r^2} + \frac{1}{r}\frac{\partial}{\partial r} + \frac{1}{r^2}\frac{\partial^2}{\partial \omega^2} \tag{4}$$

The approximate boundary conditions for the configuration are written as

$$\frac{\partial \varphi}{\partial r}\left(x, r_b, \omega\right) = -\sin\alpha \sin\omega + \cos\alpha \frac{dr_b}{dx} \qquad (0 \leqq \omega \leqq 2\pi) \tag{5}$$

and

$$\frac{1}{r}\frac{\partial \varphi}{\partial \omega}(x, r, 0) = -\frac{1}{r}\frac{\partial \varphi}{\partial \omega}(x, r, \pi) = -\sin\alpha \qquad \left(y_2(x) \geqq r \geqq y_1(x) \quad \text{or} \quad r_b(x)\right) \tag{6}$$

In this report the potential φ is made nondimensional with $U_\infty \ell$ where U_∞ is the free-stream speed, and all lengths are made nondimensional with ℓ.

DESCRIPTION OF METHOD

At present, nonlinear solutions to transonic flow problems can be obtained only with numerical methods. Numerical computation of three-dimensional mixed-flow problems is a costly task with current methods. In this section the analytical treatment of reference 13, which is reviewed in appendix B, is used to reduce the three-dimensional problem of transonic flow about lifting configurations with aspect ratios of order one to two simpler computational problems. It is shown that the dominant part of the lift potential is governed by a linear equation; and that once this part of the lift potential is known, the dependence of the perturbation velocity potential φ on the cross-flow angle ω can be determined. Consequently, the perturbation velocity potential can be obtained as the solution of a two-variable problem in a plane of constant ω.

Approximate Governing Equations

From the equations in appendix B which govern the outer potentials Φ_1, Φ_2, and Φ_3, and the first- and second-order inner potentials, it can be seen that to second order in $\sin\alpha$ and δ, the equation which governs the perturbation velocity potential φ in both the inner and outer regions at near-sonic speeds is

$$\left[1 - M_\infty{}^2 - (\gamma + 1)M_\infty{}^2 \frac{\partial\varphi}{\partial x}\right]\frac{\partial^2\varphi}{\partial x^2} + \nabla_2{}^2\varphi = 2M_\infty{}^2 \sin^2\alpha\left(\frac{\partial\phi_\alpha}{\partial r}\frac{\partial^2\phi_\alpha}{\partial x\,\partial r} + \frac{1}{r^2}\frac{\partial\phi_\alpha}{\partial \omega}\frac{\partial^2\phi_\alpha}{\partial x\,\partial \omega}\right) \tag{7}$$

12

where ϕ_α is the linear lift potential. At near-sonic speeds ϕ_α is the same as ϕ_1 and, as a result, is governed by the equation

$$\nabla_2{}^2 \phi_\alpha = 0 \tag{8}$$

The nonlinear terms in equation (7) have been made proportional to $M_\infty{}^2$ to be consistent with other transonic theories and to insure the proper behavior in the incompressible limit. The terms on the right-hand side of equation (7) are of higher order than necessary in the outer region but are included to facilitate transition between the two regions.

For Mach numbers appreciably different from 1, equation (7) is more than adequate for describing the behavior of φ. However, at these Mach numbers the linear lift potential ϕ_α is governed by the equation

$$\left(1 - M_\infty{}^2\right)\frac{\partial^2 \phi_\alpha}{\partial x^2} + \nabla_2{}^2 \phi_\alpha = 0 \tag{9}$$

rather than by equation (8).

Solutions for Linear Lift Potential

At near-sonic speeds the linear lift potential ϕ_α is governed by equation (8) and, as a result, is obtained from slender-wing theory. The Brown and Michael model (ref. 20) for leading-edge separation is used at these speeds. Slender-wing solutions for ϕ_α for attached and separated flow are given in appendix C.

The linear lift potential ϕ_α is governed by equation (9) at subsonic and supersonic speeds. In this report ϕ_α is obtained from the theory of Lawrence and Flax (ref. 21) for subsonic flow and from a modified form of the theory of Carafoli et al. (ref. 22) for supersonic flow. A modified form of the Brown and Michael model for leading-edge separation which accounts for Mach number effects is used for subsonic and supersonic flows. These methods for determining ϕ_α for attached and separated flows at subsonic and supersonic speeds are presented in appendix D.

The theory of Lawrence and Flax for subsonic flow and the modified theory of Carafoli et al. for supersonic flow were chosen for use in this report because they both reduce to slender-wing theory in the limit as the free-stream Mach number M_∞ approaches 1, and because they are simple theories which do not involve much numerical computation. Consequently, the linear lift solutions which are used in this report vary consistently with Mach number in the range from incompressible to low supersonic flow and are easy to implement. However, it should be noted that more sophisticated subsonic and supersonic linear lift theories could have been employed for both attached and separated flow.

Two-Variable Computation of Perturbation Velocity Potential

The perturbation velocity potential φ is calculated with an approximate equation obtained by evaluation of the right-hand side of equation (7) and the derivative $\partial^2\varphi/\partial\omega^2$ in that equation with the known solution of the linear lift potential ϕ_α. This approximate equation, which has the two independent variables x and r, is solved with the method of relaxation. Different approximations for ϕ_α are used in the outside flow field, where $r > y_2$, and the inside flow field, where $r < y_2$.

<u>Outside flow field</u>.- At transonic speeds the outside flow field $\left(r > y_2\right)$ includes the outer part of the inner region (where the governing equation is parabolic), the outer region (where the governing equation is of mixed elliptic-hyperbolic type), and the far field (where the governing equation is elliptic if the free-stream Mach number is subsonic and hyperbolic if the free-stream Mach number is supersonic). From equation (B20) or equations (B26), (B27), and (B28) it is seen that the perturbation velocity potential φ and the linear lift potential ϕ_α for configurations with one plane of symmetry can be expressed in the forms

$$\varphi(x,r,\omega) = \varphi_0(x,r) + \sin\alpha\ \varphi_1(x,r)\sin\omega + \sin^2\alpha\ \varphi_2(x,r)\cos 2\omega + \ldots \tag{10}$$

and

$$\phi_\alpha = \varphi_1(x,r)\sin\omega + \ldots \tag{11}$$

where φ_0 is of second order in $\sin\alpha$ and δ. It is tempting to separate equation (7) into its Fourier components and solve the component equations simultaneously. However, this procedure cannot be used for transonic flow fields because the basic nonlinear term $\left[1 - M_\infty^2 - (\gamma+1)M_\infty^2\varphi'\right]\varphi''$, which depends on the angle ω, would be represented by the term $\left[1 - M_\infty^2 - (\gamma+1)M_\infty^2\varphi_0'\right]\varphi_0''$, which is independent of ω. As a result, the Fourier analysis would indicate that the locations of shock waves are independent of ω, whereas it is clear that, in general, the shock-wave locations depend on ω.

Another approach, which is the one employed in this paper, is to use equations (10) and (11) to approximate the derivative $\partial^2\varphi/\partial\omega^2$ and the terms involving ϕ_α in equation (7) and to integrate the resulting equation in half planes of constant ω. With this method the shock-wave locations can vary with ω, and the computational problem is reduced to a two-variable calculation in the half planes. A separate integration must be performed for each value of ω for which results are desired. In the horizontal plane $(\omega = 0)$, results are calculated both above and beneath the wing.

The functions $\varphi_1(x,r)$ and $\varphi_2(x,r)$ which are used to evaluate the derivative $\partial^2\varphi/\partial\omega^2$ are approximated analytically in this paper. Account is taken of the fact that the forms of these functions are different for large and small values of r since the governing equation is parabolic near the configuration and either elliptic or hyperbolic in the far field. For the present it will be assumed that the lifting configuration is traveling in free air.

Consider the function φ_1 for $M_\infty < 1$. It can be shown from the results of appendix C that in the parabolic inner region where slender-wing theory applies, the form is

$$\varphi_1(x,r) = \frac{f(x)}{r} \tag{12}$$

Klunker (ref. 23) shows that the far-field solution for φ_1 is

$$\varphi_1(x,r) = \frac{1}{2r}\left(1 + \frac{x}{R}\right)f(1) \tag{13}$$

where

$$R = \sqrt{x^2 + \left(1 - M_\infty^{\,2}\right)r^2} \tag{14}$$

Note that the x-coordinate is measured from the nose of the configuration, and that the configuration has a nondimensional length of 1. In this paper the function φ_1 is approximated in the outer part of the flow field by the composite solution

$$\varphi_1(x,r) = \frac{1}{2r}\left[2\frac{x}{R}f(x) + \left(1 - \frac{|x|}{R}\right)f(1)\right] \tag{15}$$

for $M_\infty < 1$, where

$$f(x) = f(1) \qquad (x > 1)$$

$$f(x) = 0 \qquad (x < 0)$$

Note that this equation is correct in the asymptotic limits of the parabolic inner region, where equation (12) applies, and the elliptic far field, where equation (13) applies. It is assumed to be correct in the intervening mixed outer region.

Consider the function φ_1 for $M_\infty > 1$. In appendix E it is shown that in the far field in the interval

$$0 \leqq x - \beta r \leqq 1 \tag{16}$$

the function φ_1 can be approximated as

$$\varphi_1(x,r) = \frac{f(x - \beta r)}{r(1 - \beta r/x)^2}\left[\sqrt{1 - \beta^2 r^2/x^2} + \left(\frac{\beta r}{x}\right)^2 \log_e\left(\frac{\beta r/x}{1 + \sqrt{1 - \beta^2 r^2/x^2}}\right)\right] \tag{17}$$

where

$$\beta = \sqrt{M_\infty^2 - 1} \tag{18}$$

In this report the function φ_1 is evaluated with equation (17) in the outer part of the flow field in the interval given by inequalities (16). Outside of this interval the function φ_1 is assumed to vanish. In order to obtain equation (17), it is necessary to assume that the variation of y_2 with x is essentially linear. It should be noted that the right side of equation (17) approaches that of equation (12) as r becomes small.

Consider the function φ_2. It can be seen from equation (B20) that this function can be written in the inner region as

$$\varphi_2(x,r) = \left(\frac{\gamma + 1}{8} f'f'' - \frac{ff'}{2r^2}\right)M_\infty^2 \tag{19}$$

Note that the first term in equation (19) does not approach zero as r becomes large. In order to insure the proper asymptotic behavior for large values of r, it is assumed that for $M_\infty < 1$, the function φ_2 is given by the equation

$$\varphi_2(x,r) = \left(\frac{\gamma + 1}{8}\frac{x^2}{R^2} f'f'' - \frac{ff'}{2r^2}\right)M_\infty^2 \tag{20}$$

in the outer part of the flow field. For $M_\infty > 1$, φ_2 is evaluated with equation (19) in the region

$$\left.\begin{array}{c} r < x/\beta \\[2mm] 0 \leqq x \leqq 1 \end{array}\right\} \tag{21}$$

Outside of this region φ_2 is assumed to vanish.

16

It is shown in appendix C that the function $f(x)$ for attached transonic flow past configurations with straight trailing edges is

$$f(x) = \frac{1}{2} y_2^2(x) \left[1 + \frac{r_b^4(x)}{y_2^4(x)} \right]$$ (22)

In calculating the derivatives f' and f'', it is assumed that r_b' is negligible compared with y_2'. Although the quantity $(r_b/y_2)^4$ is very small except near the point where the wing leading edge intersects the body, it is included so that the derivative $f'(x)$ will vanish at the point where the wing leading edge intersects the body rather than at the apparent wing apex inside the body. The derivative $f'(x)$ for values of x where the wing has both a leading edge $y_2(x)$ and a trailing edge $y_1(x)$ can be evaluated exactly with slender-wing theory. However, this evaluation is very tedious. In this report an approximate form, which is a generalization of the approximate form developed for wings by Mangler (ref. 24), is used. This approximate form is written as

$$\frac{df}{dx} = 0.85 y_2 \frac{dy_2}{dx} \left(1 - \frac{r_b^4}{y_2^4} \right) \sqrt{\frac{y_2 - y_1}{y_2 + y_1}}$$ (23)

The function $f(x)$ is determined by numerical integration of equation (23).

For subsonic Mach numbers appreciably different from 1, solutions to equation (9) for ϕ_α for attached flow are obtained with the approximate method of Lawrence and Flax (ref. 21) for wing-body configurations. A brief discussion of this method, which is an extension of that of Lawrence (ref. 25) for wings alone, is given in appendix D. The method is applicable to configurations with unswept trailing edges and aspect ratios of order one or less. With this method solutions for the function $f(x)$ are obtained which to lowest order satisfy the trailing-edge Kutta condition. The terms in equations (12), (13), (15), (17), (19), and (20) which depend on the function $f(x)$ and its derivatives are evaluated with this solution. It should be noted that the slender-wing solution for $f(x)$ does not, in general, satisfy the Kutta condition at the trailing edge.

It is shown in appendix D that the function $f(x)$ is related to the values of ϕ_α on the upper and lower surfaces of the wing, which are designated as $\phi_{\alpha,u}$ and $\phi_{\alpha,\ell}$, respectively, by the equation

$$f(x) = \frac{1}{\pi} \int_{\eta=0}^{\eta=\eta_2} \left[\phi_{\alpha,u}(x,\eta) - \phi_{\alpha,\ell}(x,\eta) \right] d\eta + r_b^2(x)$$ (24)

17

where the transformed coordinate η is related to the physical coordinates y and z by the equation

$$\eta = y\left(1 - \frac{r_b^2}{y^2 + z^2}\right) \tag{25}$$

Since the function $f(x)$ is determined directly with the method of Lawrence and Flax, an additional assumption concerning the spanwise variation of ϕ_α must be made in order to evaluate the pressure distribution. In this report it is assumed that the spanwise variation of ϕ_α on the surface is the same as that predicted by slender-wing theory.

For supersonic attached flow an approximate solution to equation (9) is obtained with a method which is based on the quasiconical method of Carafoli et al. (ref. 22) for supersonic flow past wings with subsonic leading edges. The supersonic applications of the present method and the method of reference 22 are restricted to wings with unswept trailing edges. It is assumed that the forms of the potential ϕ_α on the upper and lower surfaces of the wing, respectively, can be approximated as

$$\phi_{\alpha,u}(x,\eta) = -\phi_{\alpha,\ell}(x,\eta) = \frac{1}{A}\sqrt{\left(b_1 - \eta\right)\left(b_2 + \eta\right)} \tag{26}$$

where η is given by equation (25). The quantities A, b_1, and b_2 are slowly varying functions of x and y (or z) which correspond to the quantities A^*, ℓ_1, and ℓ_2 in reference 22. The method which is used to evaluate the functions A, b_1, and b_2 is given in appendix D.

The function $f(x)$ for attached flow is obtained from equation (24) by numerical integration. Values for the integrand are obtained from equation (26). The derivatives of $f(x)$ used in equations (19) and (20) are determined numerically with upwind difference formulas.

If the flow is separated at the leading edge of the wing so that there is a vortex above the wing near the leading edge, or if the flow is attached at the leading edge but there is a vortex over the wing which was generated by a strake ahead of the wing, there is an additional contribution to the function $f(x)$ of the form

$$f_v(x) = 2\gamma_v(x)\,\lambda_v(x)\left[y_2(x) + \frac{r_b^2(x)}{y_2(x)}\right] \tag{27}$$

An expression for the product $\gamma_v(x)\lambda_v(x)$ can be obtained from equation (C26).

Consider the case of flow past a model in a tunnel. If the tunnel walls are solid, the boundary condition at the wall $\left(r = r_{max}\right)$ is

$$\frac{\partial \varphi}{\partial r}\left(x, r_{max}, \omega\right) = 0 \qquad\qquad (28)$$

Baldwin, Turner, and Knechtel (ref. 26) show that if the tunnel has slotted walls, the boundary condition is

$$\frac{\partial^2 \varphi}{\partial x\, \partial r} + \frac{1}{\kappa}\frac{\partial \varphi}{\partial x} = 0 \qquad\qquad \left(r = r_{max}\right) \qquad (29)$$

where κ is related to the slot width a_w and the slot spacing b_w by the equation

$$\kappa = -\frac{b_w}{\pi}\log_e\left(\sin\frac{\pi a_w}{2 b_w}\right) \qquad\qquad (30)$$

Chen and Mears (ref. 27) also obtain equation (29) as the boundary condition for slotted-wall tunnels where κ is related to the slot-width parameter $\bar{a}_w$, slot spacing b_w, and slot-thickness parameter $\bar{c}_w$ by the equation

$$\kappa = \frac{b_w}{2}\frac{\cos\left(\frac{\pi \bar{a}_w}{b_w}\right) + \cosh\left(\frac{\pi \bar{c}_w}{b_w}\right)}{\sin\left(\frac{\pi \bar{a}_w}{b_w}\right)} \qquad\qquad (31)$$

It should be noted that no assumptions concerning Mach number were made in the derivation of equation (29). In this report it is assumed that the slot geometry does not vary with x. Consequently, equation (29) can be integrated with respect to x to yield

$$\frac{\partial \varphi}{\partial r} = -\frac{1}{\kappa}\varphi \qquad\qquad \left(r = r_{max}\right) \qquad (32)$$

This form is used in this report. For tunnels with porous walls the boundary condition is

$$\frac{\partial \varphi}{\partial r} = -P\frac{\partial \varphi}{\partial x} \qquad\qquad \left(r = r_{max}\right) \qquad (33)$$

It is assumed that the tunnel wall lies in the region where the Fourier expansion (eq. (10)) applies. Since the boundary conditions are linear, each component on the right side of equation (10) must satisfy them. Assume that the functions $\varphi_1(x,r)$ and $\varphi_2(x,r)$ are of the form

$$\varphi_1(x,r) = \frac{f(x)}{r} + B_w(x)r \tag{34}$$

$$\varphi_2(x,r) = \left(\frac{\gamma + 1}{8} f'f'' - \frac{ff'}{2r^2}\right)M_\infty^2 + C_w(x)r^2 \tag{35}$$

where the coefficients $B_w(x)$ and $C_w(x)$ are to be determined from the boundary conditions. The forms of the last terms in equations (34) and (35) are chosen so that the terms in equation (10) proportional to $B_w(x)$ and $C_w(x)$ are solutions to the two-dimensional Laplace equation.

When equations (34) and (35) are substituted into the slotted-wall boundary condition (eq. (32)), it can be seen that the quantities $B_w(x)$ and $C_w(x)$ are given by the equations

$$B_w(x) = \frac{f(x)}{r_{max}^2} \frac{1 - r_{max}/\kappa}{1 + r_{max}/\kappa} \tag{36}$$

and

$$C_w(x) = -\frac{4f(x) f'(x)\left(2 - r_{max}/\kappa\right) + (\gamma + 1)f'(x) f''(x) r_{max}^3}{8r_{max}^4\left(2 + r_{max}/\kappa\right)} \tag{37}$$

Note that the solid-wall boundary condition (eq. (28)) is simply the special case of the slotted-wall condition (eq. (32)) with $1/\kappa = 0$.

When equations (34) and (35) are substituted into the porous-wall boundary condition (eq. (33)), it is found that $B_w(x)$ and $C_w(x)$ are governed by the ordinary differential equations

$$B_w' + \frac{1}{Pr_{max}} B_w = -\frac{1}{r_{max}^2}\left(f' - \frac{1}{Pr_{max}} f\right) \tag{38}$$

and

$$C_W' + \frac{2}{Pr_{max}} C_W = -\frac{\gamma + 1}{8r_{max}^2}(f'f'')' + \frac{1}{2r_{max}^4}\left[(ff')' - \frac{2}{Pr_{max}} ff'\right] \qquad (39)$$

The solutions to equations (38) and (39) are

$$B_W(x) = -\frac{\exp\left(-\dfrac{x}{Pr_{max}}\right)}{r_{max}^2} \int_{s=-\infty}^{s=x} \exp\left(\frac{2s}{Pr_{max}}\right)\frac{d}{ds}\left[f(s) \exp\left(-\frac{s}{Pr_{max}}\right)\right]ds \qquad (40)$$

and

$$C_W(x) = -\frac{(\gamma + 1)M_\infty^2}{8r_{max}^2} \exp\left(-\frac{2x}{Pr_{max}}\right) \int_{s=-\infty}^{s=x} \exp\left(\frac{2s}{Pr_{max}}\right)\frac{d}{ds}\left[f'(s) f''(s)\right] ds$$

$$+ \frac{\exp\left(-\dfrac{2x}{Pr_{max}}\right)}{2r_{max}^4} \int_{s=-\infty}^{s=x} \exp\left(\frac{4s}{Pr_{max}}\right)\frac{d}{ds}\left[f(s) f'(s) \exp\left(-\frac{2s}{Pr_{max}}\right)\right]ds$$

$$(41)$$

To summarize, the equation which is solved in the outside flow field is

$$\Lambda \frac{\partial^2 \varphi}{\partial x^2} + \frac{1}{r}\frac{\partial}{\partial r}\left(r \frac{\partial \varphi}{\partial r}\right) = \frac{1}{r^2}\left[\sin \alpha \; \varphi_1(x,r) \sin \omega + 4 \sin^2\alpha \; \varphi_2(x,r) \cos 2\omega\right]$$

$$+ 2M_\infty^2 \sin^2\alpha \; \frac{f(x) f'(x)}{r^4} \qquad (42)$$

where

$$\Lambda = 1 - M_\infty^2 - (\gamma + 1)M_\infty^2 \frac{\partial \varphi}{\partial x} \qquad (43)$$

and where φ_1 and φ_2 are given by equations (15) and (20) for $M_\infty \leq 1$ and equations (17) and (19) for $M_\infty > 1$. If a tunnel wall is present, equation (28), (32), or (33) is used for the boundary condition, and the quantity

$$\Delta F = \frac{1}{r} \sin \alpha \; B_W(x) \sin \omega + 4 \sin^2\alpha \; C_W(x) \cos 2\omega \qquad (44)$$

is added to the right side of equation (42). The functions $B_W(x)$ and $C_W(x)$ are obtained from equations (36) and (37) for solid or slotted walls and equations (40) and (41) for porous walls.

<u>Flow field near configuration.</u>- Consider the flow in the close vicinity of the configuration. Assume that in this region the perturbation velocity potential φ can be approximated as

$$\varphi(x,r,\omega) = \sin \alpha \; \phi_\alpha(x,r,\omega) + \Phi_0(x,r,\omega) \qquad (45)$$

where the potential ϕ_α is the linear lift potential and the potential Φ_0 is of second order in the parameters δ and $\sin \alpha$. Solutions for ϕ_α are given in appendixes C and D. It can be shown from equations (5) and (6) that the boundary conditions for ϕ_α and Φ_0 are

$$\left. \begin{array}{l} \dfrac{\partial \phi_\alpha}{\partial r}\left(x,r_b,\omega\right) = 0 \\[4mm] \dfrac{\partial \phi_\alpha}{\partial \omega}(x,r,0) = -r \qquad\qquad \left(y_2(x) \geqq r \geqq y_1(x) \quad \text{or} \quad r_b(x)\right) \end{array} \right\} \qquad (46)$$

and

$$\left. \begin{array}{l} \dfrac{\partial \Phi_0}{\partial r}\left(x,r_b,\omega\right) = \cos \alpha \; \dfrac{dr_b}{dx} \\[4mm] \dfrac{\partial \Phi_0}{\partial \omega}(x,r,0) = 0 \qquad\qquad \left(y_2(x) \geqq r \geqq y_1(x) \quad \text{or} \quad r_b(x)\right) \end{array} \right\} \qquad (47)$$

From equations (7), (8), (9), and (45), it follows that Φ_0 is governed by the equation

$$\Lambda \frac{\partial^2 \Phi_0}{\partial x^2} + \nabla_2{}^2 \Phi_0 = -\lambda \sin \alpha \frac{\partial^2 \phi_\alpha}{\partial x^2} + 2M_\infty{}^2 \sin^2\alpha \left(\frac{\partial \phi_\alpha}{\partial r} \frac{\partial^2 \phi_\alpha}{\partial x \, \partial r} + \frac{1}{r^2} \frac{\partial \phi_\alpha}{\partial \omega} \frac{\partial^2 \phi_\alpha}{\partial x \, \partial \omega} \right) \qquad (48)$$

22

where

$$\lambda = \Lambda \qquad (49)$$

if ϕ_α is governed by equation (8) and

$$\lambda = \Lambda - \left(1 - M_\infty{}^2\right) \qquad (50)$$

if ϕ_α is governed by equation (9). It should be noted in passing that for near-sonic flow, equation (48) can be approximated as

$$\nabla_2{}^2 \Phi_0 = (\gamma + 1) \sin^2\alpha \, \frac{\partial \phi_\alpha}{\partial x} \frac{\partial^2 \phi_\alpha}{\partial x^2} + 2 \sin^2\alpha \left(\frac{\partial \phi_\alpha}{\partial r} \frac{\partial^2 \phi_\alpha}{\partial x \, \partial r} + \frac{1}{r^2} \frac{\partial \phi_\alpha}{\partial \omega} \frac{\partial^2 \phi_\alpha}{\partial x \, \partial \omega} \right) \qquad (51)$$

It is assumed that in the region $\left(r < y_2(x) \right)$ the potential ϕ_α in the governing equation (48) for Φ_0 can be approximated by the three-term expansion about the axis $(r = 0)$ of the slender-wing potential for attached flow past a wing with no trailing edge. This approximation for ϕ_α is written as

$$\phi_\alpha \approx \pm y_2(x) \left[1 - \frac{1}{2} \frac{r^2}{y_2{}^2(x)} \cos 2\omega \right] - r \sin \omega \qquad (52)$$

where the plus and minus signs apply above and beneath the wing, respectively. For wings with swept trailing edges, it is assumed that equation (52) applies ahead of the point where the trailing edge emerges from the body, and that the right side of equation (48) vanishes aft of this point.

The particular solution to equation (51), and hence, for practical purposes, equation (48), with ϕ_α approximated by equation (52) is

$$\Phi_0{}^P(x,r,\omega) = \frac{\sin^2\alpha}{4} r^2 \left\{ y_2{}' y_2{}'' - \frac{1}{4} \frac{r^2 y_2{}'}{y_2{}^3} \pm r \frac{y_2{}'}{y_2{}^2} \sin \omega \right.$$

$$\left. + \frac{1}{3}\left(\frac{r}{y_2}\right)^2 \left[y_2{}' y_2{}'' - \left(\frac{y_2{}'}{y_2}\right)^3 \right] \cos 2\omega \right\} \qquad (53)$$

Since the complementary solution for Φ_0 is a source term (a term proportional to $\log_e r$) and hence dominates the particular solution near the axis, it is concluded that there is a substantial region around the axis where the dominant part of Φ_0 is independent of ω.

In this report it is assumed that $\Phi_0(x,r,\omega)$ can be approximated by a function which is independent of ω. This function is defined as

$$\varphi_0(x,r) = \frac{2}{\pi} \int_{\omega=0}^{\omega=\pi/2} \Phi_0(x,r,\omega) \, d\omega \tag{54a}$$

for points above the wing ($\omega > 0$) and as

$$\varphi_0(x,r) = \frac{2}{\pi} \int_{\omega=-\pi/2}^{\omega=0} \Phi_0(x,r,\omega) \, d\omega \tag{54b}$$

for points below the wing ($\omega < 0$). If the computational plane is the wing plane ($\omega = 0$), values for $\varphi_0(x,r)$ are calculated both above and below the wing. The governing equation for $\varphi_0(x,r)$ is

$$\Lambda \frac{\partial^2 \varphi_0}{\partial x^2} + \frac{1}{r}\frac{\partial}{\partial r}\left(r \frac{\partial \varphi_0}{\partial r}\right) = \mp \sin \alpha \left[\lambda y_2'' - 2M_\infty^2 \sin \alpha \left(\frac{1}{\pi}\frac{y_2' r}{y_2^2} - \frac{r^2 y_2'}{y_2^3}\right)\right] \tag{55}$$

The right side of this equation was obtained by integrating the right side of equation (48) with ϕ_α approximated by equation (52) over the regions above and beneath the wing. The equation for the function Λ used in equation (55) is

$$\Lambda = 1 - M_\infty^2 - (\gamma + 1)M_\infty^2\left[\frac{\partial \varphi_0}{\partial x} + \sin \alpha \, u_\alpha(x)\right] \tag{56}$$

The quantity $u_\alpha(x)$ is the average velocity due to lift in the regions above and beneath the wing near the axis and is given by the equations

$$u_\alpha(x) = \pm y_2' \tag{57a}$$

for attached flow,

$$u_\alpha(x) = \pm\left[y_2' + \frac{2(\gamma_v \lambda_v)'}{1 \mp \tau_v}\right] \tag{57b}$$

24

for flow which separates at the leading edge with a vortex, and

$$u_\alpha(x) = \pm \left[y_2' + \frac{2\gamma_v \left(1 \mp \tau_v\right)\lambda_v'}{\left(1 \mp \tau_v\right)^2 + \lambda_v^2} \right] + \frac{2\gamma_v \lambda_v \tau_v'}{\left(1 \mp \tau_v\right)^2 + \lambda_v^2} \tag{57c}$$

for flow which is attached at the leading edge but which has a strake-generated vortex inboard of the wing tip. The plus and minus signs apply above and beneath the wing, respectively. Equations (57) are derived in appendix C. The boundary condition which is used at the axis is obtained from the first of equations (47) as

$$\underset{r \to 0}{\text{Limit}} \left(r \frac{\partial \varphi_0}{\partial r} \right) = r_b(x) \frac{dr_b(x)}{dx} \tag{58}$$

For free-stream Mach numbers below 1, the trailing-edge Kutta condition must be satisfied at least approximately in order for the solutions to be physically realistic. For a configuration with an unswept trailing edge located at $x = x_t$, this condition can be expressed as

$$\varphi\left(x_t + \Delta x, y, +0\right) - \varphi\left(x_t + \Delta x, y, -0\right) = \varphi\left(x_t, y, +0\right) - \varphi\left(x_t, y, -0\right) \tag{59}$$

where Δx is the mesh spacing for the x-coordinate and $z = \pm 0$ designates the upper and lower surfaces of the wing and trailing vortex sheet. For shockless flow which is attached at the leading edge, this condition is enforced automatically if ϕ_α is obtained from the theory of Lawrence and Flax. If ϕ_α is obtained from slender-wing theory, the condition is met for shockless attached leading-edge flow by requiring that the derivative y_2' approach zero at the trailing edge of the wing. It is shown in appendix C that if there is a vortex over the wing, the contribution of the vortex system to the derivative $\Delta \phi_\alpha'$ on the inboard portion of the wing is of the form

$$\Delta \phi_\alpha' = \pm \frac{2}{1 \mp \tau_v} \left(\gamma_v \lambda_v\right)' \tag{60a}$$

if the flow is separated at the wing leading edge and

$$\Delta \phi_{\alpha,u}' = 2\gamma_v \frac{\left(1 - \tau_v\right)\lambda_v' + \lambda_v \tau_v'}{\left(1 - \tau_v\right)^2 + \lambda_v^2} \tag{60b}$$

25

$$\Delta\phi'_{\alpha,\ell} = -\frac{2\gamma_v}{1 + \tau_v}\left(\lambda_v' - \frac{\lambda_v}{1 + \tau_v}\tau_v'\right) \tag{60c}$$

if the vortex is strake generated. Of course, equations (60) are not valid on the outboard portion of the wing near the vortex. If the computational plane is the wing plane where $\omega = 0$, partial account of the effect of shock waves and leading-edge separation on the Kutta condition is taken by imposing the condition

$$\Phi_{0,u}(x_t+\Delta x,r) - \Phi_{0,\ell}(x_t+\Delta x,r) = \Phi_{0,u}(x_t,r) - \Phi_{0,\ell}(x_t,r) - \sin\alpha\left[\Delta\phi'_{\alpha,u}(x_t) - \Delta\phi'_{\alpha,\ell}(x_t)\right]$$
$$\tag{61}$$

The subscripts u and ℓ designate values on the upper and lower surfaces of the wing and vortex sheet. This additional adjustment for the Kutta condition is not made for computational planes other than the wing plane.

Method of solution.- The method of successive line overrelaxation is used to solve equations (42) and (55). The procedure used here is very similar to that used by Bailey (ref. 28). However, the shock difference operator developed by Murman (ref. 29) is incorporated in the method since it tends to predict the jump condition at strong shock waves more accurately than other difference operators. The details of the numerical procedure are given in appendix F. The solution procedure used to find the vortex core strength and location is given in appendix G.

Determination of Surface Pressures, Lift,

and Pitching Moment

Although the velocity potential is calculated in wind-oriented coordinates in this report, the surface pressure coefficients are calculated in body-oriented coordinates. The velocity potential is used in the form

$$\varphi(x,r,\theta) = \sin\alpha\ \phi_\alpha(x,r,\theta) + \varphi_0(x,r) - \frac{1}{2}\sin^2\alpha\ f'(x) \tag{62}$$

where the coordinates x, r, and θ in this equation are body oriented. The angle θ is zero in the wing plane and positive above the wing. One of the forms discussed in appendixes C and D is used for the cross-flow potential ϕ_α, and the solution determined numerically in terms of wind-oriented coordinates is used for the potential φ_0. The last term in equation (62) is a correction factor which accounts for the fact that the wing boundary condition for the lift potential ϕ_α is enforced in the horizontal plane ($\omega = 0$) when wind-oriented coordinates are used and in the wing plane ($\theta = 0$) when body-oriented

coordinates are used. Let the body-oriented perturbation velocity components in the axial, radial, and cross-flow directions be u, v, and w, respectively. The pressure coefficient is written to second order in $\delta \sin \alpha$ as

$$C_p = -2\left[u + \sin \alpha \left(v \sin \theta + w \cos \theta\right)\right] - v^2 - w^2 \tag{63}$$

It was shown by Munk (ref. 30) that the lift acting on that part of a slender configuration between the nose and the points x upstream of the trailing edge is

$$L(x) = -\cos \alpha \left[\oint_C \varphi(x,y,z) \, dy + \pi r_b^2(x) \sin \alpha\right] \tag{64}$$

where L is made nondimensional with the factor $\rho_\infty U_\infty^2 \ell^2$ where ρ_∞ is the free-stream density. The path of integration C for the integral in equation (64) is the contour around the configuration in the cross-flow plane which intersects the axis at x, and the velocity potential φ is given by equation (62). Equation (64) can be expressed as

$$L(x) = L_0(x) + L_1(x)$$

where

$$L_0(x) = 2 \cos \alpha \int_{y=0}^{y=y_2(x)} \Delta\varphi_0(x,y) \, dy \tag{65}$$

and

$$L_1(x) = -\cos \alpha \sin \alpha \left[\oint_C \phi_\alpha(x,y,z) \, dy + \pi r_b^2(x)\right] \tag{66}$$

The quantity $\Delta\varphi_0(x,y)$ is the difference in the potential φ_0 on the upper and lower surfaces of the configuration at the point x,y. The lift term $L_0(x)$ in equation (65) is evaluated numerically in this report.

It can be seen from the results of Wei, Levinsky, and Su (ref. 31) that for slender-wing flow past a configuration with a vortex over the wing and an unswept trailing edge, the lift term $L_1(x)$ can be written as

$$L_1(x) = \pi \cos \alpha \sin \alpha \left\{\left[y_2(x) - \frac{r_b^2(x)}{y_2(x)}\right]^2 + r_b^2(x) + 4\gamma_v(x) \lambda_v(x)\left[y_2(x) + \frac{r_b^2(x)}{y_2(x)}\right]\right\} \tag{67}$$

The functions γ_v and λ_v are associated with the vortex and are discussed in appendix C. As is pointed out in the appendix, these functions have different forms for leading-edge separation and for a vortex inboard of the leading edge. If there is no vortex over the wing, the last term on the right side of equation (67) vanishes. It should be noted that equation (67) applies from the nose of the configuration to the trailing edge of the wing.

It has been shown by Mirels (ref. 32) that if the trailing edge as well as the leading edge of the wing is swept at x, the derivative dL_1/dx for a configuration with a constant body radius can be written as

$$\frac{dL_1}{dx}(x) = 2\pi \cos \alpha \sin \alpha \, \eta_2 \frac{d\eta_2}{dx} S(x)\left[1 - \frac{E(k)}{K(k)}\right] \tag{68}$$

where η_2 is given by equations (C11) and $K(k)$ and $E(k)$ are complete elliptic integrals of the first and second kinds, respectively, with the modulus k given by equation (C12). The function $S(x)$ is discussed in appendix C. It can be seen that with the approximations given by equations (C15) and (C16), equation (68) can be approximated as

$$\frac{dL_1}{dx}(x) = 2\pi \cos \alpha \sin \alpha\left(\frac{df}{dx} - r_b \frac{dr_b}{dx}\right) \tag{69}$$

where the derivative df/dx is given by equation (23). The last term in equation (69) is added so that this equation will be consistent with equation (67). The lift term $L_1(x)$ at points where there is a swept trailing edge must be determined by numerical integration of equation (69).

Neither equation (67) nor (69) is valid at points aft of the trailing edge of the wing unless the body radius is constant behind the wing. Adams and Sears (ref. 33) derived an integral expression for the load on the aft end of a configuration with an unswept trailing edge and a body which closes. It is observed in reference 33 that because the flow in the aft cross-flow planes is essentially incompressible, the area of a stream tube with the outer and inner radii r_t and $r_b(x_t)$ at the trailing edge is constant over the afterbody of the configuration. Consequently, the outer boundary of this stream tube is

$$r = \sqrt{r_t^2 - r_b^2(x_t) + r_b^2(x)} \tag{70}$$

Aft of the trailing edge equation (66) for the lift term $L_1(x)$ can be written as

$$L_1(x) = -\cos\alpha\,\sin\alpha\left[\oint_C \phi_\alpha(x,y,z)\,dy + \pi r_b^2(x)\right]$$

$$= \cos\alpha\,\sin\alpha\left[r_b(x_t)\int_{\omega=0}^{\omega=2\pi}\phi_\alpha\left(x_t, r_b(x_t),\omega\right)\sin\omega\,d\omega\right.$$

$$\left. + 2\int_{y_t=r_b(x_t)}^{y_t=y_2(x_t)}\Delta\phi_\alpha\left(x_t,y_t\right)\frac{dy}{dy_t}\,dy_t - \pi r_b^2(x)\right] \qquad (71)$$

where $\Delta\phi_\alpha$ is the difference in the linear lift potential ϕ_α above and beneath the wing. The derivative dy/dy_t can be evaluated with equation (70).

The pitching moment about the nose is calculated with the equation

$$M_p = \int_{x=0}^{x=1} x\,\frac{dL}{dx}\,dx \qquad (72)$$

TRANSONIC AREA RULE FOR LIFTING CONFIGURATIONS

It is well known that the effect of thickness is to deflect streamlines outward from the configuration. It can be shown that for near-sonic flow, lift can also have this effect in addition to the usual downwash effect. The manner in which lift causes the outward deflection of streamlines is depicted schematically in figure 3. The cross-sectional area of stream tubes is minimum where the flow is sonic. The effect of lift is to increase the fluid speed in stream tubes above the wing and to decrease the speed in the tubes
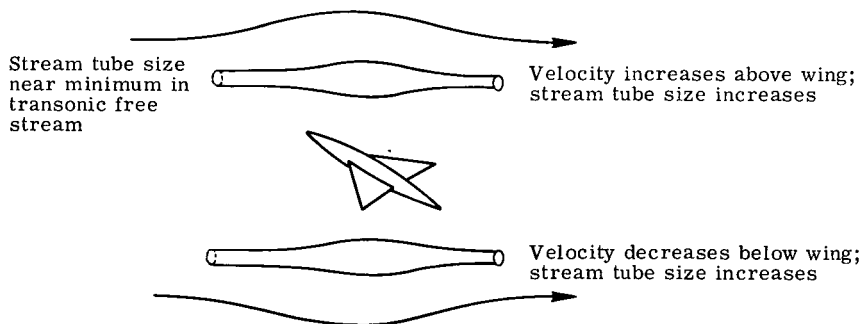

Figure 3.- Outward displacement of streamlines by both lift and thickness effects.

beneath the wing. For configurations traveling at Mach numbers near 1, both the increase and decrease in fluid speed are deviations from near-sonic flow. Thus the cross sections of practically all the stream tubes about the body increase so that the streamlines are deflected outward more than they would be by thickness effects alone. It should be noted that this phenomenon does not occur for completely subsonic or completely supersonic flow, where an increase in stream tube size on one side of the wing is compensated by a decrease on the other.

An expression for the effective cross-sectional area of a lifting configuration traveling at transonic speed is given by equation (B32). The lift coefficient is defined in terms of the present notation as

$$C_L = \frac{2L}{S_{ref}} \tag{73}$$

where S_{ref} is the reference area. With equation (D23) and the fact that to lowest order the linear lift L_1 and the total lift L are the same, equation (B32) can be written to lowest order as

$$S_{eff}(x) = \pi r_b^2(x) + \frac{\gamma + 1}{2}\, \pi B \left(\frac{S_{ref}}{4\pi} \frac{dC_L}{dx} \right)^2 + \frac{1}{2} S_{ref} C_L(x)\, \sin \alpha \tag{74}$$

An expression for the coefficient B is given by equation (B33). The right side of this equation is at best only a weak function of x and can, for practical purposes, be considered constant. However, a unique value for B cannot be determined with this equation because the length scale ℓ cannot be determined with the theory of appendix B. A value for B can be obtained numerically with the present method by comparing the flow fields of lifting configurations and axisymmetric bodies with cross-sectional area distributions obtained from equation (74).

It should be noted that the last term in equation (74) can be ignored for practical purposes because both C_L and $\sin \alpha$ tend to be much smaller than the gradient of C_L in the region where the effects of lift are large. It should also be noted that the results of references 13 and 14 indicate that there are higher order terms in the expression for the effective cross-sectional area which are proportional to the derivatives of the wing twist and camber. These terms are negligible unless the wing twist and camber are of the same order of magnitude as $\sin \alpha$. Since the wing is assumed to be flat in this report, the additional terms do not appear.

RESULTS

In this section results are presented for axisymmetric flow fields and flow fields about lifting configurations. In addition, the results of a numerical study of the transonic area rule for lifting configurations are presented.

Axisymmetric Flow Fields

Parabolic arc of revolution.- The present method calculates axisymmetric flow fields in essentially the same manner as the method of Bailey (ref. 28). The only major difference is that the present method employs the shock difference operator of Murman (ref. 29) and the method of reference 28 does not. In figure 4 results of the present method and that of Bailey are compared for flow past a parabolic arc of revolution with a fineness ratio of 10. The free-stream Mach number is 0.99. Results for the sonic-line and shock-wave locations and the surface pressure distributions are given. It is seen that the use of the shock difference operator influences the results for the location of the shock wave and the pressure in the region behind the shock.
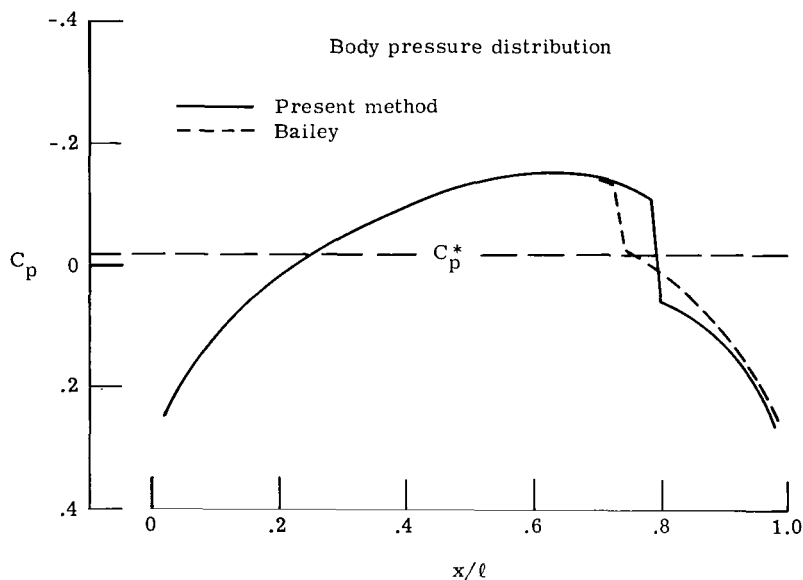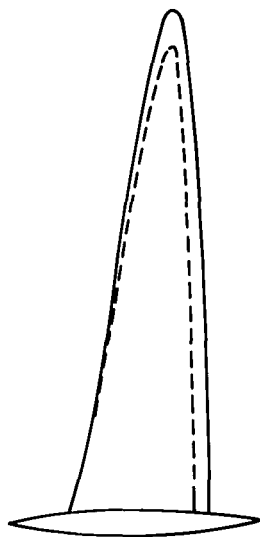

Figure 4.- Comparison of methods for parabolic arc of revolution with fineness ratio of 10. $M_\infty = 0.99$; $\alpha = 0°$.

Parabolic arc of revolution with bump.- Equation (74) indicates that the flow fields about wing-body combinations traveling at near-sonic speeds at angle of attack are similar to flow fields about bodies with bumps on them. Therefore, the present method should be capable of calculating flow about bodies with irregular thickness distributions. In figure 5 the results of the present method are compared with the experimental results of Taylor (ref. 34) for a body with a bump on it. The basic body is a parabolic arc of revolution with a fineness ratio of 14 and the amount the bump, which extends from $x = 0.393$ to $x = 0.607$, adds to the configuration radius is given by the equation

$$\Delta r = \Delta r_{max} \sin^2\left[\pi\left(\frac{x - 0.393}{0.214}\right)\right]$$

where Δr_{max} is 20 percent of the basic body diameter. It should be noted that r_0, the radius of the surface on which the boundary condition given by equation (58) is applied, was given the value of 0.03. This value is approximately the body radius where the bump begins and ends. The results for the pressure distribution differ slightly for other values of r_0.
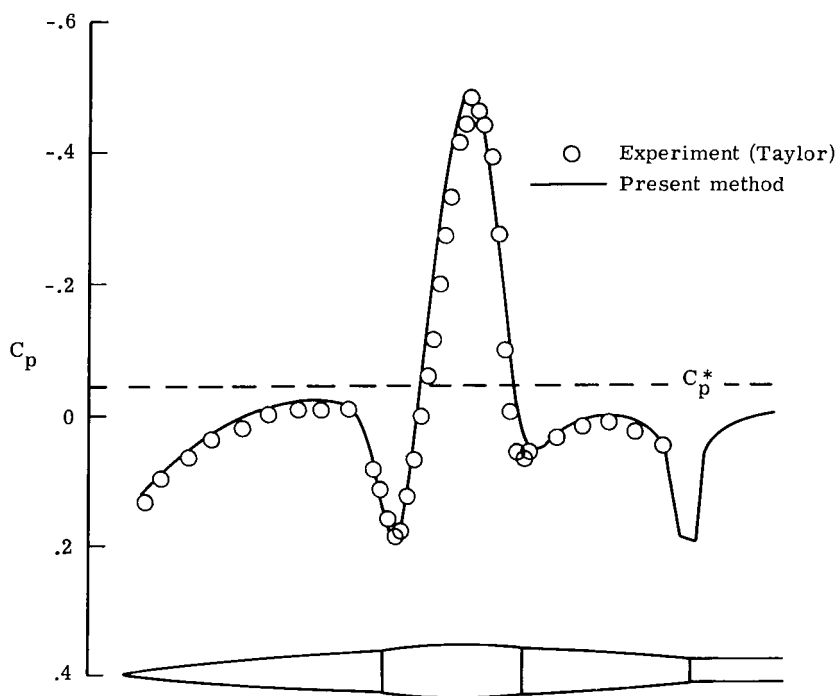

Figure 5.- Pressure distribution for bumpy body. $M_\infty = 0.975$; $\alpha = 0^\circ$.

Ellipse of revolution.- The results of the present method for an elliptic body with a fineness ratio of 10 are compared with the results of the method of South and Jameson (ref. 35) in figures 6 and 7 for Mach numbers 0.99 and 0.997, respectively. In the present method the small-disturbance approximation is used, whereas in the method of reference 35 the full potential equation is solved. It can be seen from figures 6 and 7 that, in general, the results of the two methods for the pressure distributions are in reasonable agreement. The results of the two methods differ in the region of the nose for $M_\infty = 0.99$. This difference is probably due to the fact that the small-disturbance approximation, which tends to be inaccurate in stagnation regions, was used in the present method. It should be noted that the method of reference 35 does not employ the Murman shock difference operator. Consequently, the results of the present method in the region of the shock are mathematically more realistic than those of the method of reference 35. It can be seen from the figures that the present method predicts a smaller supersonic region at large radial distances from the configuration than the method of reference 35.

Parabolic arc of revolution in slotted and porous tunnels.- The results of the present method for transonic flow past a parabolic-arc body with a fineness ratio of 10 in a slotted-wall tunnel are shown in figure 8. The free-stream Mach number is 0.99. The body has a sting which extends downstream from $x = 0.84$. Comparisons are made with the results of the present method for flight in free air and the experimental results of Taylor and McDevitt (ref. 36). The experimental results were obtained in the Ames
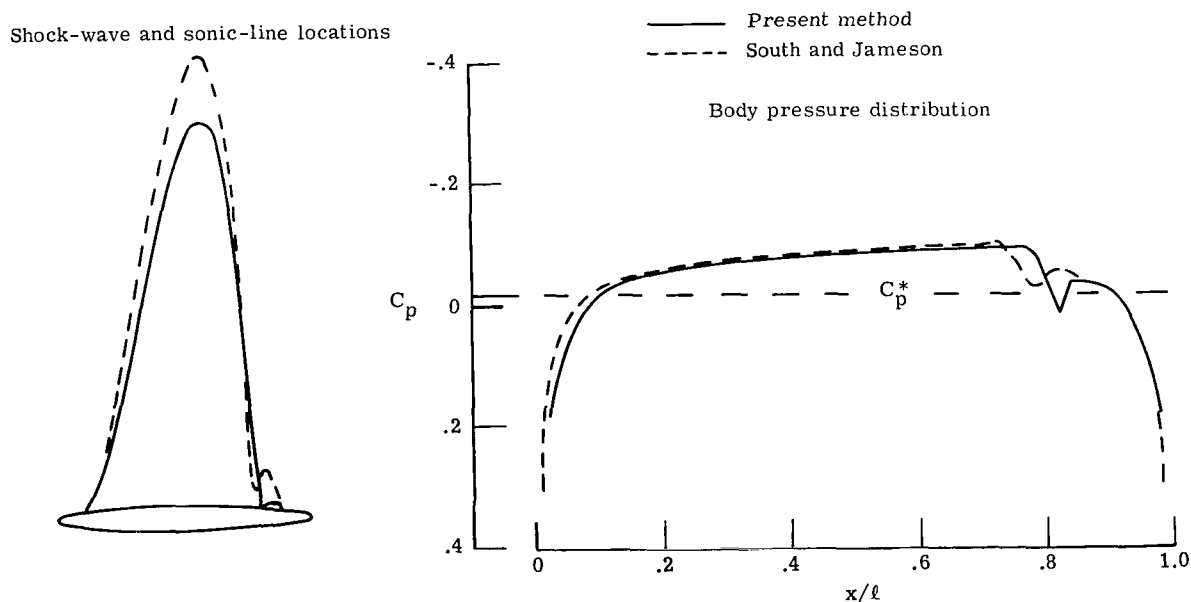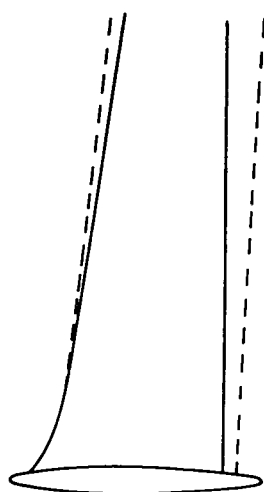

Figure 6.- Comparison of methods for ellipse of revolution with fineness ratio of 10. $M_\infty = 0.99$; $\alpha = 0^\circ$.

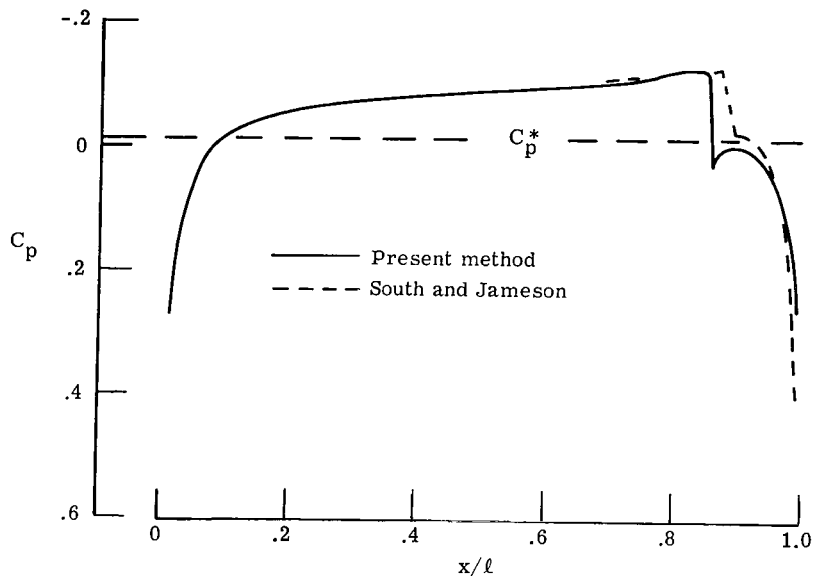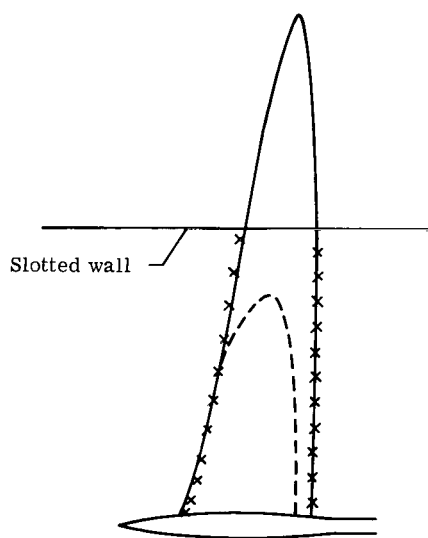Shock-wave and sonic-line locations

Body pressure distribution

Figure 7.- Comparison of methods for ellipse of revolution with fineness ratio of 10. $M_\infty = 0.997$; $\alpha = 0^O$.
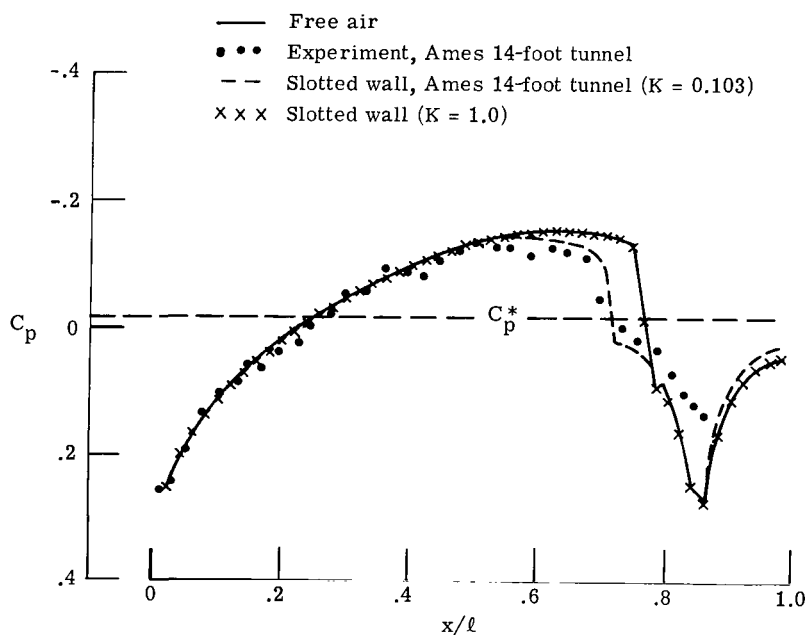
Shock wave and sonic line

Surface pressure distribution

Figure 8.- Parabolic arc of revolution in slotted-wall tunnel. $M_\infty = 0.99$; $\alpha = 0^O$.

34

14-foot wind tunnel. This tunnel has the same type of slots on all four walls, is essentially square, and has an openness ratio of 0.054 and a slot spacing of 24.77 cm (9.75 in.). The walls are actually neither slotted nor porous in the usual sense because the slots are subdivided with a corrugated strip. The theoretical length of the symmetric parabolic-arc body is 203.2 cm (80 in.). Results for two slotted-wall computations are shown. The dashed line depicts the results when the constant κ in the slotted-wall boundary condition (eq. (29)) is evaluated with equation (30), which was developed by Baldwin, Turner, and Knechtel (ref. 26), and the characteristics of the Ames 14-foot tunnel. It is seen that the computation is in reasonable agreement with the experimental results except at the rear where the flow is probably separated. A comparison with the free-air results shows that the effect of the wall is to truncate the supersonic region and move the shock wave forward. It is known that the shock can be moved rearward by reducing the tunnel openness, and hence by increasing the value of κ. It is seen that for the choice $\kappa = 1$ the tunnel results and the free-air results are essentially coincident. Note that the shock location and the pressure level ahead of the shock are both in agreement.

Results for flow in free air and a porous-wall wind tunnel are compared in figure 9. It is seen that the shock wave is located upstream of the free-air shock if the constant P in the porous-wall boundary condition (33) has a value of 0.5. This is the value of P which was recommended for the Ames 14-foot tunnel by Bailey (ref. 28). When P is
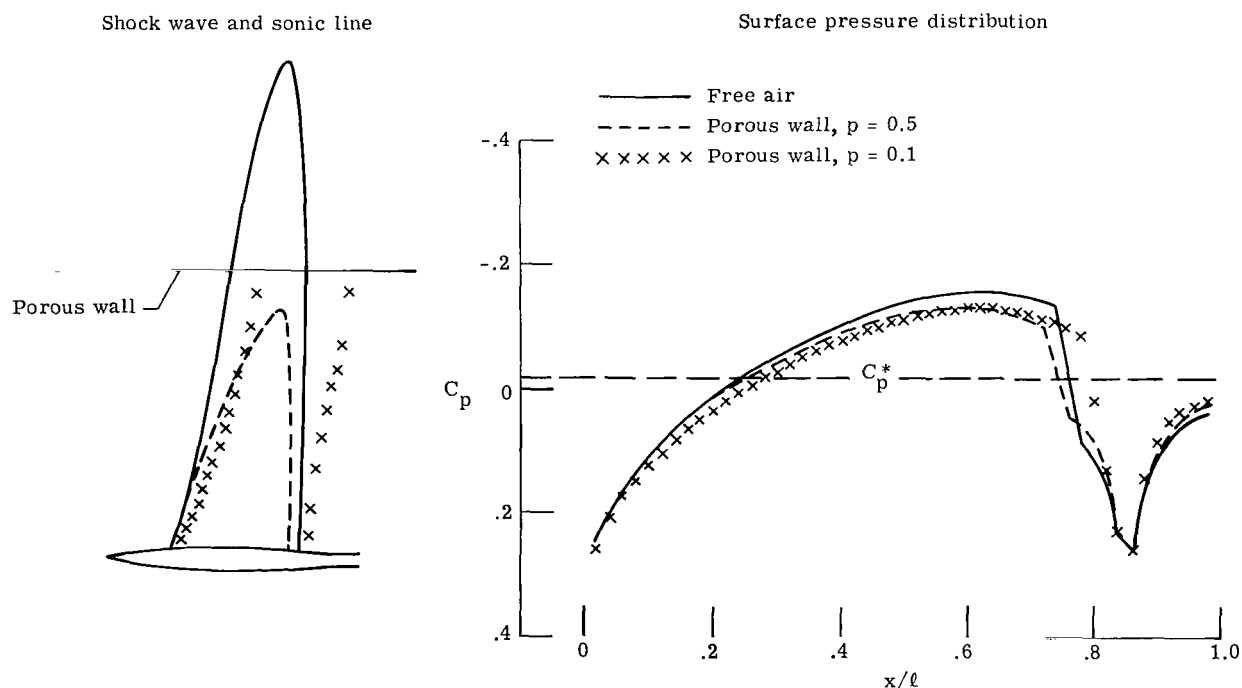

Figure 9.- Parabolic arc of revolution in porous-wall tunnel. $M_\infty = 0.99$; $\alpha = 0^\circ$.

given the value 0.1, it is seen that the shock wave is located downstream of the free-air shock. However, the same minimum pressure level upstream of the shock, which differs from the free-air level, is obtained for both values of P. It appears from these calculations that slotted-wall tunnels are more capable of reproducing free-air results than porous-wall tunnels.

Flow Fields About Lifting Configurations

Comparisons with linear subsonic and supersonic methods.- The results of the present method for incompressible attached flow past two wing-body combinations are compared with those of a standard linear panel method (ref. 37) in figure 10. The linear lift potential used in the present method is obtained from the theory of Lawrence and Flax (ref. 21). The body is an ogive-cylinder-ogive with each ogive being one quarter of the body length. A configuration which has a flat-plate delta wing with a 45° leading-edge sweep and a configuration which has a truncated flat-plate delta wing with the same sweep are treated. The results for the body pressure distribution in the wing plane, that is, the pressure distribution along the intersection of the body surface and the wing plane, are compared. The results of the two methods are in fair agreement. It can be seen that the panel-method results for the afterbody pressure depicted in figure 10(a) contain large oscillations and are probably in error.
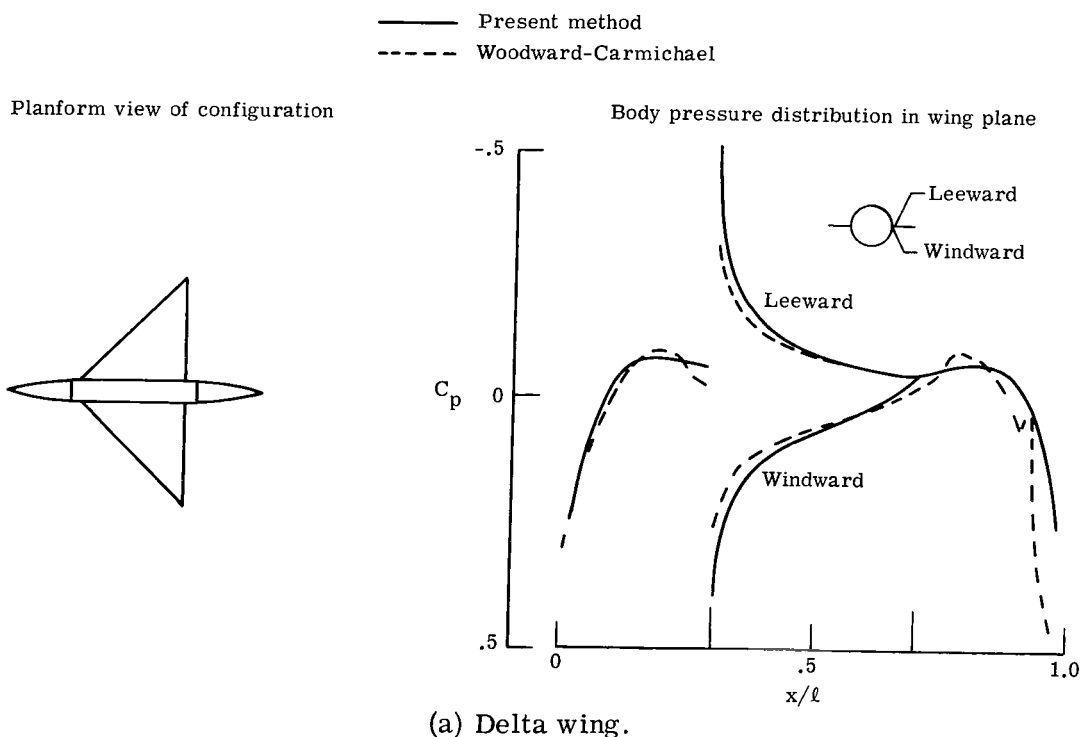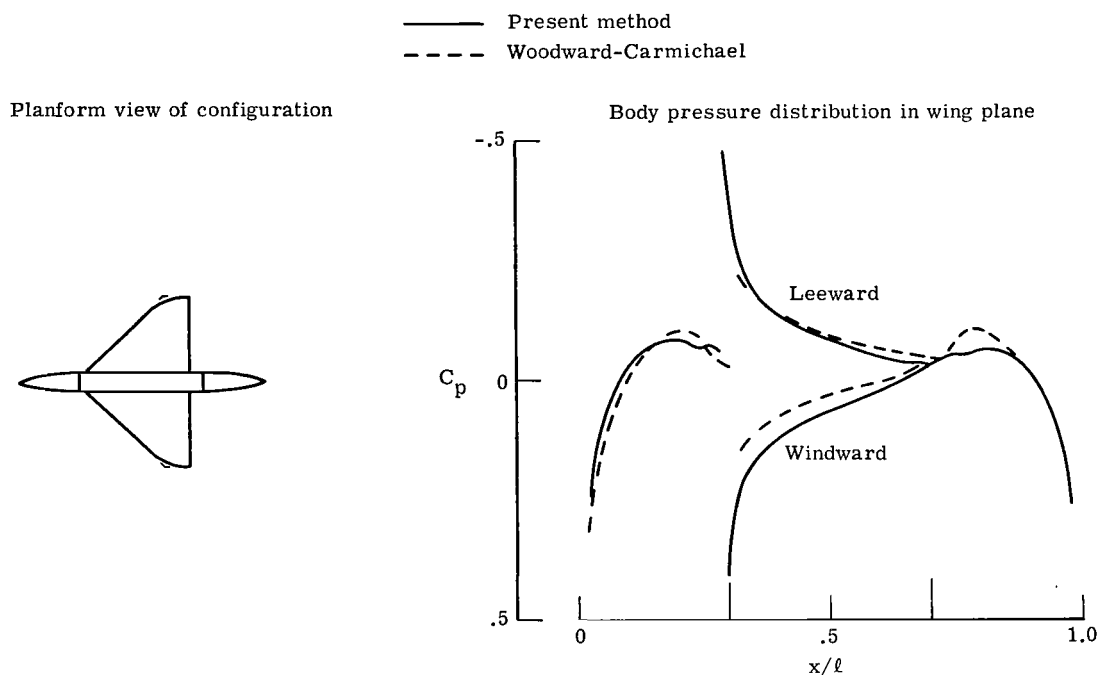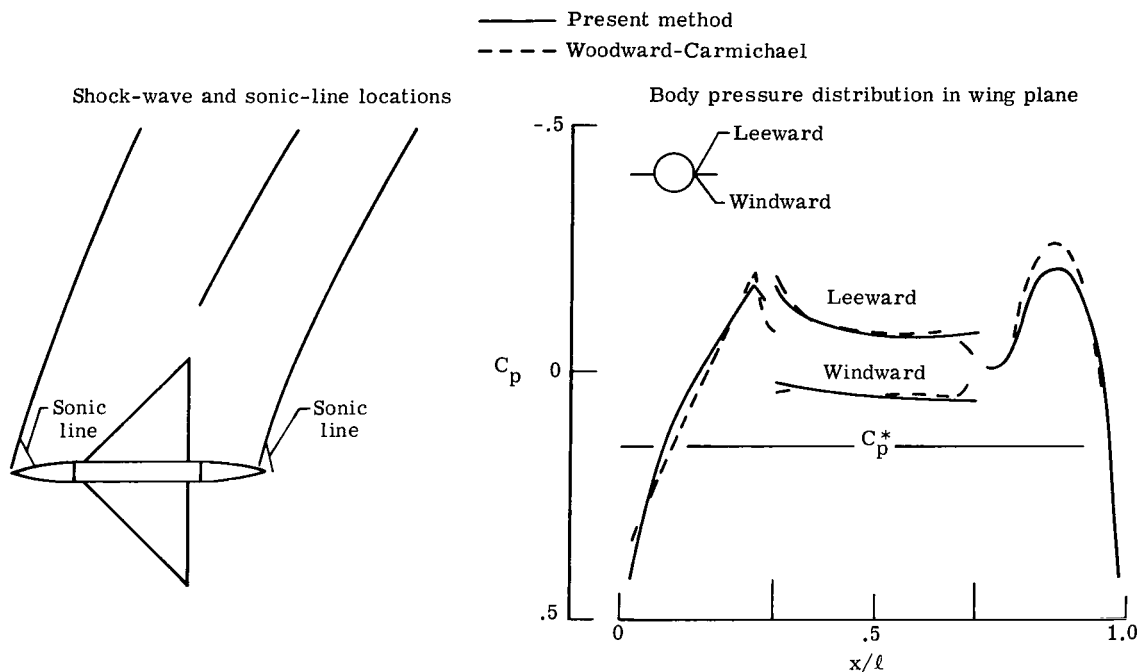

Planform view of configuration   Body pressure distribution in wing plane

(a) Delta wing.

Figure 10.- Comparison of results for body pressure distribution in wing plane. $M_\infty = 0$; $\alpha = 4^O$.

————— Present method
– – – – Woodward-Carmichael

Planform view of configuration
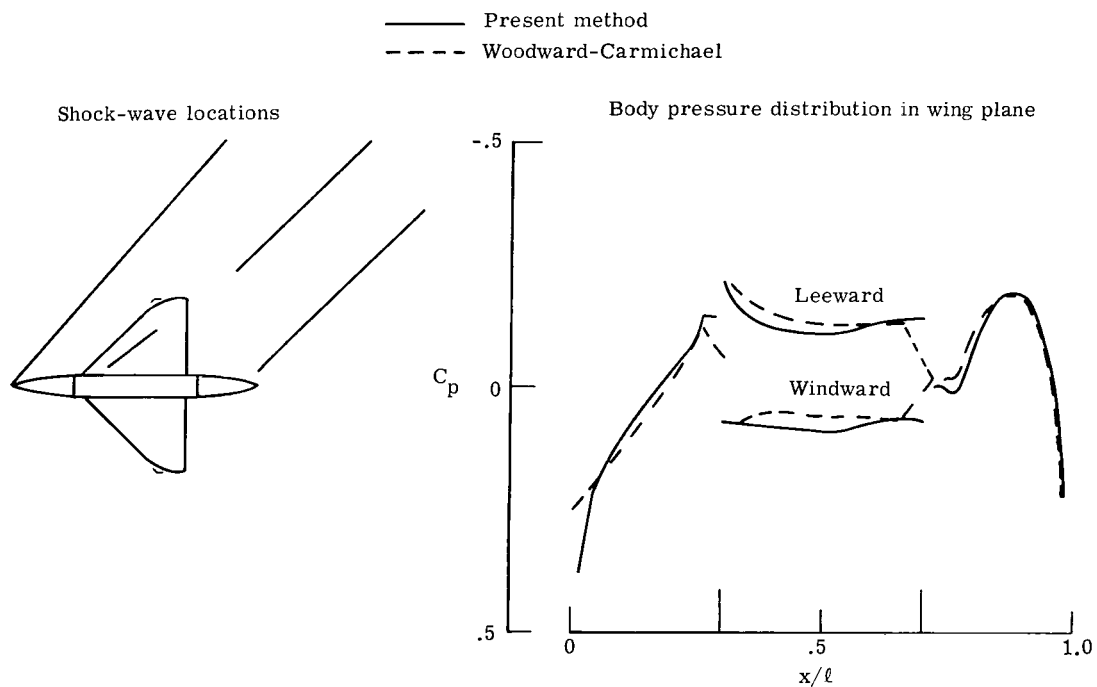
Body pressure distribution in wing plane

(b) Cropped delta wing.

Figure 10.- Concluded.

In figure 11 the results of the two methods are compared for supersonic attached flow past two configurations. The linear lift potential which is used in the present method is obtained from a quasiconical theory. The shock-wave and sonic-line locations as predicted by the present method are shown on the left, and the surface pressure distributions in the wing plane are compared on the right. Sonic-line and strong-shock-wave locations are determined from the longitudinal Mach number distributions. It is assumed that weak shock waves are located at points in regions of supersonic flow where the derivative φ'' has a negative minimum. The free-stream Mach numbers for the delta-wing and the truncated delta-wing configurations are 1.1 and 1.4, respectively. For the lower free-stream Mach number there is a slightly detached bow shock, a tail shock which intersects the body just upstream of the rear apex, a weak shock in the vicinity of the wing, and small pockets of subsonic flow at the ends of the body. The results of the two methods for the surface pressure distribution are in good agreement in the vicinity of the wing. There is some disagreement on the forebody where the flow is transonic and hence where linear methods tend to be inaccurate. There is also some disagreement in the results for the afterbody pressure distribution. For the flow field with $M_\infty = 1.4$, the shock-wave pattern is qualitatively the same as that with $M_\infty = 1.1$, but there are no pockets of subsonic flow. The results of the two methods for the pressure distributions

37

(a) Delta wing. $M_\infty = 1.1$; $\alpha = 2^O$.

(b) Cropped delta wing. $M_\infty = 1.4$; $\alpha = 4^O$.

Figure 11.- Comparison of results for shock-wave and sonic-line locations and body pressure distribution in wing plane.

38

in the vicinity of the wing disagree somewhat, but the pressure difference across the wing is the same. The results for the afterbody pressure distributions are in agreement. The pressure increase on the rear part of the wing indicated in figure 11(b) is due to the first term on the right side of equation (55). This is the nonlinear $\dfrac{\partial \varphi}{\partial x} \dfrac{\partial^2 \varphi}{\partial x^2}$ term as approximated in the present method at points inside the wing tip. As has been pointed out previously, this term is evaluated on the basis of slender-wing theory and, as a result, the Mach lines are assumed to be perpendicular to the free-stream direction. Of course, this approximation is poor for a Mach number of 1.4.

Results obtained with the present method and the method of reference 37 for the chordwise pressure distributions at two span stations on the delta-wing configuration traveling at both subsonic and supersonic speeds are compared in figure 12. It is seen that the results of the two methods are in reasonable agreement.

Transonic lift effects for subsonic free-stream speeds.- The effect of lift on the shock-wave and sonic-line locations in the wing plane of a wing-body combination traveling at a Mach number of 0.99 is shown in figure 13. The linear lift solution is obtained from slender-wing theory. The configuration is composed of a body with a fineness ratio of 12 and the maximum-thickness point at $x = 0.4$ and a "hyperbolic" wing. (See appendix A.) It is seen that for angles of attack of 6° and less, the effects of thickness are dominant, and for angles of attack of 9° and larger, the effects of lift are dominant. For the lift-dominated cases, the flow decelerates with a shock immediately ahead of the apparent bump due to lift, then overexpands past the bump, and finally decelerates with a shock near the trailing edge.

In figure 14 the effect of lift on the sonic-line and shock-wave locations for flow past another wing-body combination traveling at the lower free-stream Mach number of 0.98 is shown. The configuration is composed of a circular-arc body with a fineness ratio of 10 and a flat-plate truncated delta wing with a rounded tip. As before, the linear solution is obtained from slender-wing theory. It is seen that the lift effect for this case is qualitatively the same as before, but that the angle-of-attack range for thickness-dominated flow is smaller. Lift-dominated flow exists for angles of attack of 6° and larger.

The pressure distributions along the intersection of the body surface and the wing plane of the configuration shown in figure 14 for $\alpha = 0^{\text{o}}$ and $\alpha = 9^{\text{o}}$ are compared in figure 15. For the larger angle of attack, the distributions both above and beneath the wing are shown. It is seen that the strength of the shock wave due to lift on the upper surface of the wing for $\alpha = 9^{\text{o}}$ is much larger than the thickness-induced shock for $\alpha = 0^{\text{o}}$. It is also seen that there is a small supersonic region and shock wave beneath

———— Present method

– – – – Woodward-Carmichael

Pressure distribution at y/b = 0.35

Pressure distribution at y/b = 0.70

C_p

-.5

0

.5

$\frac{x-x_{le}}{c(y)}$

0   1.0

C_p

-.5

0

.5

$\frac{x-x_{le}}{c(y)}$

0   1.0

Leeward

Windward

Leeward

Windward

y/b = 0.70

0.35

(a) $M_\infty = 0$; $\alpha = 4^O$.

———— Present method

– – – – Woodward-Carmichael

Pressure distribution at y/b = 0.35

Pressure distribution at y/b = 0.65

C_p

-.4

0

.4

$\frac{x-x_{le}}{c(y)}$

0   1.0

C_p

-.4

0

.4

$\frac{x-x_{le}}{c(y)}$

0   1.0

Leeward

Windward

Leeward

Windward

y/b = 0.65

0.35

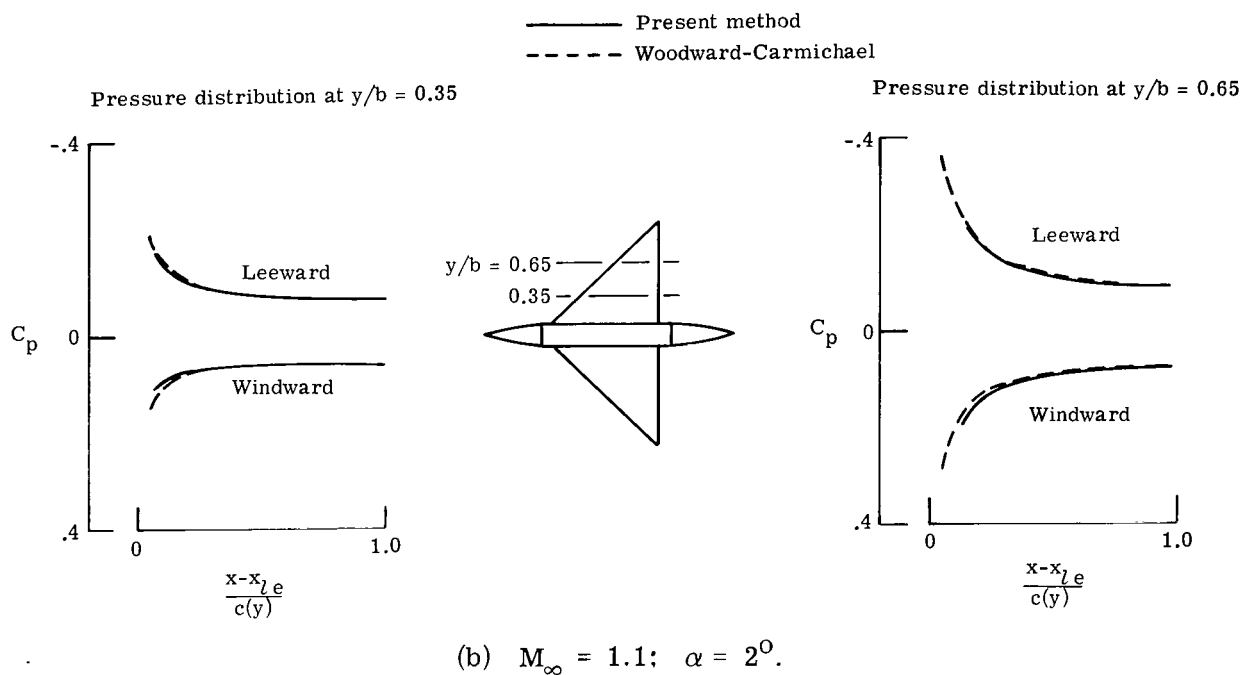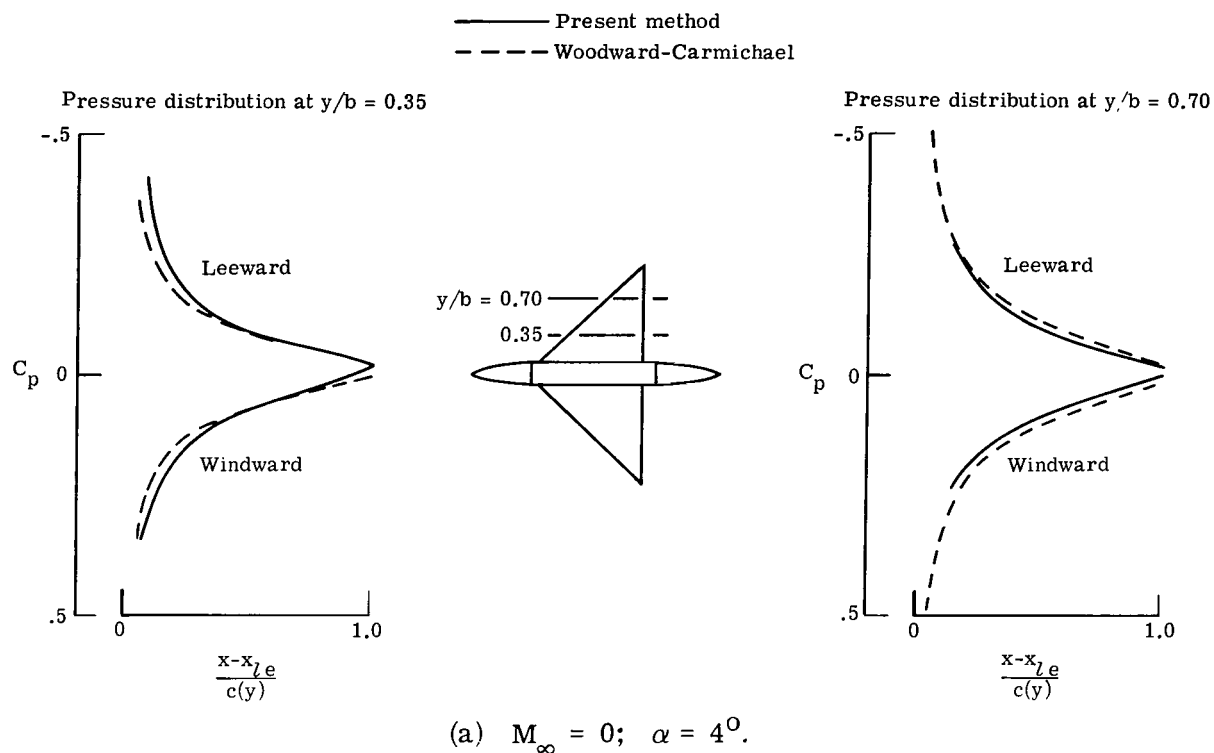(b) $M_\infty = 1.1$; $\alpha = 2^O$.

Figure 12.- Comparison of results for chordwise pressure distributions at
two span stations on a delta-wing configuration.

40

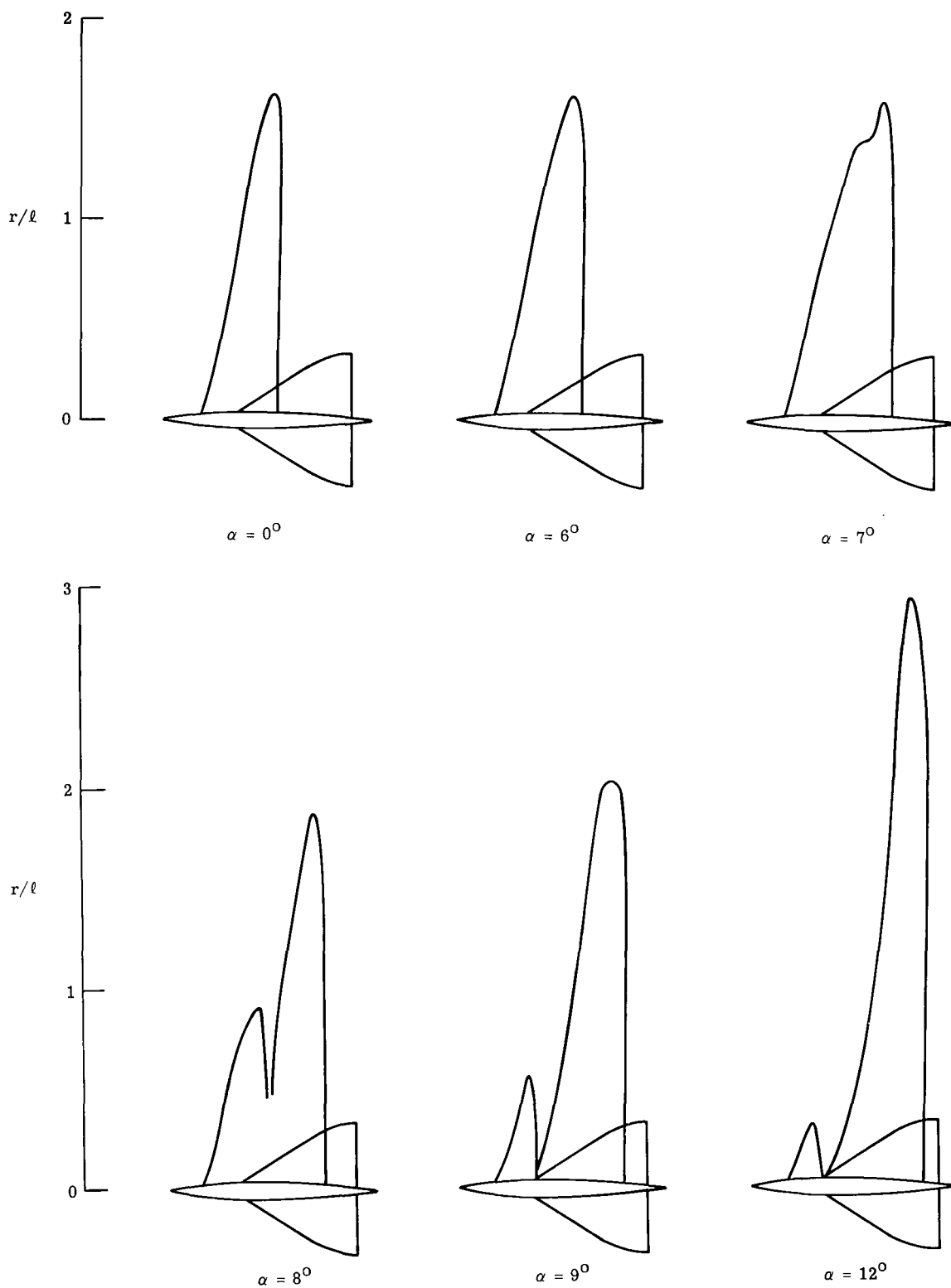Figure 13.- Effect of lift on transonic shock-wave and sonic-line locations in wing plane. $M_\infty = 0.99$.

$\alpha = 0^O$ $\alpha = 3^O$ $\alpha = 4^O$

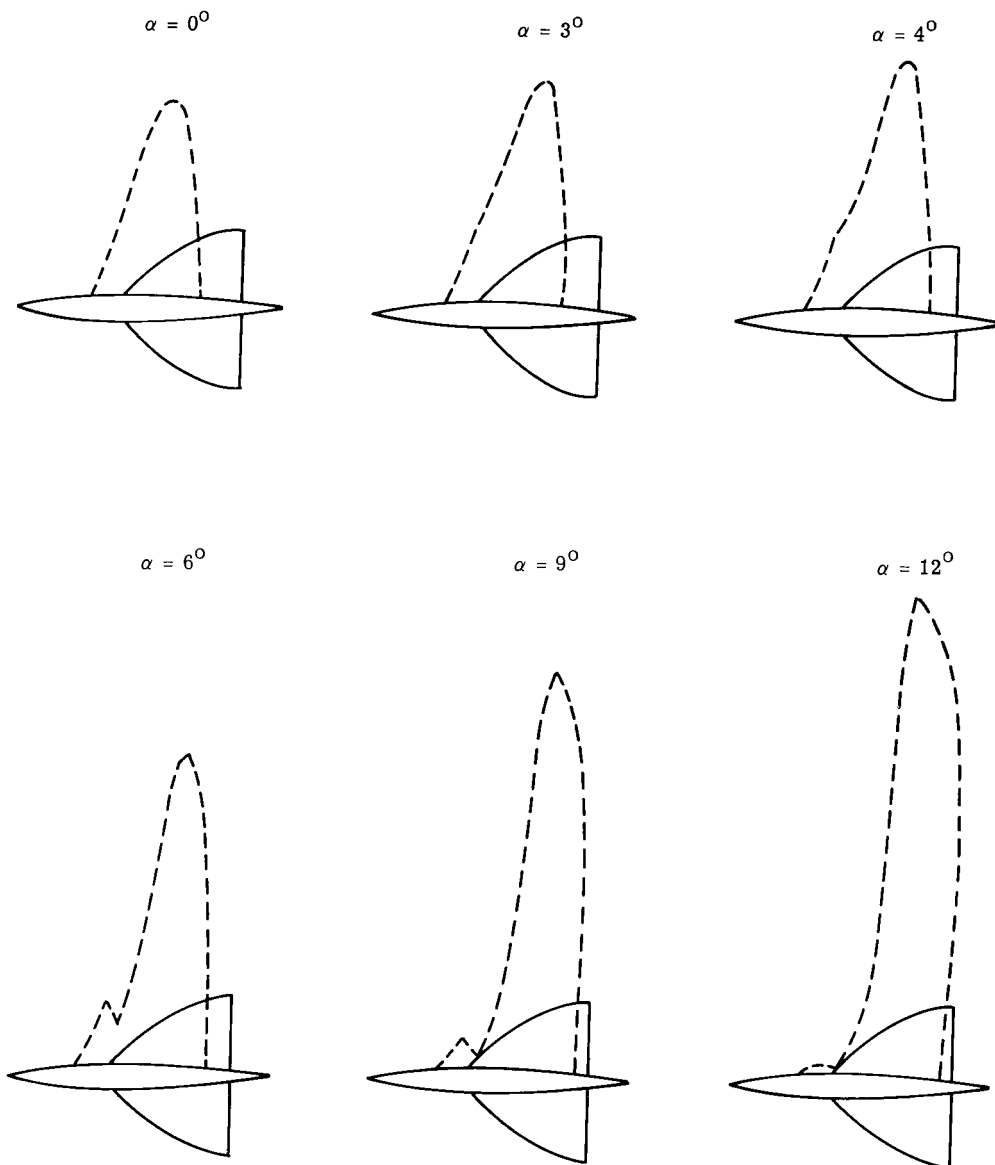$\alpha = 6^O$ $\alpha = 9^O$ $\alpha = 12^O$

Figure 14.- Effect of lift on transonic shock-wave and sonic-line locations in wing plane. $M_\infty = 0.98$.
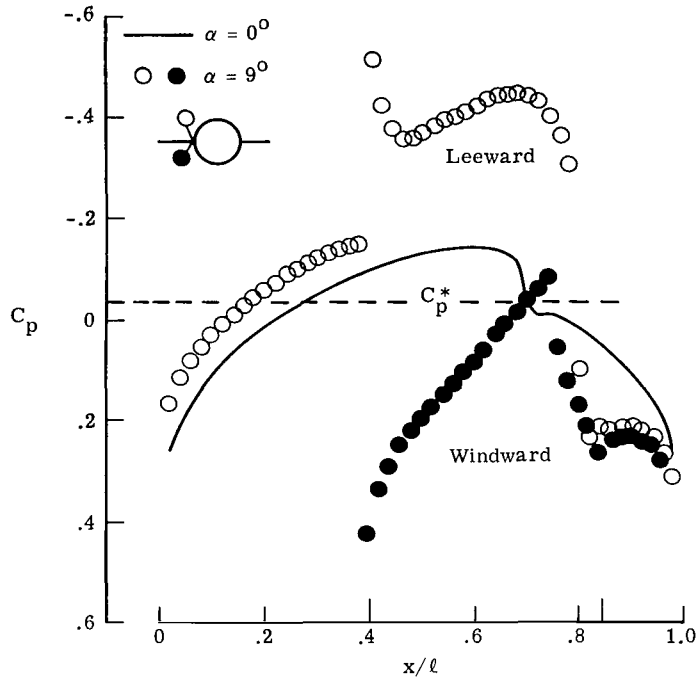
Figure 15.– Comparison of body pressure distributions in wing plane for two angles of attack. $M_{\infty} = 0.98$.

the wing. It should be noted that the results shown in this figure were calculated in the horizontal plane ($\omega = 0^{\circ}$).

As discussed in a previous section, the linear lift solution can be obtained from the theory of Lawrence and Flax if M_{∞} is less than 1, slender-wing theory if M_{∞} is near 1, and the modified theory of Carafoli et al. if M_{∞} is greater than 1. For high subsonic values of M_{∞}, either slender-wing theory or the theory of Lawrence and Flax can be used since the latter reduces to the former as M_{∞} approaches 1. In order to demonstrate that both theories are applicable in this range, results obtained with them are compared in figure 16 for a free-stream Mach number of 0.98 and an angle of attack of 6°. It is seen that the results of the two theories are in good agreement except near the point where the wing emerges from the body. The differences in the pressure distributions in this region are due to the fact that some of the derivatives associated with the geometry are calculated analytically for slender-wing theory and numerically for the theory of Lawrence and Flax. Closer agreement can be obtained with a refined grid.

In figure 17 the shock-wave and sonic-line locations for $\alpha = 9^{\circ}$ calculated in the plane of symmetry ($\omega = 90^{\circ}$, -90°) are compared with those calculated in the horizontal plane ($\omega = 0^{\circ}$). The extent of the supersonic region in the upper part of the plane of symmetry ($\omega = 90^{\circ}$) is about the same as that in the horizontal plane. However, it is seen
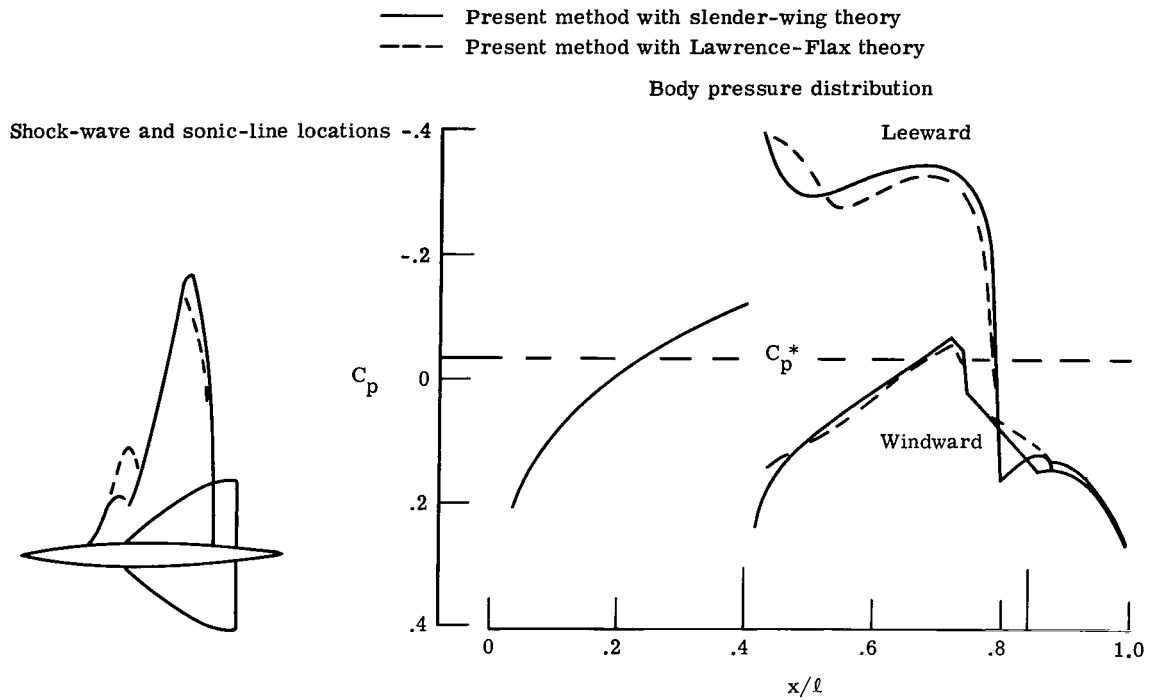
43

Body pressure distribution

Shock-wave and sonic-line locations

C_p

C_p^*

Leeward

Windward

x/ℓ

Figure 16.- Comparison of wing-plane results obtained with slender-wing theory and Lawrence-Flax theory. $M_\infty = 0.98$; $\alpha = 6^O$.

Wing plane

Vertical plane
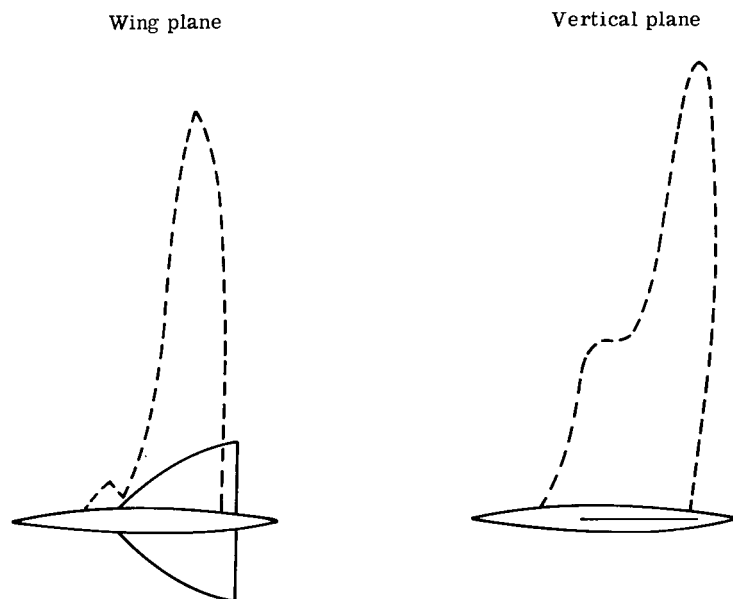
Figure 17.- Comparison of shock-wave and sonic-line locations in wing plane and vertical plane. $M_\infty = 0.98$; $\alpha = 9^O$.

that the computation for $\omega = -90^O$ indicates that there is no supersonic bubble in the lower part of the symmetry plane so that the flow is entirely subsonic. This lack of supersonic flow is caused by the decelerating effect of the lift-dipole term on the flow beneath the wing. There is a difference in the results calculated for $\omega = 0^O$ and $\omega = -90^O$ since the former indicates the existence of the small region of supersonic flow beneath the wing. This difference is probably due to the simple flow model in the region $r < y_2(x)$ and indicates a limitation of the present method.

Transonic lift effects for supersonic free-stream speeds.- In figure 18 the horizontal-plane results for the shock-wave and sonic-line locations for slightly supersonic flow past a wing-body combination at angles of attack $\alpha = 0^O$ and $\alpha = 10^O$ are compared. The free-stream Mach number M_∞ is 1.02. It is seen that two of the effects of increasing the angle of attack are to move the rear shock forward onto the trailing edge of the wing and to increase the size of the subsonic region behind the rear shock.

The pressure distributions along the intersection of the body surface and wing plane are compared in figure 19. In addition to moving the rear shock forward and increasing the size of the rear subsonic region, lift is seen to increase the strength of the shock above the wing.

The results shown in figures 18 and 19 were obtained with a lift solution obtained from slender-wing theory. It is shown in figure 20 that virtually the same results can be obtained for $M_\infty = 1.02$ when the lift solution is obtained from the quasiconical theory of Carafoli et al. (ref. 22). This is to be expected since conical theory for supersonic flow reduces to slender-wing theory as the free-stream Mach number approaches 1.

Lifting transonic tunnel flows.- The results for transonic flow past a lifting configuration in free air and in a slotted tunnel are compared in figure 21. The Mach number and angle of attack are $M_\infty = 0.98$ and $\alpha = 12^O$, respectively. The slotted-tunnel computation is for a configuration with a span of 152.4 cm (60 in.) in an axisymmetric model of the Ames 14-foot transonic wind tunnel. The results show that the outer part of the supersonic region is truncated by the tunnel wall and that the presence of the wall causes the shock to be shifted forward.

The effects of a solid wall on the shock-wave and sonic-line locations in the wing plane for slightly supersonic flow past a lifting wing-body combination are shown in figure 22. The Mach number and angle of attack are $M_\infty = 1.02$ and $\alpha = 10^O$, respectively. The results for free air are shown on the left, and those for flow in the tunnel are shown at the right. It is seen that the bow shock is reflected at the tunnel wall and that the reflected shock intersects the aft shock in such a manner that the subsonic pocket at the rear of the configuration is enlarged considerably. The location of the reflected shock in the region of the intersection is not shown because of the difficulty in locating weak oblique shock waves.
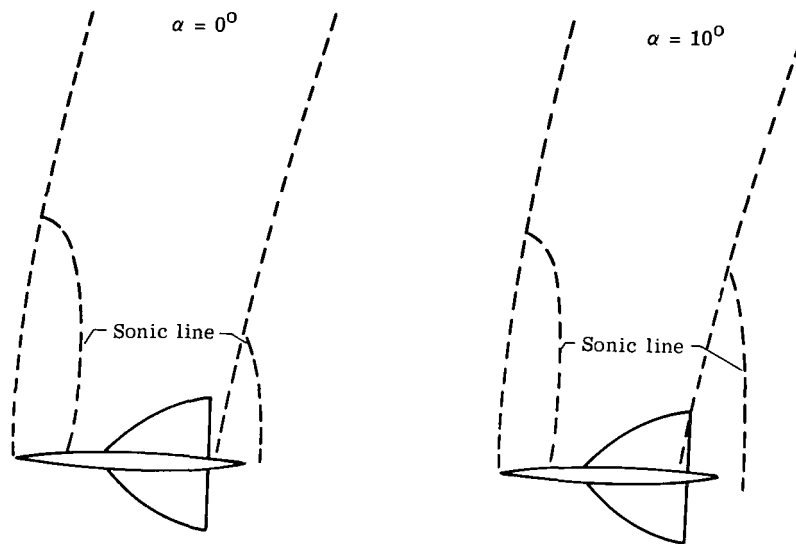
Figure 18.- Comparison of shock-wave and sonic-line locations in wing plane for two angles of attack. $M_\infty = 1.02$.
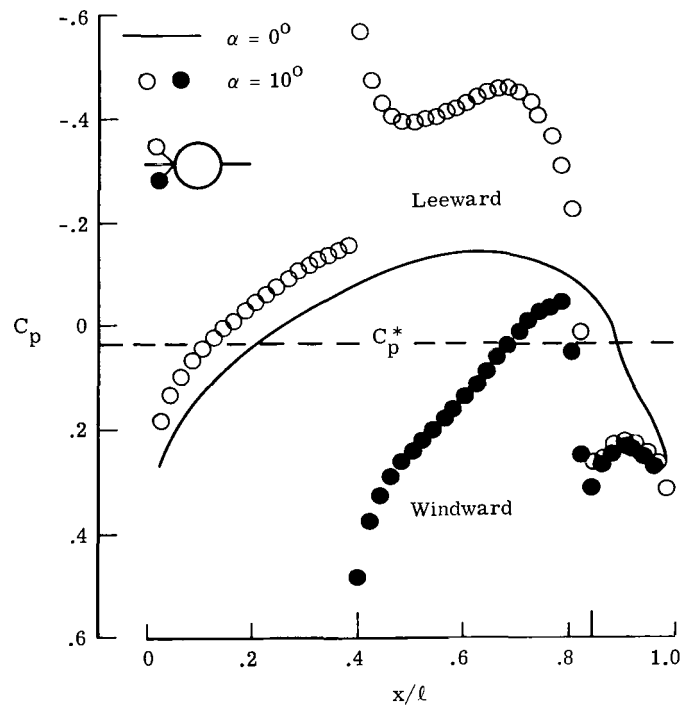
Figure 19.- Comparison of body pressure distributions in wing plane for two angles of attack. $M_\infty = 1.02$.

— Present method with slender-wing theory
--- Present method with quasiconical theory

Shock-wave and sonic-line locations   Body pressure distribution

Figure 20.- Comparison of wing-plane results obtained with slender-wing theory and quasiconical theory. $M_\infty = 1.02$; $\alpha = 6^O$.

--- Free air
— Slotted tunnel

Shock wave and sonic line   Body pressure distribution

Figure 21.- Wing-plane results for free air and slotted-wall tunnel. $M_\infty = 0.98$; $\alpha = 12^O$.

47

Figure 22.- Effect of tunnel wall on shock-wave and sonic-line locations. $M_\infty = 1.02$; $\alpha = 10^\circ$.
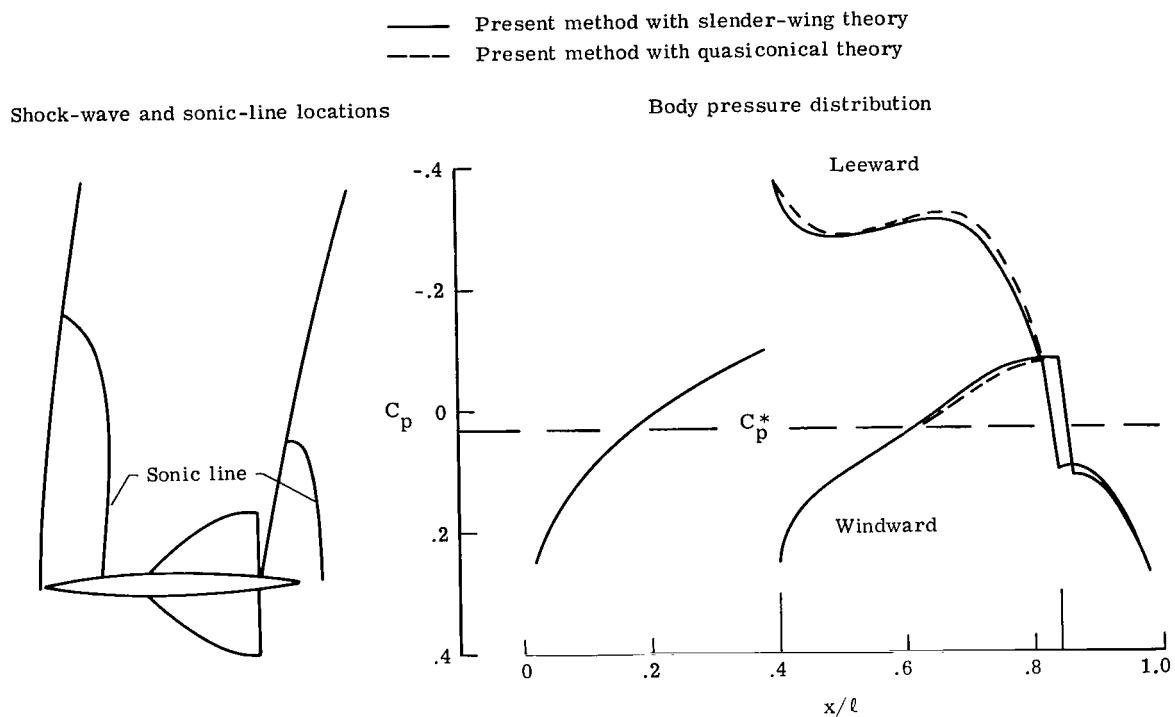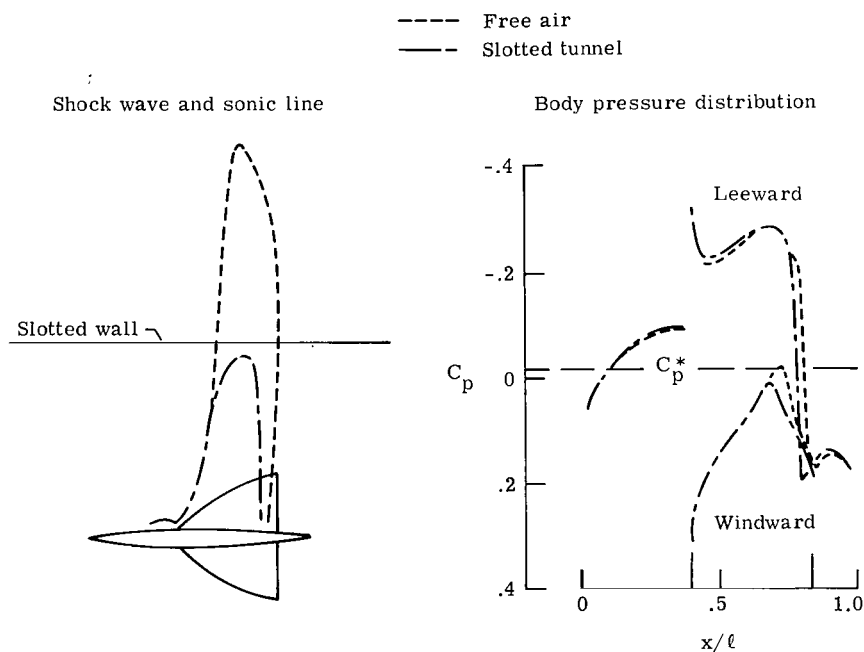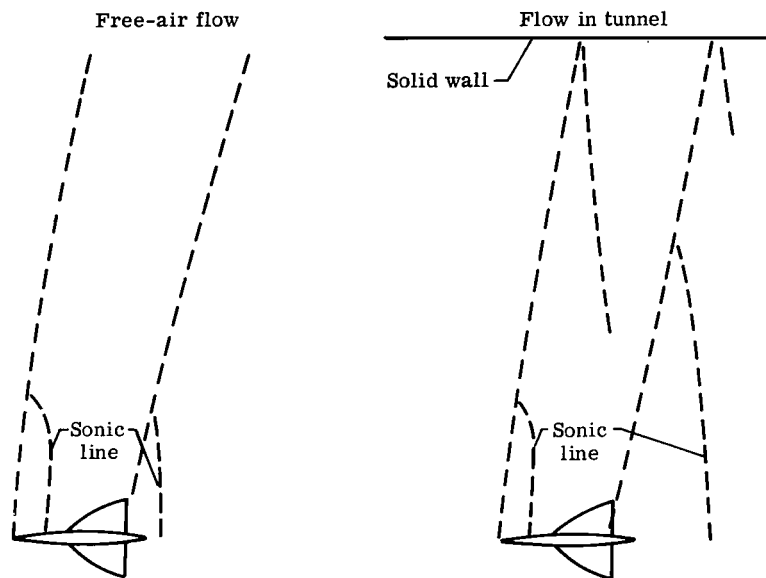
Leading-edge separation.- The results of the present method for the dependence of the lift coefficient C_L on the angle of attack α for separated flow past a delta wing are compared with experiment and the results of other methods in figure 23. The comparisons for low-speed flow are presented on the left side of the figure. The experimental data are those of Peckham (ref. 38). It is seen that the results of both Brown and Michael (ref. 20) and Smith (ref. 39) overpredicted the data, the latter being more accurate than the former, and the results of the suction analogy of Polhamus (ref. 40) are essentially in agreement with the data. It is also seen that the results of the present method overpredict the data to about the same degree as those of Smith. The suction analogy was not employed in the present method because the spanwise effects of vorticity cannot be determined with it in its present form. Results for supersonic flow with $M_\infty = 1.96$ are shown on the right side of the figure. The experimental data are those of Hill (ref. 41). It is seen that the trends for supersonic flow are the same as those for low-speed flow. The suction-analogy results for supersonic flow were obtained from reference 42.

The effects of leading-edge separation on transonic flow past a lifting wing body are shown in figure 24. In this figure the results for attached and separated flow past a wing-body combination with $M_\infty = 0.98$ and $\alpha = 6^\circ$ are compared. On the left side of the figure it can be seen that the only effect of leading-edge separation on the shock-wave and sonic-line locations in the wing plane is the slight backward shift of the rear shock toward the trailing edge of the wing. The body surface pressure distributions in the wing
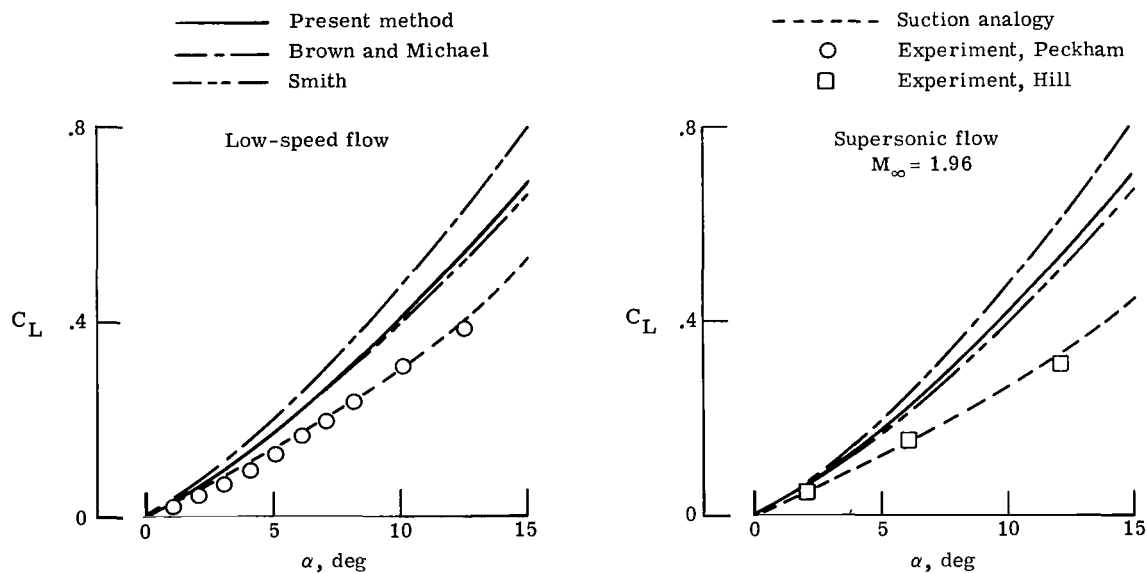
48

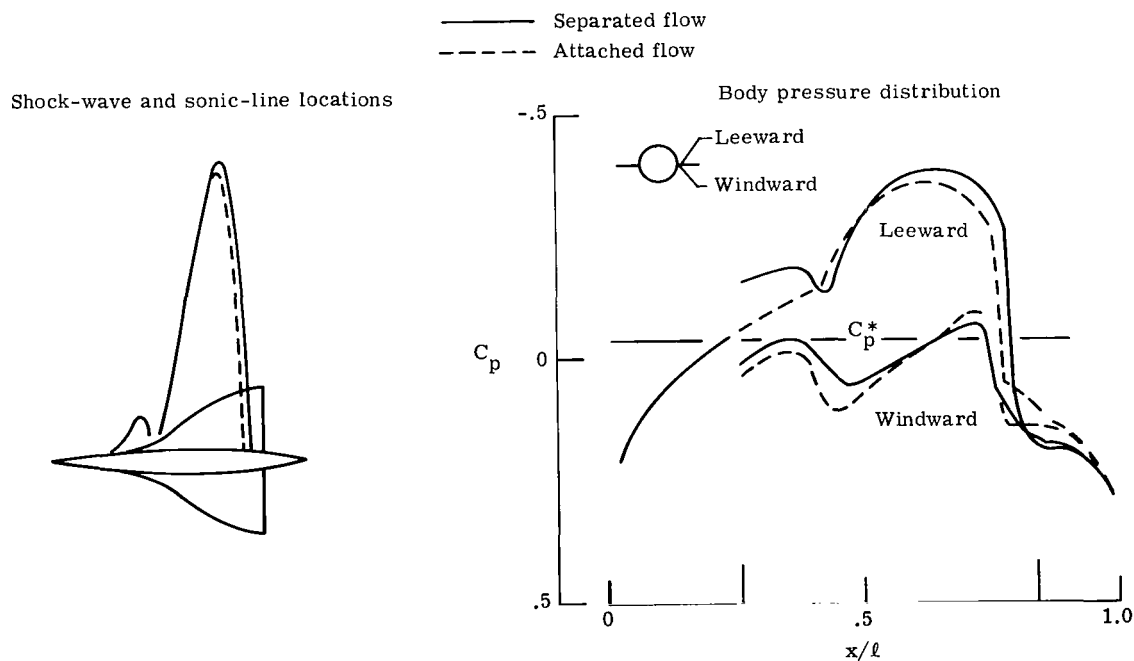Figure 23.- Leading-edge separation for delta wing with aspect ratio of one.

Figure 24.- Effect of leading-edge separation on flow in wing plane. $M_\infty = 0.98$; $\alpha = 6^O$.

49

plane are compared on the right side of the figure. It is seen that separation affects the pressure distribution both above and beneath the wing considerably.

The coefficients for the total lift $L = L_0 + L_1$ and the linear lift L_1 for attached and separated transonic flow past the configuration depicted in figure 24 are compared in figure 25. The Mach number is $M_\infty = 0.98$ and the angle-of-attack range is $0^O < \alpha < 9^O$. The nonlinear lift term L_0 is due primarily to the presence of shock waves. It should be noted that the Brown and Michael model for leading-edge separation, which was used to obtain these results, overpredicts the effect of separation on the lift coefficient. It can be seen that the present results show a small increase in lift due to nonlinear effects.

The results for flow past a configuration which has a strake-generated vortex over the wing are compared with the results for attached flow for a Mach number and angle of attack of $M_\infty = 0.98$ and $\alpha = 6^O$, respectively, in figure 26. The flow is separated on the strake and attached on the main part of the wing. The vortex which was generated by the strake is located over the inboard portion of the wing aft of the point where attached-leading-edge flow begins. It is seen that the shock-wave and sonic-line locations are essentially unaffected by the vortex and that the pressure distribution is affected appreciably only on the strake.

The effects of leading-edge separation on the pressure distribution of the wing body depicted in figures 10(a) and 11(a) for Mach numbers appreciably different from 1 are shown in figure 27. The configuration is composed of a flat-plate delta wing and an ogive-cylinder-ogive body where the length of each ogive is one quarter of the body length. The angle of attack is 9°. Results for separated and attached flow are compared for Mach numbers 0 and 1.4. The pressure distributions which are shown are those along the intersection of the body surface and the wing plane. This distribution in the vicinity of the wing is the root-chord pressure distribution. It is seen that for incompressible flow the load at the wing root is larger for attached than for separated flow. However, the lift coefficients for attached and separated incompressible flow for $\alpha = 9^O$ are 0.63 and 1.14, respectively. The apparent discrepancy is due to the fact that the lift due to the leading-edge vortex is exerted mostly on the outboard portion of the wing. In figure 27(b) it is seen that the effect of the leading-edge vortex on the root-chord pressure distribution is also small for supersonic flow. However, the lift coefficients for attached and separated flow at these conditions are 0.80 and 1.02, respectively.

Swept trailing edge.- The results for attached and separated flow past a configuration with a swept trailing edge are compared in figure 28. The free-stream Mach number and angle of attack are $M_\infty = 0.98$ and $\alpha = 4^O$, respectively. It is evident from the figure that the rear shock wave intersects the body upstream of the swept trailing edge. The present method does not yield good results at points where a shock wave intersects a swept trailing edge.

50
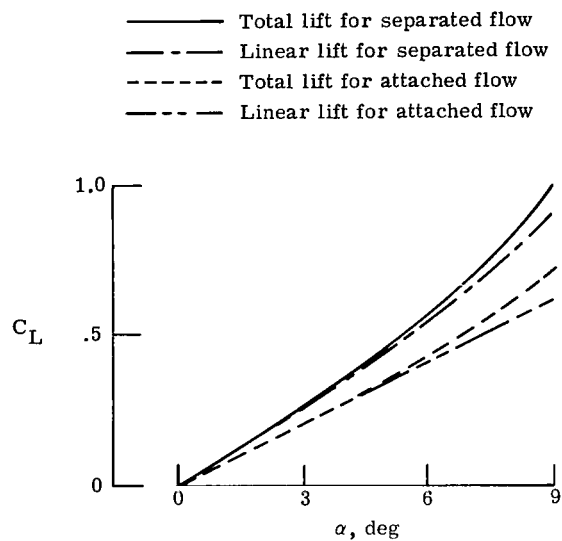
Figure 25.- Total and linear lift for attached and separated flow about configuration depicted in figure 24. $M_\infty = 0.98$.
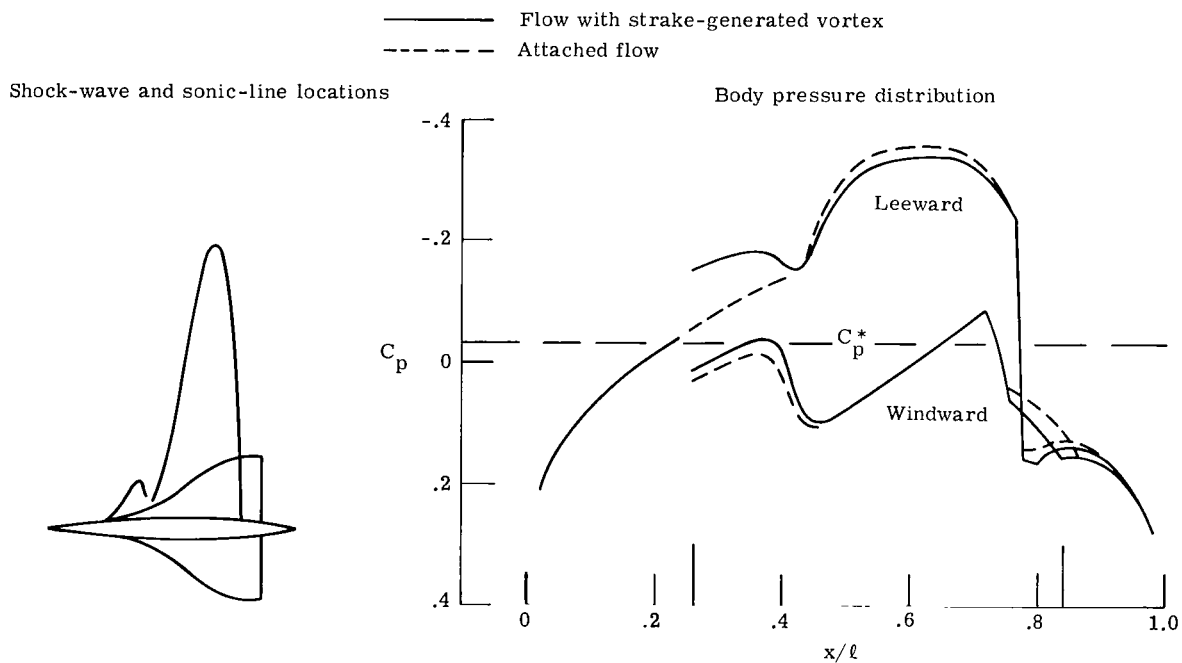
Figure 26.- Effect of strake-generated vortex on flow in wing plane. $M_\infty = 0.98$; $\alpha = 6^\circ$.

51
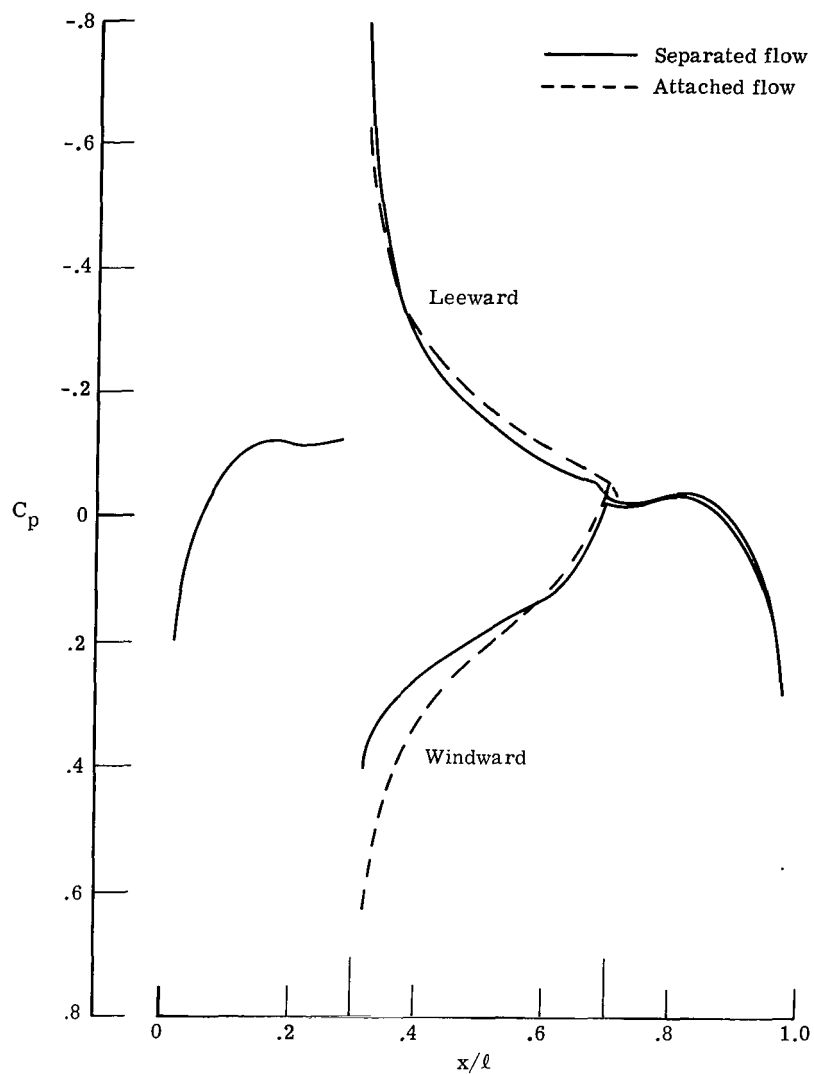
(a) $M_\infty = 0$.

Figure 27.- Effect of leading-edge separation on body pressure distribution in wing plane of configuration shown in figure 10(a). $\alpha = 9^O$.

-.6

Separated flow
- - - - - Attached flow

-.4

-.2

C_p

Leeward

0

.2

Windward

.4

0   .2   .4   .6   .8   1.0

x/ℓ

(b) $M_\infty = 1.4$.

Figure 27.- Concluded.

Separated flow
- - - - - Attached flow

Shock-wave and sonic-line locations

Body pressure distribution

-.4

Leeward

-.2

C_p^*

C_p

0

Windward

.2

.4

0   .2   .4   .6   .8   1.0

x/ℓ

Figure 28.- Comparison of wing-plane results for separated and attached flow past configuration with swept trailing edge. $M_\infty = 0.98$; $\alpha = 4^0$.

Lifting Transonic Area Rule

It has been shown that far from a lifting configuration traveling at near-sonic speed, the flow field is similar to that about an axisymmetric body with a cross-sectional area distribution which depends on both the lift and thickness distributions of the configuration. This modified area distribution is given by equation (74). As noted previously, the second term on the right side of this equation has a coefficient which must be determined experimentally or analytically. In figure 29 the shock-wave and sonic-line locations in the wing plane of a lifting configuration are compared with those of several axisymmetric bodies with cross-sectional area distributions obtained from equation (74) with several different values of the constant B. The Mach number and angle of at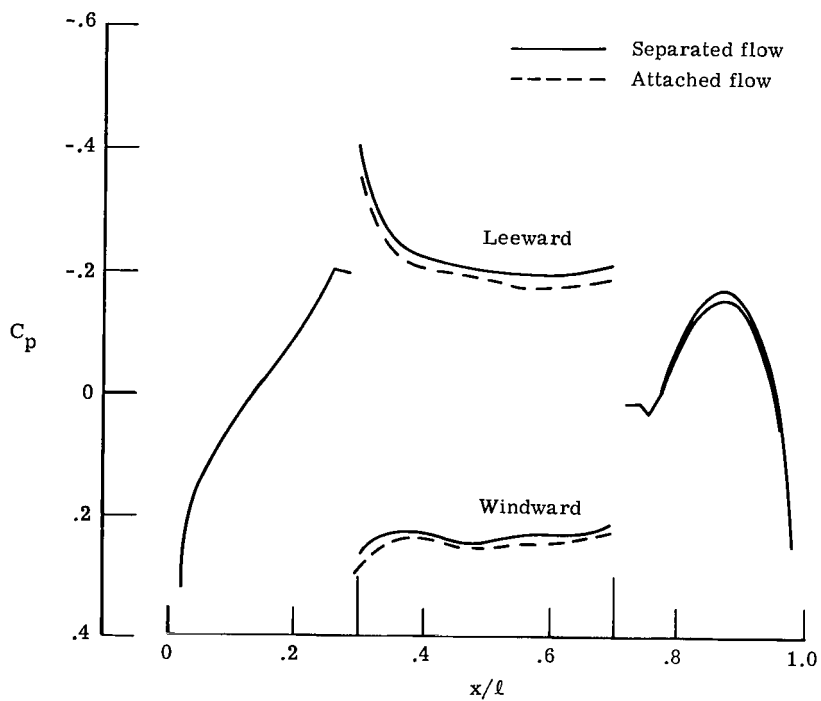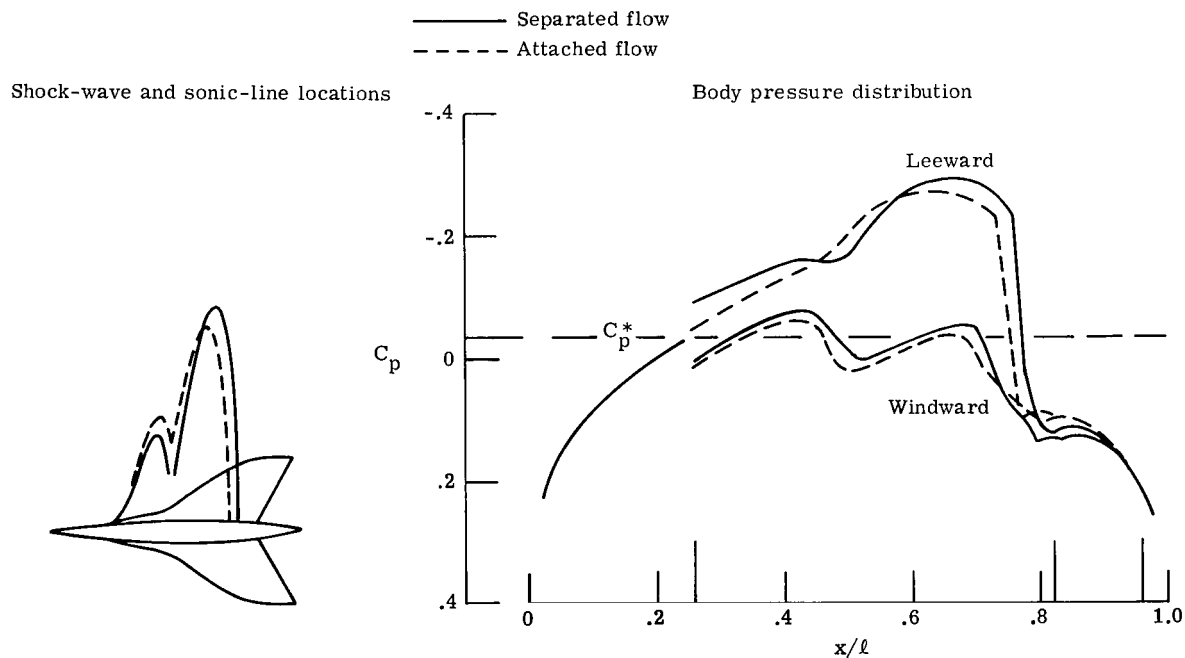tack are $M_\infty = 0.98$ and $\alpha = 6^O$, respectively. It can be seen in figures 29 and 30 that the supersonic region for the axisymmetric configurations lies behind those for the lifting configuration. This phenomenon occurs because it is assumed in the present approximate method for lifting configurations that the lift solution is of the slender-wing type. Consequently, the characteristics of the lift solution are vertical. As a result, the present approximate method tends to locate those nonlinear lift effects which occur at large radial distances from the configuration slightly upstream of their actual location. It is seen that the radial extent of the supersonic region for the axisymmetric lift-equivalent body obtained with the value $B = 3.8$ is the same as that for the wing-plane results for the lifting configuration.

The constant B should depend only on the configuration geometry for near-sonic flow; it should be independent of the angle of attack and Mach number. In figure 30, axisymmetric results obtained with the value $B = 3.8$ and lifting-configuration results are compared for different Mach numbers and angles of attack. It is seen that reasonable agreement is obtained with this value of B at different angles of attack and excellent agreement is obtained at different Mach numbers.

It can be shown that the coefficient B is dependent on the configuration geometry. The configuration depicted in figures 29 and 30 is composed of a flat-plate wing with the planform shown and a body of revolution with a parabolic-arc generator and a fineness ratio of 10. In figure 31 results are presented for a configuration composed of the same wing and a body with an elliptic generator and a fineness ratio of 10. The Mach number and angle of attack are $M_\infty = 0.98$ and $\alpha = 6^O$, respectively. It is seen that for this configuration the coefficient B has a value of 2.9.

———— Lift solution in wing plane

— — — Axisymmetric solution

B = 2.2   B = 3.8   B = 5.0
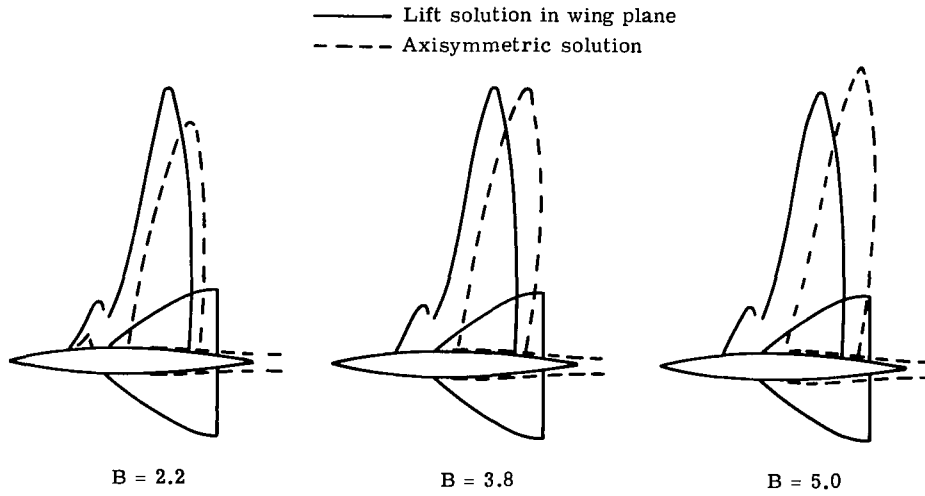
Figure 29.- Determination of coefficient B in lifting transonic area rule.
$M_\infty = 0.98$; $\alpha = 6^O$.

———— Lift solution

— — — Axisymmetric solution (B = 3.8)

$M_\infty = 0.98$; $\alpha = 6^O$ $M_\infty = 0.98$; $\alpha = 10^O$ $M_\infty = 0.99$; $\alpha = 6^O$
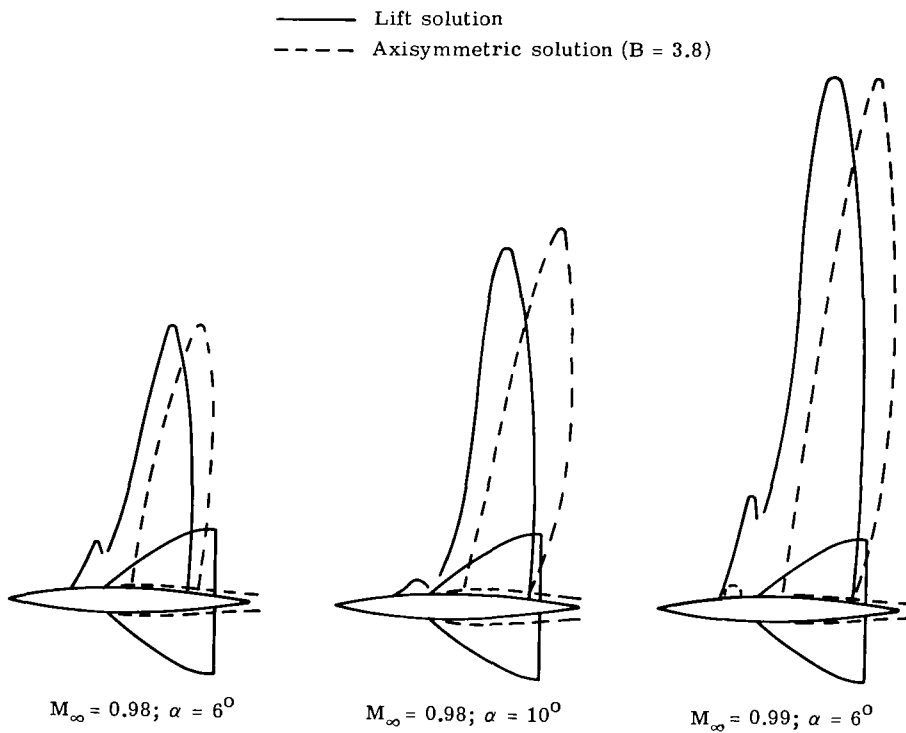
Figure 30.- Comparison of wing-plane results for lifting and equivalent axisymmetric
flow past configuration with parabolic-arc body.
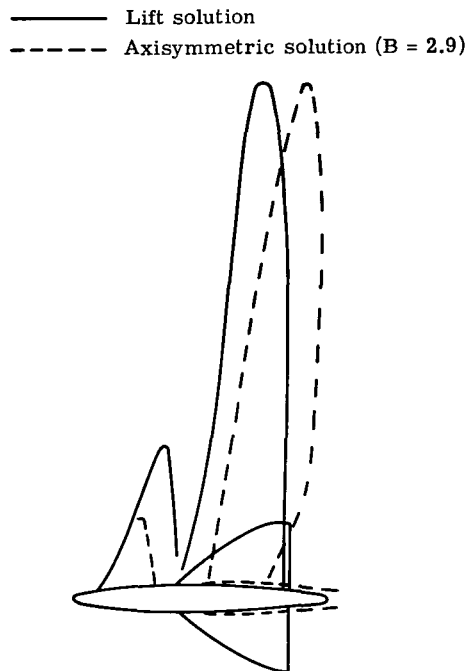
Figure 31.- Comparison of wing-plane results for lifting and equivalent axisymmetric flow past configuration with elliptic body. $M_\infty = 0.98$; $\alpha = 6^\circ$.

CONCLUDING REMARKS

An approximate method for calculating transonic flow about lifting wing-body con-figurations has been developed. The nonlinear, three-dimensional physical problem is reduced to a two-variable computational problem which is solved with the method of relaxation. The Mach number range in which the method is applicable extends from zero to low supersonic and the angle-of-attack range extends to angles of the order of the con-figuration thickness-length ratio. The method accounts for shock waves, leading-edge separation, and wind-tunnel wall effects. A modified form of the transonic area rule which accounts for the effect of lift is developed. This effect is explained from simple physical considerations.

Langley Research Center
National Aeronautics and Space Administration
Hampton, Va. 23665
November 26, 1975

APPENDIX A

CONFIGURATION GEOMETRY

The configurations which are treated in this report are composed of axisymmetric bodies and flat-plate wings. The body and wing geometry which were incorporated into the computer program (ref. 18) used to calculate the results presented in this report are discussed in this appendix.

Body Geometry

In this report the body shape $r_b(x)$ is specified by equation (2), where t is the maximum body thickness and $F_e(x)$ is the body thickness distribution. Four basic body shapes are treated. These are the ellipse with

$$F_e(x) = 2\sqrt{x - x^2}$$

a general pointed body with

$$F_e = C\left[(1 - x) - (1 - x)^n\right]$$

where the maximum radius is located at

$$x_c = 1 - \left(\frac{1}{n}\right)^{\frac{1}{n-1}} < \frac{1}{2}$$

and where

$$C = \frac{1}{\left(1 - x_c\right) - \left(1 - x_c\right)^n}$$

or

$$F_e(x) = C\left(x - x^n\right)$$

where the maximum radius occurs at

$$x_c = \left(\frac{1}{n}\right)^{\frac{1}{n-1}} > \frac{1}{2}$$

APPENDIX A

and where

$$C = \frac{1}{x_c - x_c{}^n}$$

a cone with

$$F_e(x) = x$$

and an ogive-cylinder-ogive with

$$F_e(x) = 8x(1 - 2x) \qquad\qquad (0 \leqq x \leqq 0.25)$$

$$F_e(x) = 1 \qquad\qquad (0.25 \leqq x \leqq 0.75)$$

$$F_e(x) = 8(1 - x)(2x - 1) \qquad\qquad (0.75 \leqq x \leqq 1)$$

The equations for the general pointed bodies were developed by McDevitt and Taylor (ref. 43). The basic body shapes are depicted in figure 32. As the figure indicates, a sting can be simulated at the rear.

Wing Geometry

The leading and trailing edges of the wing are specified by the function $y_2(x)$ and $y_1(x)$, respectively. In this report the trailing edge is a straight line; it may be normal to the axis or swept. Two types of leading-edge shapes are considered. Both shapes satisfy the condition $dy_2/dx = 0$ at the trailing edge so that the Kutta condition is satisfied.

The first leading-edge shape, which is depicted in figure 33, is a portion of a hyperbola. The leading edge intersects the x-axis at x_1, the wing ends at x_3, and the wing semispan is b. The foci of the hyperbola lie on the line $x = x_3$, and the asymptotes of the hyperbola have the slopes B_1 and $-B_1$ and intersect at the point $x = x_3$, $y = (1 + \Delta)b$. The equation for this leading edge is

$$y_2(x) = b\left[(1 + \Delta) - \sqrt{\Delta^2 + (1 + 2\Delta)\left(\frac{x_3 - x}{x_3 - x_1}\right)^2}\right]$$

58

Ellipse

Cone

General pointed body, maximum
radius ahead of midpoint

Ogive-cylinder-ogive

General pointed body, maximum
radius behind midpoint
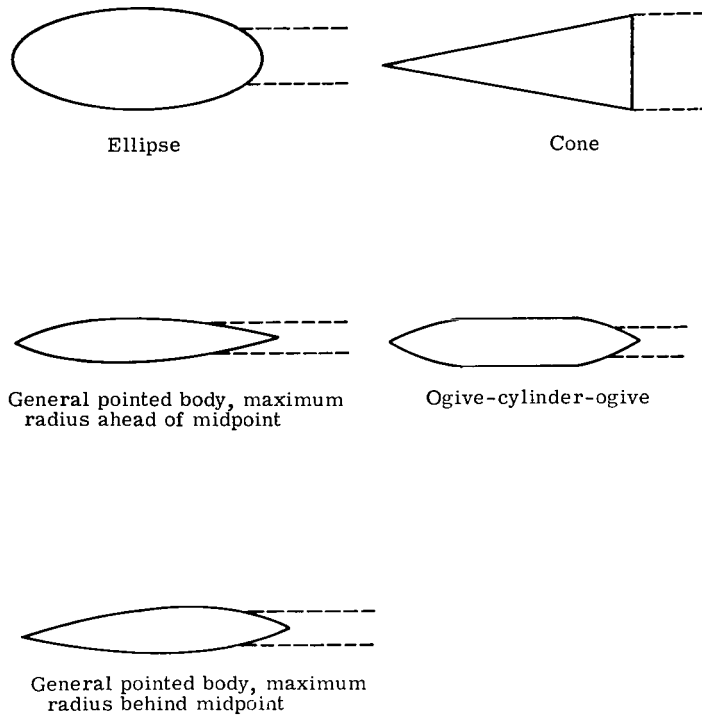
Figure 32.- Basic body shapes.
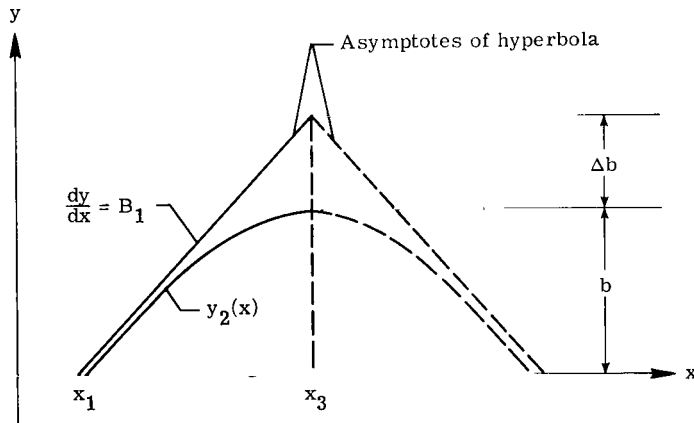
Figure 33.- First leading-edge shape.

The second leading-edge shape, which is depicted in figure 34, is constructed of two or three straight-line segments which are connected with the transition function of the
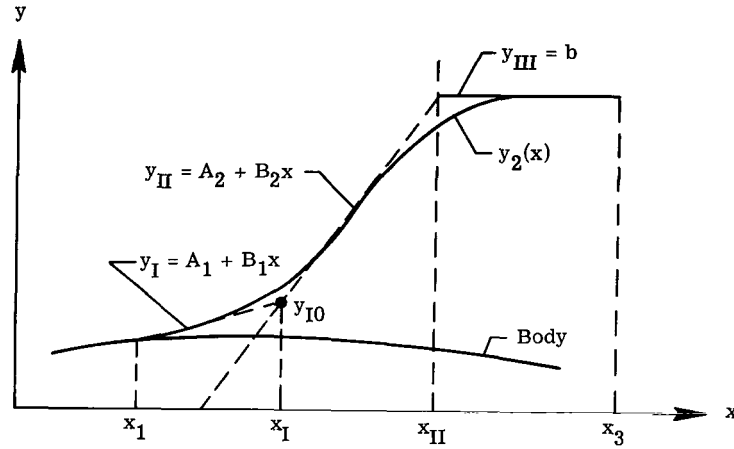
Figure 34.- Second leading-edge shape.

first kind of Grabau (ref. 44). Three straight-line segments are used if the wing has a strake; otherwise, two segments are used. As before, the wing ends at $x = x_3$. If the wing has a strake, the leading edge emerges from the body at $x = x_1$. For wings with no strake the point $x = x_1$ is where the leading edge crosses the x-axis. The line segments y_I and y_{II} intersect at the point

$$x_I = \frac{A_1 - A_2}{B_2 - B_1} \qquad\qquad y_{I0} = \frac{B_2 A_1 - B_1 A_2}{B_2 - B_1}$$

and the segments y_{II} and y_{III} intersect at the point

$$x_{II} = \frac{b - A_2}{B_2} \qquad\qquad y_{II0} = b$$

The values of y_2 at x_I and x_{II} are

$$y_2(x_I) = y_{I0}(1 + \Delta_1)$$

$$y_2(x_{II}) = b(1 - \Delta_2)$$

APPENDIX A

For a wing with a strake the equation for $y_2(x)$ is

$$y_2(x) = A_1 + B_1 x + \frac{\left(B_2 - B_1\right)\left(x - x_I\right)}{1 - \exp\left[-k_1\left(x - x_I\right)\right]} - \frac{B_2\left(x - x_{II}\right)}{1 - \exp\left[-k_2\left(x - x_{II}\right)\right]}$$

where

$$k_1 = \frac{B_2 - B_1}{y_{I0}\Delta_1}$$

$$k_2 = \frac{B_2}{b\Delta_2}$$

For a wing without a strake the equation for $y_2(x)$ is

$$y_2(x) = A_2 + B_2 x - \frac{B_2\left(x - x_{II}\right)}{1 - \exp\left[-k_2\left(x - x_{II}\right)\right]}$$

If the trailing edge is swept, the function $y_1(x)$ is

$$y_1(x) = b \frac{x - x_2}{x_3 - x_2}$$

where x_2 is the point where the trailing edge intersects the x-axis.

61

APPENDIX B

REVIEW OF ANALYTICAL SOLUTION FOR TRANSONIC FLOW
ABOUT LIFTING CONFIGURATIONS

In this appendix the analyses of references 13 and 15, on which the approximations used in this report are based, are reviewed. These analyses, which use slender-wing and slender-body theory and which are performed with the method of matched asymptotic expansions, show the general form of the solution but do not completely determine it.

It is well known that in the transonic flow regime disturbances propagate large distances outward in directions perpendicular to the free-stream velocity vector. Consequently, the characteristic length scale in the radial direction must be large except in the immediate vicinity of the configuration, where radial disturbances are scaled by the characteristic radial dimension of the configuration. The regions close to the configuration and at large distances from the configuration are generally referred to as the inner and outer regions, respectively. For the present problem the radial length scales of the disturbances in the inner and outer region are written as ℓ and ℓ/ν, respectively, where ν is a positive dimensionless parameter such that

$$\nu \ll 1 \tag{B1}$$

and where ℓ is the longitudinal length scale of the disturbances. It should be noted that the same longitudinal length scale applies in both the inner and outer regions. The value of ℓ is of the order of the configuration length, but its precise value is not known. The radial variables in the outer and inner regions are related as

$$\bar{r} = \nu r \tag{B2}$$

In the outer region the perturbation velocity potential can be expressed as

$$\varphi(x,r,\omega) = \epsilon_1 \Phi_1(x,\bar{r},\omega) + \epsilon_2 \Phi_2(x,\bar{r},\omega) + \ldots \tag{B3}$$

where the gage functions ϵ_i satisfy the inequalities

$$\epsilon_1 \ll 1$$

$$\epsilon_{i+1} \ll \epsilon_i$$

APPENDIX B

The relative magnitudes of ν, ϵ_1, and the quantity $1 - M_\infty{}^2$ can be determined from a study of the governing equation (3). In the outer region this equation can be expressed as

$$\left(1 - M_\infty{}^2\right)\frac{\partial^2 \Phi_1}{\partial x^2} + \nu^2 \overline{\nabla}_2{}^2 \Phi_1 = \epsilon_1 (\gamma + 1) \frac{\partial \Phi_1}{\partial x} \frac{\partial^2 \Phi_1}{\partial x^2} \tag{B4}$$

Since equation (B4) must reduce to the standard linear forms for subsonic and supersonic flows, the two terms on the left must be of the same order of magnitude. Since the coefficient of the derivative $\partial^2 \Phi_1/\partial x^2$ must change sign in the transonic region, the term on the right must be of the same order of magnitude as the first term on the left. It follows that ν, ϵ_1, and $1 - M_\infty{}^2$ may be related as

$$\nu^2 = \epsilon_1 = \frac{1 - M_\infty{}^2}{K} \tag{B5}$$

where K is an order-one constant. Cheng and Hafez (ref. 15) argue that the similarity laws for flow about lifting configurations must reduce to those for flow about nonlifting configurations as the angle of attack is diminished. Consequently, ν must be proportional to δ. In this report it is assumed that

$$\nu = \delta \tag{B6}$$

The relationship between the angle of attack α and the other parameters can be established only after the nature of the solution in the inner region is determined.

It is shown in reference 13 that the perturbation velocity potential in the inner region can be expressed to second order in α and δ as

$$\varphi(x,r,\omega) = \delta^2 \log_e\left(\frac{1}{\delta}\right)\varphi_{\delta,1}(x) + \delta^2 \varphi_\delta(x,r,\omega) + \sin \alpha\, \phi_1(x,r,\omega)$$

$$+ \sin^2\alpha\left[\log_e{}^2\left(\frac{1}{\delta}\right)\phi_{2,2}(x,r,\omega) + \log_e\left(\frac{1}{\delta}\right)\phi_{2,1}(x,r,\omega) + \phi_2(x,r,\omega)\right] \tag{B7}$$

The governing equations for the component potentials in this expansion are obtained following substitution of the expansion into equation (2) and collection of terms of the same magnitude. It is found that all the potentials in the expansion (eq. (B7)) except ϕ_2 satisfy the two-dimensional Laplace equation in the cross-flow plane. For example,

$$\nabla_2{}^2 \phi_1 = 0$$

APPENDIX B

The potential ϕ_2 satisfies the Poisson equation

$$\nabla_2^2 \phi_2 = (\gamma + 1)\frac{\partial \phi_1}{\partial x}\frac{\partial^2 \phi_1}{\partial x^2} + 2\left(\frac{\partial \phi_1}{\partial r}\frac{\partial^2 \phi_1}{\partial x\,\partial r} + \frac{1}{r^2}\frac{\partial \phi_1}{\partial \omega}\frac{\partial^2 \phi_1}{\partial x\,\partial \omega}\right) \tag{B8}$$

The potentials $\varphi_{\delta,1}$ and φ_δ are the slender-body thickness potentials, and ϕ_1 is the slender-wing lift potential. It is well known that $\varphi_{\delta,1}$ can be written as

$$\varphi_{\delta,1} = -F_e(x)\,F_e'(x) \tag{B9}$$

and that for large values of r, φ_δ and ϕ_1 can be written as

$$\varphi_\delta = g_\delta(x) + F_e(x)\,F_e'(x)\,\log_e r \tag{B10}$$

$$\phi_1 = f(x)\frac{\sin \omega}{r} \tag{B11}$$

where $g_\delta(x)$ is an unknown function of x, $F_e(x)$ is the nondimensional thickness distribution of the equivalent axisymmetric body for the configuration, and $f(x)$ is the axial distribution of the dipole strength for the lifting configuration. The prime denotes differentiation with respect to x. It is also well known that equation (B10) for φ_δ applies for all the way to the body surface if the body is axisymmetric, and that very near the configuration surface ϕ_1 can be written as

$$\phi_1 = m_\pm(x,y) - z \tag{B12}$$

where the plus and minus signs apply on the leeward and windward sides of the configuration, respectively. The lift potential ϕ_1 is discussed in detail in appendix C.

Now consider the second-order potentials $\phi_{2,2}$, $\phi_{2,1}$, and ϕ_2. It is shown in reference 13 that the pertinent solutions for $\phi_{2,2}$ and $\phi_{2,1}$ are

$$\left.\begin{aligned}\phi_{2,2} &= g_{2,2}(x)\\[6pt]\phi_{2,1} &= g_{2,1}(x)\end{aligned}\right\} \tag{B13}$$

where the functions $g_{2,2}$ and $g_{2,1}$ are, at this point, unknown. It can be seen from the results of reference 13 that the particular solution for ϕ_2, which is governed by equation (B8), can be written as

64

$$\phi_2{}^P = \frac{\gamma + 1}{8} \frac{\partial}{\partial x} \int dX \int dX^* \left[\phi_1{}'(x,X,X^*) \right]^2 + \frac{1}{\lambda^2} \phi_1 \phi_1{}' \qquad (B14)$$

where $X = y + iz$ is the complex variable in the cross-flow plane and the asterisk denotes the complex conjugate. From equation (6) it can be shown that ϕ_2 must satisfy homogeneous Neumann boundary conditions at the wing surface. Consequently, the complementary solution for ϕ_2 can be written as

$$\phi_2{}^C = g_2(x) - \frac{1}{4\pi} \int_{s=y_1(x)}^{s=y_2(x)} \left[\frac{\partial \phi_2{}^P}{\partial z}(x,s,+0) - \frac{\partial \phi_2{}^P}{\partial z}(x,s,-0) \right] \log_e \left[(s - X)(s - X^*) \right] ds \qquad (B15)$$

where the function $g_2(x)$ is unknown. If the trailing edge of the wing is not swept, the lower limit of integration in equation (B15) is 0. It was pointed out by Cheng and Hafez (ref. 15) that the solution $\phi_2{}^C$ for attached flow exists only if the derivative $\phi_1{}'$ is finite at the leading edge of the wing. Note that for this case it is necessary to bend the leading edge of the wing in order to enforce the condition on $\phi_1{}'$. In reference 13 it is shown that the solution obtained in reference 15 is valid to a first approximation for the case of leading-edge separation. As a result, it is possible to treat the problem of flow past flat-plate wings.

It is shown in reference 13 that the sum of equations (B14) and (B15) can be written for large values of r as

$$\phi_2 = g_2(x) + H'(x) \log_e r + \frac{\gamma + 1}{8} f'(x) f''(x) \left(2 \log_e{}^2 r + \cos 2\omega \right) + \frac{f(x) f'(x)}{4} \frac{1}{r^2} (1 - \cos 2\omega)$$

$$(B16)$$

where

$$H(x) = \frac{\gamma + 1}{16\pi} \int_{s=-y_2(x)}^{s=y_2(x)} m'(x,s) \text{ P.V.} \int_{t=-y_2(x)}^{t=y_2(x)} m'(x,t) \left(\frac{s}{t - s} + \log_e |t - s| \right) ds \, dt + \frac{1}{2\pi} \int_{s=-y_2(x)}^{s=y_2(x)} m(x,s) \, ds \qquad (B17)$$

The function $m(x,y)$ in equation (B17) is written as

$$m(x,y) = \frac{1}{2} \left[m_+(x,y) - m_-(x,y) \right] \qquad (B18)$$

and the notation P.V. designates the principal value of the integral. It should be noted that with the aid of equation (B11), equation (B8) for ϕ_2 can be written for large values of r as

APPENDIX B

$$\nabla_2^2 \phi_2 = \frac{\gamma + 1}{2} \frac{f'f''}{r^2}\left(1 - \cos 2\omega\right) + \frac{2ff'}{r^4} \tag{B19}$$

and that the particular-solution terms on the right side of equation (B16) can be obtained easily from equation (B19).

The dependence of the angle of attack α and the gage functions ϵ_2 and ϵ_3 in the outer expansion for φ on the equivalent thickness ratio δ can now be determined by inspection. By assumption, the effects of lift and thickness in the outer region are comparable. Formally, this means that the leading term in the outer expansion must depend on both lift and thickness effects. The procedure is to write the inner expansion for φ for large values of the inner radial variable r in terms of the outer radial variable $\bar{r}$ and to require that the gage function of the largest lift term in the resulting expression be equal to $\epsilon_1 = \delta^2$. The gage functions of the second and third largest terms are then equated to ϵ_2 and ϵ_3, respectively. From equations (B2), (B6), (B9), (B10), (B11), (B13), and (B16), it is seen that the inner expansion (eq. (B7)) can be written for $r \gg 1$ in terms of $\bar{r}$ as

$$\varphi = \delta^2\Big[g_\delta(x) + F_e(x) F_e'(x) \log_e \bar{r}\Big] + \delta \sin\alpha \, f(x) \frac{\sin\omega}{\bar{r}}$$

$$+ \sin^2\alpha \, \log_e^2\left(\frac{1}{\delta}\right)\left[g_{2,2}(x) + \frac{\gamma + 1}{4} f'f''\right] + \sin^2\alpha \, \log_e\left(\frac{1}{\delta}\right)\Big[g_{2,1}(x)$$

$$+ H'(x) + \frac{\gamma + 1}{2} f'f'' \log_e \bar{r}\Big] + \sin^2\alpha\Big[g_2(x) + H'(x) \log_e \bar{r}$$

$$+ \frac{\gamma + 1}{8} f'f''\left(2 \log_e^2 \bar{r} + \cos 2\omega\right)\Big] + \ldots \tag{B20}$$

In reference 13 it is shown that if equation (B6) is to be valid, the term with the gage function $\sin^2\alpha \, \log_e^2\left(\frac{1}{\delta}\right)$ must vanish identically. It can be shown that if this were not the case, the terms in the inner expansion (eq. (B7)) of third and higher order in $\sin\alpha$ when written in terms of $\bar{r}$ for $r \gg 1$ would have gage functions larger than $\epsilon_1 = \delta^2$. As a result, it follows from equation (B20) that

$$g_{2,2}(x) = -\frac{\gamma + 1}{4} f'(x) f''(x)$$

$$\sin \alpha = \frac{a\delta}{\sqrt{\log_e\left(\frac{1}{\delta}\right)}} \tag{B21}$$

where   a   is an order-one constant.   The second and third largest gage functions in equation (B20) are

$$\epsilon_2 = \delta \sin \alpha = \frac{a\delta^2}{\sqrt{\log_e\left(\frac{1}{\delta}\right)}} \tag{B22a}$$

$$\epsilon_3 = \sin^2\alpha = \frac{a^2\delta^2}{\log_e\left(\frac{1}{\delta}\right)} \tag{B22b}$$

It can be seen from equations (B4) and (B5) that the governing equation for the outer potential Φ_1 is

$$K\frac{\partial^2\Phi_1}{\partial x^2} + \overline{\nabla}_2{}^2\Phi_1 = (\gamma + 1)\frac{\partial\Phi_1}{\partial x}\frac{\partial^2\Phi_1}{\partial x^2} \tag{B23}$$

When the outer expansion (eq. (B3)) is substituted into the governing equation (3) for φ, it is found with the aid of equations (B5), (B6), and (B22) for the gage functions ϵ_1, ϵ_2, and ϵ_3 that the outer potentials Φ_2 and Φ_3 are governed by the equations

$$K\frac{\partial^2\Phi_2}{\partial x^2} + \overline{\nabla}_2{}^2\Phi_2 = (\gamma + 1)\frac{\partial}{\partial x}\left(\frac{\partial\Phi_1}{\partial x}\frac{\partial\Phi_2}{\partial x}\right) \tag{B24}$$

and

$$K\frac{\partial^2\Phi_3}{\partial x^2} + \overline{\nabla}_2{}^2\Phi_3 = (\gamma + 1)\left[\frac{\partial}{\partial x}\left(\frac{\partial\Phi_1}{\partial x}\frac{\partial\Phi_3}{\partial x}\right) + \frac{\partial\Phi_2}{\partial x}\frac{\partial^2\Phi_2}{\partial x^2}\right] \tag{B25}$$

respectively.

Equations (B23), (B24), and (B25) can be solved iteratively in the inner part of the outer region where $\bar{r} \ll 1$.   For example, equation (B23) is written as

$$\overline{\nabla}_2{}^2\Phi_1 = \left[(\gamma + 1)\frac{\partial\Phi_1}{\partial x} - K\right]\frac{\partial^2\Phi_1}{\partial x^2}$$

The complementary solution to the left side of this equation is obtained. This solution is used to evaluate the terms on the right-hand side of the equation to render it a Poisson equation. Then the particular solution is obtained. This process can be continued until the desired number of terms has been found. It should be noted that the coefficients of the complementary solutions are arbitrary functions of x. These coefficients can be evaluated by matching the outer expansion with equation (B20). The outer potentials Φ_1, Φ_2, and Φ_3 are thus found to be

$$\Phi_1 = G_1(x) + \left[F_e(x) F_e'(x) + \frac{\gamma + 1}{2} a^2 f'(x) f''(x)\right] \log_e \bar{r} + \dots \tag{B26}$$

$$\Phi_2 = f(x) \frac{\sin \omega}{\bar{r}} + \dots \tag{B27}$$

$$\Phi_3 = G_3(x) + H'(x) \log_e \bar{r} + \frac{\gamma + 1}{8} f'(x) f''(x)\left(2 \log_e^2 \bar{r} + \cos 2\omega\right) + \dots \tag{B28}$$

The functions $G_1(x)$ and $G_3(x)$ in equations (B26) and (B28), respectively, cannot be determined with this method. Note that to lowest order the effect of lift is that of a source. The doublet effect appears in the second approximation.

An expression for the effective cross-sectional area of a lifting wing-body configuration can be obtained from the results of this appendix. The source strength of the potential for large values of the radial coordinate is proportional to the lengthwise derivative of the cross-sectional area. From equations (B3), (B5), (B22), (B26), (B28), and others, it can be seen that the source strength is of the form

$$\delta^2 F_e F_e' + \sin^2\alpha \log_e\left(\frac{1}{\delta}\right)\frac{\gamma + 1}{2} f'f'' + \sin^2\alpha H'$$

Consequently, the effective cross-sectional area S_{eff}, which is 2π times the integral with respect to x of the source strength, is of the form

$$S_{eff} = \pi r_b^2(x) + \frac{\gamma + 1}{2} \pi \log_e\left(\frac{1}{\delta}\right)\left[\sin \alpha \, f'(x)\right]^2 + 2\pi \sin^2\alpha \, H(x) \tag{B29}$$

The first term on the right-hand side of equation (B29) is the actual cross-sectional area of the configuration. The transonic area rule as formulated by Whitcomb only involves this term. The second term is the dominant area-due-to-lift term which was first described in reference 12. The third term in equation (B29) is the higher order

area-due-to-lift term found by Cheng and Hafez (ref. 14). It can be seen from equation (B17) that this term is composed of two integrals, the first a double integral and the second a single integral. With equations (B12), (B18), and (D25), the second integral can be approximated as

$$\int_{s=-y_2(x)}^{s=y_2(x)} m(x,s)\,ds \approx 2\pi\,f(x) \tag{B30}$$

From the form of equation (B30) it follows that the x-derivative of the function $m(x,y)$ can be written as

$$m'(x,y) = \frac{f'(x)}{y_2(x)}\,m_p\!\left(x,\frac{y}{y_2}\right) \tag{B31}$$

where m_p is a slowly varying function of x. For conical flow m_p is independent of x. It follows from equations (B17), (B29), (B30), and (B31) that the expression for the effective cross-sectional area can be written as

$$S_{eff}(x) = \pi\left\{r_b^{\,2}(x) + \frac{\gamma+1}{2}\,B\big[\sin\alpha\,f'(x)\big]^2 + 2\sin^2\alpha\,f(x)\right\} \tag{B32}$$

where

$$B = \log_e\!\left(\frac{\ell}{t}\right) + \frac{1}{8\pi}\int_{s=-1}^{s=1} m_p(x,s)\;\text{P.V.}\int_{t=-1}^{t=1} m_p(x,t)\left(\frac{s}{t-s} + \log_e|t-s|\right)dt\,ds \tag{B33}$$

A precise value for B cannot be obtained from equation (B33) since the length scale ℓ is not known. It should be noted that the double integral is, at best, a slowly varying function of x.

APPENDIX C

LIFT POTENTIAL FOR NEAR-SONIC FLOW

The slender-wing lift potential is used in this report for near-sonic flow. This potential is governed by the equation

$$\nabla_2^2 \phi_\alpha = 0$$

and satisfies the boundary conditions

$$\left.\begin{aligned}
&\frac{\partial \phi_\alpha}{\partial r}\left(x, r_b, \theta\right) = 0 \\[2ex]
&\frac{\partial \phi_\alpha}{\partial \theta}(x, r, 0) = -\frac{\partial \phi_\alpha}{\partial \theta}(x, r, \pi) = -r \qquad \left(y_2 \geqq r \geqq y_1 \quad \text{or} \quad r_b\right)
\end{aligned}\right\} \tag{C1}$$

where x, r, and θ are body-oriented cylindrical polar coordinates. In this appendix this potential is derived for attached flow past configurations with swept leading edges and swept leading and trailing edges, and separated-leading-edge flow past configurations with swept leading edges.

Attached Flow Past Configurations With
Swept Leading Edges

A cross section of the wing-body configuration is shown in figure 35. The solution for attached flow past this configuration was obtained by Spreiter (ref. 6) and Ward (ref. 7). Let the complex variable in the cross-flow plane be

$$X = y + iz = re^{i\theta} \tag{C2}$$
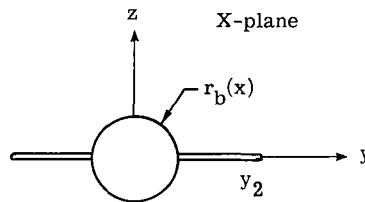
Figure 35.- Cross section of configuration composed of circular body and flat-plate wing.

APPENDIX C

The complex potential for this problem is written as

$$W(x,X) = i\left[X - Y(x,X)\right] \tag{C3}$$

where

$$Y(x,X) = \sqrt{\left(X + \frac{r_b^2}{X}\right)^2 - \left(y_2 + \frac{r_b^2}{y_2}\right)^2} \tag{C4}$$

The cross-flow perturbation velocity potential is

$$\phi_\alpha(x,r,\theta) = \text{Re}\left[W(x,X)\right]$$

$$= \pm\frac{\sqrt{2}}{2}\left\{-\left(1 + \frac{r_b^4}{r^4}\right)r^2 \cos 2\theta + y_2^2\left(1 + \frac{r_b^4}{r^4}\right)\right.$$

$$+ \left[r^4\left(1 + \frac{r_b^4}{r^4}\right)^2 + 4r_b^4 \cos^2 2\theta + y_2^4\left(1 + \frac{r_b^4}{y_2^4}\right)^2\right.$$

$$\left.\left. - 2y_2^2\left(1 + \frac{r_b^4}{y_2^4}\right)\left(1 + \frac{r_b^4}{r^4}\right)r^2 \cos 2\theta\right]^{1/2}\right\}^{1/2} - r \sin \theta \tag{C5}$$

For large values of r, equation (C3) can be written as

$$W(x,X) = iX\left\{1 - \left[1 - \frac{1}{X^2}\left(y_2^2 + \frac{r_b^4}{y_2^2}\right) + \frac{r_b^4}{X^4}\right]^{1/2}\right\}$$

$$= iX\left[\frac{1}{2}y_2^2\left(1 + \frac{r_b^4}{y_2^4}\right) - \frac{1}{8}\frac{y_2^4}{X^2}\left(1 - \frac{r_b^4}{y_2^4}\right) + \cdots\right]$$

Thus, the perturbation velocity potential for large values of r can be written as

$$\phi_\alpha(x,r,\theta) = f(x) \frac{\sin\theta}{r} \tag{C6}$$

where

$$f(x) = \frac{1}{2} y_2^2 \left(1 + \frac{r_b^4}{y_2^4}\right) \tag{C7}$$

The quantity $f(x)$ is the local dipole strength of the lifting configuration.

Attached Flow Past Configurations With

Swept Leading and Trailing Edges

The derivative $\partial\phi_\alpha/\partial x$ for this problem has been derived by Mirels (ref. 32) and Mangler (ref. 24). It should be noted that in addition to the boundary conditions given by equations (C1), the boundary condition

$$\frac{\partial\phi_\alpha}{\partial x}(x,y,0) = 0 \qquad\qquad \left(y_1(x) \geqq y \geqq r_b(x)\right) \tag{C8}$$

is also used. The solution is obtained in terms of the transformed complex variable

$$Z = X - \frac{r_b^2}{X} \tag{C9}$$

The physical and transform planes are shown in figure 36. It is shown in reference 32 that the derivative $\dfrac{\partial^2 W}{\partial x\,\partial Z}$ is written as

$$\frac{\partial^2 W}{\partial x\,\partial Z} = -i\eta_2\eta_2{}' \, S(x) \left[\frac{Z^2 - \eta_1^2}{Z^2 - \eta_2^2} - \frac{E(k)}{K(k)}\right] \frac{1}{\sqrt{Z^2 - \eta_1^2}\sqrt{Z^2 - \eta_2^2}} \tag{C10}$$

where

$$\left.\begin{array}{l} \eta_1 = y_1 - \dfrac{r_b^2}{y_1} \\[4mm] \eta_2 = y_2 - \dfrac{r_b^2}{y_2} \end{array}\right\} \tag{C11}$$

(a) Physical plane.   (b) Transform plane.
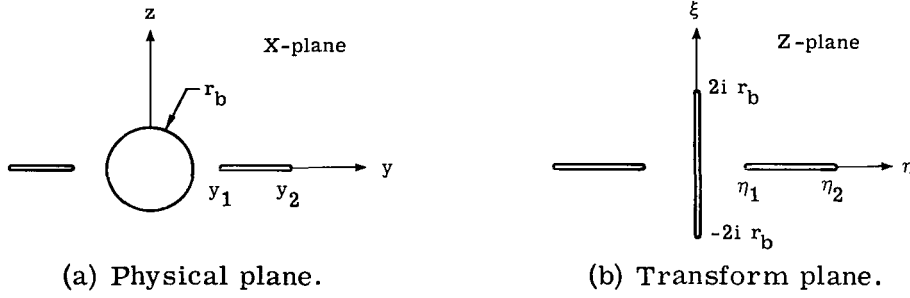
Figure 36.- Cross-flow planes for attached flow past configurations with swept leading and trailing edges.

The function $S(x)$ is the function Mirels (ref. 32) developed for enforcing the Kutta condition at the trailing edge, and K and E are complete elliptic integrals of the first and second kinds with the modulus

$$k = \sqrt{1 - \frac{\eta_1^2}{\eta_2^2}} \tag{C12}$$

It should be noted that Mirels' S-function is identical to the function H used by Mangler (ref. 24).

The complex potential W, and consequently the perturbation potential ϕ_α, can be obtained by integrating equation (C10) with respect to Z and x. However, as Mirels and Mangler point out, it is very difficult to perform these integrations and the lift can be obtained from equation (C10) comparatively easily without first obtaining ϕ_α. Consequently, ϕ_α and $\partial\phi_\alpha/\partial x$ are not determined at points near the configuration in this report.

The derivative $\partial\phi_\alpha/\partial x$ can be determined approximately in the outer part of the flow field. At large distances from the configuration equation (C10) can be written as

$$\frac{\partial^2 W}{\partial x \, \partial Z} = -i\eta_2 \eta_2' \frac{1}{Z^2} S(x) \left[1 - \frac{E(k)}{K(k)} \right]$$

Consequently, the derivative $\partial W/\partial x$ can be approximated as

$$\frac{\partial W}{\partial x} = \frac{i}{Z} \eta_2 \eta_2' S(x) \left[1 - \frac{E(k)}{K(k)} \right]$$

Therefore, for large values of r, the derivative $\partial\phi_\alpha/\partial x$ can be approximated as

$$\frac{\partial\phi_\alpha}{\partial x} = S(x)\left[1 - \frac{E(k)}{K(k)}\right]y_2 \frac{dy_2}{dx}\left(1 - \frac{r_b^4}{y_2^4}\right)\frac{\sin\theta}{r} \tag{C13}$$

In this report two approximations are made which simplify equation (C13). First, it is assumed that the derivatives y_1' and y_2' satisfy the inequality

$$y_2'(x) \ll y_1'(x) \tag{C14}$$

Mirels (ref. 32) shows that as a result of inequality (C14), the function $S(x)$ for a wing can be approximated as

$$S(x) = \frac{1}{\sqrt{1 - \frac{y_1^2}{y_2^2}}} \tag{C15}$$

The second approximation is that of Mangler (ref. 24) for the function $E(k)/K(k)$ which is written as

$$\frac{E(k)}{K(k)} = 1 - 0.85\left(1 - \sqrt{1 - k^2}\right) \tag{C16}$$

With the approximations given by equations (C15) and (C16), equation (C13) can be written as

$$\frac{\partial\phi_\alpha}{\partial x} = \frac{df}{dx}\frac{\sin\theta}{r} \tag{C17}$$

where

$$\frac{df}{dx} = 0.85y_2 \frac{dy_2}{dx}\left(1 - \frac{r_b^4}{y_2^4}\right)\sqrt{\frac{y_2 - y_1}{y_2 + y_1}} \tag{C18}$$

Separated Flow Past Configurations With Swept Leading Edges

In this report two types of flow fields with vortices are considered. The first is leading-edge separation, and the second is flow with inboard strake-generated vortexes. These flow fields are depicted in figure 37.

Cross section

Cross section

Top view

Top view

Vortex-core
locations

Vortex-core
locations

(a) Leading-edge separation.   (b) Strake-generated vortex.
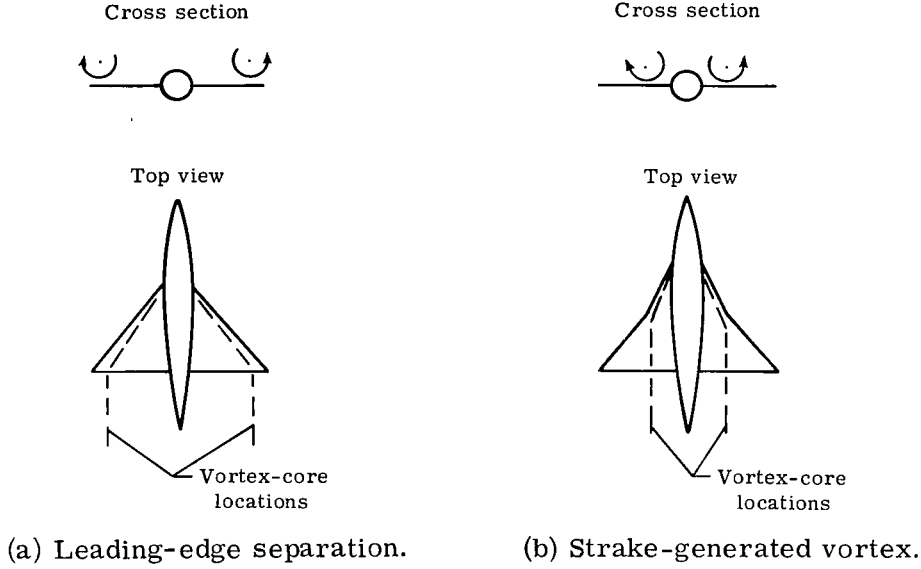
Figure 37.- Flow fields with vortexes.

The problem of leading-edge separation was first treated successfully by Brown and Michael (ref. 20) for the case of flow past a delta wing. Although several other more complicated leading-edge-separation models have been developed and could have been used, the model of reference 20 is employed here because of its simplicity.

The complex potential for the Brown and Michael model for separated-leading-edge flow past a flat-plate-wing, axisymmetric-body configuration is

$$W(x,X) = i \left\{ X - Y(x,X) - \gamma_v(x) \log_e \left[\frac{Y(x,X) - Y_v(x)}{Y(x,X) + Y_v^*(x)} \right] \right\} \tag{C19}$$

where X and Y are given by equations (C2) and (C4), respectively, and where

$$Y_v(x) = \left[y_2(x) + \frac{r_b^2(x)}{y_2(x)} \right] \left[\lambda_v(x) + i \tau_v(x) \right] \tag{C20}$$

is the vortex location in the Y-plane. The potential in equation (C19) satisfies the boundary conditions given by equations (C1). Brown and Michael show that in addition, a Kutta condition must be satisfied at the leading edge and the force on the system composed of the vortex core and vorticity feeding sheet, which extends from the leading edge to the core, must be zero. These conditions are expressed as

$$\frac{dW}{dX}\left(x, y_2(x)\right) = 0 \qquad (C21)$$

and

$$\frac{d\gamma_v}{dx}\left(X_v - y_2\right) = \gamma_v(x)\left[\underset{X \to X_v}{\text{Limit}}\left(\frac{dW^*}{dX^*} + \frac{\gamma_v}{i}\frac{1}{X^* - X_v^*}\right) - \frac{dX_v}{dx}\right] \qquad (C22)$$

respectively. For the problem of flow with a strake-generated vortex, the Kutta condition, equation (C21), is not enforced and the vortex strength becomes constant so that the left side of equation (C22) vanishes. The solution procedure is given in appendix G.

The problem of separated flow past a delta wing can be used to gage the effect of the vortex in the outer part of the flow. It is shown in reference 20 that to lowest order in $\sin \alpha$ the location of the vortex in the X-plane is

$$\left. \begin{aligned} y_v &= y_2\left[1 - \frac{1}{2}\left(\frac{z_v}{y_2}\right)^{2/3}\right] \\[2mm] z_v &= \frac{1}{4} x \sin \alpha \end{aligned} \right\} \qquad (C23)$$

It follows that in the outer part of the flow where

$$\left| X \right| \gg y_2$$

the perturbation velocity potential ϕ_α is

$$\phi_\alpha = \frac{1}{2} y_2^2 \frac{\sin \alpha}{r}\left[1 + 2\left(\frac{z_v}{y_2}\right)^{2/3}\right] \qquad (C24)$$

Consequently, for small angles of attack the second term in equation (C24), which is due to the vortex, could be ignored in the outer part of the flow. However, this term is not ignored in this report because its inclusion presents no particular difficulty.

The influence of the vortex on the flow far from a general configuration can be determined from equation (C19). For large values of r and hence large magnitudes of Y, the logarithm in equation (C19) can be approximated as

$$\log_e\left[\frac{Y(x,X) - Y_v(x)}{Y(x,X) + Y_v^*(x)}\right] \approx -\frac{Y_v(x) + Y_v^*(x)}{Y(x,X)} \approx -\frac{2\lambda_v(x)}{r}\left[y_2(x) + \frac{r_b^2(x)}{y_2(x)}\right]e^{-i\theta}$$

Consequently, the potential ϕ_α at large distances from the configuration is given by equation (C6) where

$$f(x) = \frac{1}{2}y_2^2(x)\left(1 + \frac{r_b^4}{y_2^4}\right) + 2\lambda_v\gamma_v\left(y_2 + \frac{r_b^2}{y_2}\right) \tag{C25}$$

If the flow is separated at the wing leading edge, the boundary condition given by equation (C21) applies. It can be shown that this boundary condition can be written in the form

$$\gamma_v = \frac{1}{2\lambda_v}\left(\lambda_v^2 + \tau_v^2\right)\left(y_2 + \frac{r_b^2}{y_2}\right) \tag{C26}$$

If the flow is not separated at the wing leading edge but a strake-generated vortex is present, γ_v does not vary with x aft of the strake and has the value given by equation (C26) at the time that leading-edge separation ceased.

In order to account for nonlinear behavior at points where $r < y_2(x)$, it is necessary to account for the effect of the derivative $\partial\phi_\alpha/\partial x$ on the coefficient of the $\partial^2\varphi_0/\partial x^2$ term in equation (55). In this report the value u_α of this derivative which applies in the region near the axis is used to approximate the values at all points inside the wing tip. From equation (C19) it can be shown that if $r_b \ll y_2$, the potential ϕ_α near the axis is, approximately,

$$\phi_\alpha \approx \pm y_2(x) + \gamma_v(x)\left[\tan^{-1}\left(\frac{\lambda_v}{\pm 1 - \tau_v}\right) - \tan^{-1}\left(\frac{-\lambda_v}{\pm 1 - \tau_v}\right)\right]$$

Consequently, the derivative $u_\alpha = \dfrac{\partial\phi_\alpha}{\partial x}$ in the region near the axis is

$$u_\alpha = \pm y_2'(x) + \left[\tan^{-1}\left(\frac{\lambda_v}{\pm 1 - \tau_v}\right) - \tan^{-1}\left(\frac{-\lambda_v}{\pm 1 - \tau_v}\right)\right]\gamma_v'$$

$$+ \frac{2\gamma_v\left(\pm 1 - \tau_v\right)\lambda_v'}{\left(\pm 1 - \tau_v\right)^2 + \lambda_v^2} + \frac{2\gamma_v\lambda_v\tau_v'}{\left(\pm 1 - \tau_v\right)^2 + \lambda_v^2} \tag{C27}$$

77

The function $Y_v(x)$ given in equation (C20) is related to the vortex core location $X_v = y_v + iz_v$ by the equation

$$Y_v(x) = \sqrt{X_v^2 - y_2^2} \tag{C28}$$

It can be shown from equations (C20) and (C28) that for $r_b \ll y_2$, the equations for λ_v and τ_v are

$$\lambda_v^2 = \frac{1}{2}\left\{\sqrt{\left[1 - \left(\frac{y_v}{y_2}\right)^2 + \left(\frac{z_v}{y_2}\right)^2\right]^2 + 4\left(\frac{y_v}{y_2}\right)^2\left(\frac{z_v}{y_2}\right)^2} - \left[1 - \left(\frac{y_v}{y_2}\right)^2 + \left(\frac{z_v}{y_2}\right)^2\right]\right\} \tag{C29a}$$

$$\tau_v^2 = \frac{1}{2}\left\{\sqrt{\left[1 - \left(\frac{y_v}{y_2}\right)^2 + \left(\frac{z_v}{y_2}\right)^2\right]^2 + 4\left(\frac{y_v}{y_2}\right)^2\left(\frac{z_v}{y_2}\right)^2} + \left[1 - \left(\frac{y_v}{y_2}\right)^2 + \left(\frac{z_v}{y_2}\right)^2\right]\right\} \tag{C29b}$$

If $1 - y_v/y_2 \ll 1$ and $z_v/y_2 \ll 1$, as is the case for separated-leading-edge flow past a wing at a small angle of attack, it follows from equations (C29) that

$$\left.\begin{array}{c} \lambda_v \ll 1 \\ \\ \tau_v \ll 1 \end{array}\right\} \tag{C30}$$

With the first of equations (C23) it can be shown that for the particular case of separated flow past a delta wing, equations (C29) can be written as

$$\lambda_v = \left(\frac{z_v}{y_2}\right)^{2/3} \ll 1$$

$$\tau_v = \left(\frac{z_v}{y_2}\right)^{1/3} \ll 1$$

If $1 - y_v/y_2 = O(1)$ and $z_v/y_2 \ll 1$, as is the case for a strake-generated vortex over the wing, the values of λ_v and τ_v are of the form

APPENDIX C

$$\lambda_v = \left(\frac{y_v}{y_2}\right)^2 \left(\frac{z_v}{y_2}\right)^2 \left[1 - \left(\frac{y_v}{y_2}\right)^2\right]^{-1/2} \ll 1 \qquad (C31a)$$

$$\tau_v = \sqrt{1 - \left(\frac{y_v}{y_2}\right)^2} \left\{1 + \left(\frac{z_v}{y_2}\right)^2 \left[1 - \left(\frac{y_v}{y_2}\right)^2\right]^{-2}\right\} = O(1) \qquad (C31b)$$

With equation (C26) and inequalities (C30) it can be shown that if the flow at the leading edge is separated, equation (C27) can be approximated as

$$u_\alpha = \pm\left[y_2' + \frac{2(\gamma_v \lambda_v)'}{1 \mp \tau_v}\right] \qquad (C32)$$

With equations (C31) it can be shown that if there is a strake-generated vortex over the wing, equation (C27) can be approximated as

$$u_\alpha = \pm\left[y_2' + \frac{2\gamma_v(1 \mp \tau_v)\lambda_v'}{(1 \mp \tau_v)^2 + \lambda_v^2}\right] + \frac{2\gamma_v \lambda_v \tau_v'}{(1 \mp \tau_v)^2 + \lambda_v^2} \qquad (C33)$$

In order to satisfy the Kutta condition to lowest order, it is necessary to correct for the influence of the vortex on the flow at the trailing edge. For all the slender-wing solutions used in this report, the attached-flow portion of the trailing-edge Kutta condition is satisfied by the condition that y_2' vanish at the trailing edge. Consequently, it follows from equation (C32) that if the flow at the leading edge is separated, the influence of the vortex on the flow on the inboard portion of the wing is

$$\Delta\phi_\alpha' = \pm\frac{2}{1 \mp \tau_v}(\gamma_v \lambda_v)' \qquad (C34)$$

It can be seen from equation (C33) that if there is a strake-generated vortex over the wing, the influence of the vortex on the flow on the inboard portion of the wing is

$$\Delta\phi_{\alpha}' = \frac{2\gamma_{\mathrm{v}}}{\left(1 \mp \tau_{\mathrm{v}}\right)^2 + \lambda_{\mathrm{v}}^2}\left[\left(\pm 1 - \tau_{\mathrm{v}}\right)\lambda_{\mathrm{v}}' + \lambda_{\mathrm{v}}\tau_{\mathrm{v}}'\right]$$

This equation can be simplified as

$$\Delta\phi_{\alpha,\mathrm{u}}' = 2\gamma_{\mathrm{v}}\frac{\left(1 - \tau_{\mathrm{v}}\right)\lambda_{\mathrm{v}}' + \lambda_{\mathrm{v}}\tau_{\mathrm{v}}'}{\left(1 - \tau_{\mathrm{v}}\right)^2 + \lambda_{\mathrm{v}}^2} \qquad (C35a)$$

$$\Delta\phi_{\alpha,\ell}' = -\frac{2\gamma_{\mathrm{v}}}{1 + \tau_{\mathrm{v}}}\left(\lambda_{\mathrm{v}}' - \frac{\lambda_{\mathrm{v}}}{1 + \tau_{\mathrm{v}}}\tau_{\mathrm{v}}'\right) \qquad (C35b)$$

APPENDIX D

LIFT POTENTIAL FOR SUBSONIC AND SUPERSONIC FLOW

In this report approximate methods are used to determine the lift potential ϕ_α for subsonic and supersonic flow. These methods are described in this appendix. In addition, a generalization of the Brown and Michael model to subsonic and supersonic flow is given.

Solution for Subsonic Flow

The approximate theory of Lawrence and Flax (ref. 21) for subsonic flow past wing bodies is used in this report. This theory is a generalization of the theory of Lawrence (ref. 25) for wings alone. The theory of references 21 and 25 is restricted to wings with unswept trailing edges.

The transformation given in equation (C9) is used to relate the flow past a wing body to that past a wing alone. These flow fields are depicted in figure 38. The quantity η_2 is related to y_2 and r_b by the second of equations (C11).

(a) Wing-body plane.   (b) Wing plane.
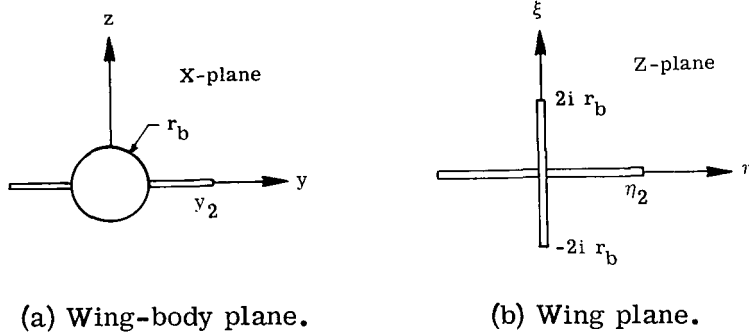
Figure 38.- Wing-body and wing cross-flow planes.

Lawrence employs the equation

$$\overline{w}(x,\eta) = -\frac{1}{2\pi}\frac{\partial}{\partial\eta}\int_{s=x_0}^{s=x_t}\int_{t=-\eta_2(s)}^{t=\eta_2(s)} ds\, dt\, \frac{\overline{u}_u(s,t)}{\eta - t}\left[1 + \frac{\sqrt{(s-x)^2 + \left(1 - M_\infty^2\right)(\eta - t)^2}}{x - s}\right] \quad (D1)$$

to determine the downwash on a wing. The foremost points on the wing and trailing edge of the wing are at x_0 and x_t, respectively, and $\overline{u}_u$ is the x component of perturbation velocity on the upper surface. Equation (D1) is an exact integral solution to

equation (9) which was developed by Reissner (ref. 45). Lawrence evaluates this equation by using the crucial approximation

$$\sqrt{(x-s)^2 + \left(1-M_\infty^2\right)(y-t)^2} \approx \frac{1}{2}\left[|x-s| + \sqrt{(x-s)^2 + \left(1-M_\infty^2\right)\eta_2^2(x)}\right] \tag{D2}$$

As noted in reference 25, this approximation was chosen because equation (D1) reduces to the limits of slender-wing theory and two-dimensional theory when η_2 approaches zero and infinity, respectively, when the approximation is used. The boundary condition on the wing is

$$\overline{w}(x,y) = -\alpha \tag{D3}$$

With equations (D2) and (D3), equation (D1) can be written as

$$\alpha = \frac{1}{2\pi} \int_{s=x_0}^{s=x_t} \left[1 + \frac{|x-s| + \sqrt{(x-s)^2 + \left(1-M_\infty^2\right)\eta_2^2(x)}}{2(x-s)}\right] \frac{\partial}{\partial\eta} \int_{t=-\eta_2(s)}^{t=\eta_2(s)} \frac{\overline{u}_u(s,t)}{\eta-t} \, dt \, ds \tag{D4}$$

Equation (D4) is used in the integral form

$$\alpha \int_{\eta=-\eta_2(x)}^{\eta=\eta_2(x)} \sqrt{\eta_2^2(x) - \eta^2} \, d\eta = \frac{1}{2\pi} \int_{s=x_0}^{s=x_t} \left[1 + \frac{|x-s| + \sqrt{(x-s)^2 + \left(1-M_\infty^2\right)\eta_2^2(x)}}{2(x-s)}\right]$$

$$\times \int_{\eta=-\eta_2(x)}^{\eta=\eta_2(x)} \sqrt{\eta_2^2(x) - \eta^2} \, d\eta \, \frac{\partial}{\partial\eta} \int_{t=-\eta_2(s)}^{t=\eta_2(s)} \frac{\overline{u}_u(s,t)}{\eta-t} \, dt \, ds \tag{D5}$$

It is shown by Lamb (ref. 46) that any two potentials ψ_1 and ψ_2 which satisfy the two-dimensional Laplace equation

$$\nabla_2^2 \psi_1 = 0$$

$$\nabla_2^2 \psi_2 = 0$$

also satisfy the integral equation

$$\oint_S \psi_2 \frac{\partial\psi_1}{\partial n} \, dS = \oint_S \psi_1 \frac{\partial\psi_2}{\partial n} \, dS \tag{D6}$$

where S is a closed path in the plane and n is the coordinate normal to the curve S. For this problem the path S is chosen along the surface of the wing so that the normal coordinate is simply ξ. Let the potential ψ_2 on the surface and its normal derivative be

$$\left.\begin{array}{l} \psi_2(x,\eta) = \pm\sqrt{\eta_2{}^2(x) - \eta^2} \\[2em] \dfrac{\partial\psi_2}{\partial\xi}(x,\eta) = -1 \end{array}\right\} \tag{D7}$$

It can be shown with slender-wing theory that ψ_1 and its normal derivative can be related as

$$\frac{\partial\psi_1}{\partial\xi}(x,\eta) = -\frac{1}{\pi}\frac{\partial}{\partial\eta}\int_{t=-\eta_2(x)}^{t=\eta_2(x)} \frac{\psi_1(x,t)}{\eta - t}\,d\eta \tag{D8}$$

For this problem let

$$\psi_1(x,\eta) = \bar{u}(x,\eta) \tag{D9}$$

With the choices given in equations (D7) and (D9) for ψ_2 and ψ_1, respectively, and with the relation given by equation (D8), it can be shown that integral equation (D6) for this problem can be written as

$$\int_{\eta=-\eta_2(x)}^{\eta=\eta_2(x)} \sqrt{\eta_2{}^2(x) - \eta^2}\,d\eta\,\frac{\partial}{\partial\eta}\int_{t=-\eta_2(s)}^{t=\eta_2(s)} \frac{\bar{u}_u(s,t)}{\eta - t}\,dt\,ds = \pi\int_{\eta=-\eta_2(x)}^{\eta=\eta_2(x)} \bar{u}_u(s,\eta)\,d\eta$$

$$= \pi \sin\alpha\,\frac{\partial}{\partial s}\int_{\eta=-\eta_2(x)}^{\eta=\eta_2(x)} \phi_u(s,\eta)\,d\eta \tag{D10}$$

where ϕ_u is the upper-surface value of a lift potential which, in general, is related to the potential $\phi_{\alpha,u}$ by the equation

$$\phi_u = \phi_{\alpha,u} - \frac{r_b{}^2}{r}\sin\omega \tag{D11}$$

APPENDIX D

Let the functions $\bar{k}(x)$ and $g(x)$ be defined as

$$\bar{k}(x) = \int_{\eta=-\eta_2(x)}^{\eta=\eta_2(x)} \sqrt{\eta_2^2(x) - \eta^2} \, d\eta = \frac{\pi}{2} \eta_2^2(x) \tag{D12}$$

$$g(x) = \int_{\eta=-\eta_2(x)}^{\eta=\eta_2(x)} \phi_u(x,\eta) \, d\eta = \frac{1}{2} \int_{\eta=-\eta_2(x)}^{\eta=\eta_2(x)} \left[\phi_u(x,\eta) - \phi_\ell(x,\eta) \right] d\eta \tag{D13}$$

With equations (D10), (D12), and (D13), equation (D5) can be written as

$$\bar{k}(x) = \frac{1}{4} \left[2g(x) + g(x_1) + \int_{s=x_0}^{s=x_t} \frac{\sqrt{(x - s)^2 + \left(1 - M_\infty^2\right) \eta_2^2(x)}}{x - s} g'(s) \, ds \right] \tag{D14}$$

Let the variables σ and τ and the function $\bar{\beta}(\sigma)$ be defined by the equations

$$\left. \begin{array}{l} x = \frac{1}{2}\left[x_t + x_0 + \left(x_t - x_0\right) \cos \sigma\right] \\[12pt] s = \frac{1}{2}\left[x_t + x_0 + \left(x_t - x_0\right) \cos \tau\right] \end{array} \right\} \tag{D15}$$

and

$$\bar{\beta}(\sigma) = \frac{2}{x_t - x_0} \sqrt{1 - M_\infty^2} \, \eta_2(\sigma) \tag{D16}$$

With equations (D15) and (D16), equation (D14) can be written as

$$4\bar{k}(\sigma) = 2g(\sigma) + g(\sigma) + \bar{\beta}(\sigma) \int_{\tau=0}^{\tau=\pi} \frac{g'(\tau) \, d\tau}{\cos \tau - \cos \sigma} + \int_{\tau=0}^{\tau=\pi} \bar{H}(\sigma,\tau) \, g'(\tau) \, d\tau \tag{D17}$$

where

$$\bar{H}(\sigma,\tau) = \frac{\sqrt{(\cos \tau - \cos \sigma)^2 + \bar{\beta}^2(\sigma)} - \bar{\beta}(\sigma)}{\cos \tau - \cos \sigma} \tag{D18}$$

84

Equation (D17) is an integral equation for the function $g(\sigma)$. This equation is solved numerically by colocation. The procedure used is that outlined in reference 25. The form assumed for $g(\sigma)$ is

$$g(\sigma) = (\pi - \sigma)\overline{A}_1 + \sum_{r=1}^{N-1} \left(\overline{A}_{r-1} - \overline{A}_{r+1}\right) \frac{\sin\,(r\sigma)}{r} \tag{D19}$$

where

$$\overline{A}_0 = \overline{A}_{N-1} = \overline{A}_N = 0$$

It will be shown that as a result of the form of equation (D19), the trailing-edge Kutta condition is satisfied to lowest order.

The function $g(x)$ is related to the load on the configuration between the apex and the station x. The linear lift is given by equation (66). With equation (D11) it can be shown that the contour integral in equation (66) can be written as

$$\oint_C \phi_\alpha(x,y,z)\,dy = \oint_C \phi(x,y,z)\,dy - 2\pi r_b^2(x) \tag{D20}$$

Let the contour C lie along the body and wing surface. It is shown in reference 21 that the integral along the body surface is related to that along the wing as

$$\int_{\omega=0}^{\omega=2\pi} \phi\left(x,r_b,\omega\right)\,dy = 2\int_{y=r_b(x)}^{y=y_2(x)} \left[\phi_u(x,y) - \phi_\ell(x,y)\right] \frac{r_b^2(x)}{y^2}\,dy$$

Consequently, the contour integral on the right side of equation (D20) can be written as

$$\oint_C \phi(x,y,z)\,dy = 2\int_{y=r_b(x)}^{y=y_2(x)} \left[\phi_u(x,y) - \phi_\ell(x,y)\right] \left[1 + \frac{r_b^2(x)}{y^2}\right]\,dy = 2g(x) \tag{D21}$$

Thus from equations (66), (D20), and (D21), it is seen that the linear lift $L_1(x)$ is related to $g(x)$ as

$$L_1(x) = \cos\alpha\,\sin\alpha\left[2g(x) + \pi r_b^2(x)\right] \tag{D22}$$

With equations (11), (12), and (66), a similar relationship between $L_1(x)$ and the function $f(x)$ can be established. This relationship is

$$L_1(x) = \pi \cos \alpha \sin \alpha \left[2f(x) - r_b{}^2(x) \right] \tag{D23}$$

From equations (D22) and (D23) it follows that $f(x)$ and $g(x)$ are related as

$$g(x) = \pi \left[f(x) - r_b{}^2(x) \right] \tag{D24}$$

and from equations (D11), (D13), and (D24), it follows that $f(x)$ is related to the integral of wing surface potentials $\phi_{\alpha,u}$ and $\phi_{\alpha,\ell}$ as

$$f(x) = \frac{1}{\pi} \int_{\eta=0}^{\eta=\eta_2(x)} \left[\phi_{\alpha,u}(x,\eta) - \phi_{\alpha,\ell}(x,\eta) \right] d\eta + r_b{}^2(x) \tag{D25}$$

The method of Lawrence does not provide a means for determining the pressure at isolated points. In this report approximate values for the pressure are obtained by using the assumption that the spanwise pressure distribution is functionally the same as that obtained with slender-wing theory. The linear lift on the configuration can be written as

$$L_1(x) = \cos \alpha \left\{ 2 \int_{s=x_0}^{s=x} \int_{\eta=-\eta_2(s)}^{\eta=\eta_2(s)} \left[C_{p,\ell}(s,\eta) - C_{p,u}(s,\eta) \right] ds \, d\eta + \pi \sin \alpha \, r_b{}^2(x) \right\} \tag{D26}$$

A comparison of equations (D22) and (D26) shows that

$$g(x) = \frac{2}{\sin \alpha} \int_{s=x_0}^{s=x} \int_{\eta=-\eta_2(s)}^{\eta=\eta_2(s)} C_{p,\ell}(s,\eta) \, ds \, d\eta \tag{D27}$$

The spanwise integral of the pressure coefficient is obtained from equation (D27) as

$$\int_{\eta=-\eta_2(x)}^{\eta=\eta_2(x)} C_{p,\ell}(x,\eta) \, d\eta = \frac{1}{2} \sin \alpha \, \frac{dg}{dx} \tag{D28}$$

The pressure coefficient $C_{p,\ell}$ on the wing alone is expressed in a form proportional to that of slender-wing theory as

$$C_{p,\ell}(x,\eta) = \frac{R_0 \sin \alpha}{\sqrt{\eta_2{}^2(x) - \eta^2}} \tag{D29}$$

APPENDIX D

where R_0 is to be determined. When equation (D29) is substituted into equation (D28), the expression for R_0 is found to be

$$R_0 = \frac{1}{2\pi} \frac{dg}{dx} \tag{D30}$$

The pressure coefficients on the upper and lower surfaces of the wing of the wing-body configuration are approximated as

$$C_{p,\ell}(x,y) = -C_{p,u}(x,y) = \frac{dg/dx}{2\pi\sqrt{\left(y_2 - \frac{r_b^2}{y_2}\right)^2 - \left(y - \frac{r_b^2}{y}\right)^2}} \tag{D31}$$

The expression for the derivative dg/dx can be obtained from equation (D19) and the first of equations (D15) as

$$\frac{dg}{dx} = \frac{4}{x_t - x_0} \sum_{r=1}^{N-2} A_r \sin(r\sigma)$$

It can be seen that dg/dx vanishes at the trailing edge where $\sigma = 0$. Thus, the approximate expression for the wing-surface pressure coefficient given in equation (D31) vanishes at the trailing edge so that the Kutta condition is satisfied.

Solution for Supersonic Flow

The quasiconical theory of Carafoli et al. (ref. 22) is used to evaluate the linear lift potential for supersonic flow. As in the subsonic case, the wing body is mapped to a wing alone with the transformation given in equation (C9). This mapping is depicted in figure 38.

The form which is assumed for the potential ϕ_α is given by equation (26). The form of the constant A used by Carafoli et al. is

$$A = \sqrt{\frac{b_1 + b_2}{b_1} \frac{\eta_2'(x_1)}{\eta_2'(x_1) + \eta_2'(x_2)}} E(k) \tag{D32}$$

87

where the distances b_1 and b_2 and the positions x_1 and x_2 are depicted in figure 39 and where $E(k)$ is the complete elliptic integral of the second kind with the modulus

$$k = \sqrt{1 - \frac{1}{4}\left(M_\infty^2 - 1\right)\left[\eta_2'\left(x_1\right) + \eta_2'\left(x_2\right)\right]^2}$$

(a) Geometry of Carafoli et al.   (b) Present geometry.
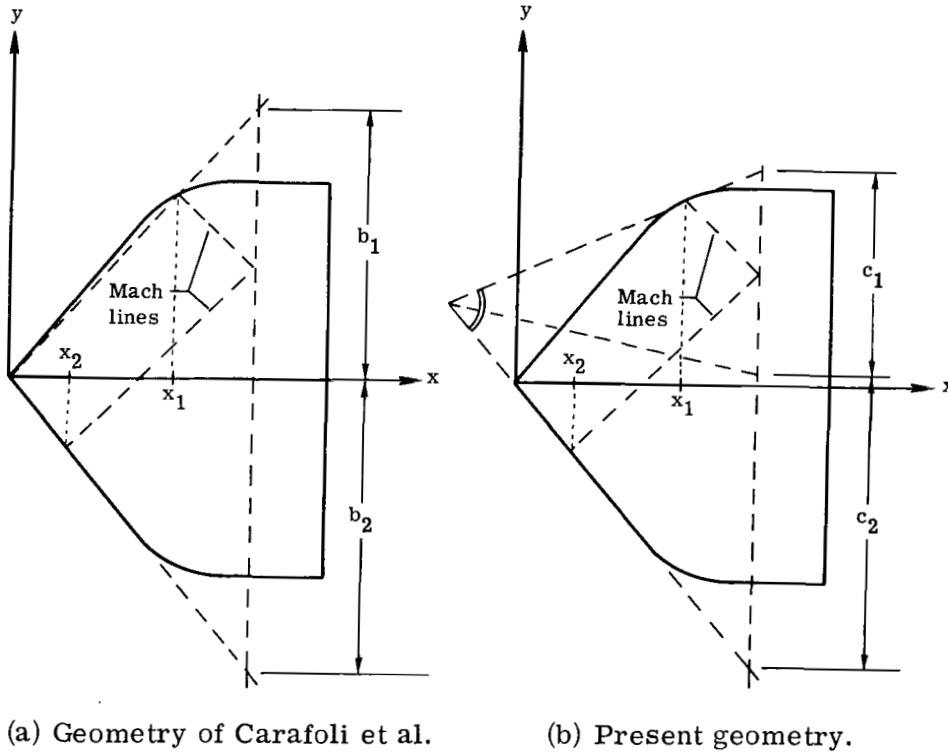
Figure 39.- Wing parameters for supersonic solution for ϕ_α.

It can be seen that the value of A given by equation (D32) becomes small as $\eta_2'\left(x_1\right)$ becomes small so that the potential ϕ_α becomes large. In order to avoid this difficulty, a form for A given by the equation

$$A = \sqrt{\frac{c_1 + c_2}{2c_1}}\, E(k)$$

where

$$k = \sqrt{1 - \frac{1}{4}\left(M_\infty^2 - 1\right)\left[y_2'\left(x_1\right) + y_2'\left(x_2\right)\right]^2}$$

is used in this report. The distances c_1 and c_2 are depicted in figure 39. It can be seen from the equation for k that a real value for k exists if the wing leading edge is sonic or subsonic. Consequently, the present method is limited to flow about configurations with sonic or subsonic leading edges as determined by simple sweep theory.

Brown and Michael Model for Subsonic and Supersonic Flow

The leading-edge separation models of both Brown and Michael (ref. 20) and Smith (ref. 39) are for lift potentials governed by equation (8), the Laplace equation in the cross-flow plane. In this section the Brown and Michael model is generalized for lift potentials governed by equation (9) for subsonic and supersonic flow. It should be noted that Sacks, Lundberg, and Hanson (ref. 47) have generalized both the Brown and Michael model and the Smith model for subsonic flow.

The potential ϕ_α is written as

$$\phi_\alpha = \phi_a + \Phi_v \tag{D33}$$

where ϕ_a and Φ_v are the attached flow and the vortex potentials. It is assumed that these potentials are governed by the equations

$$\left(1 - M_\infty^2\right)\frac{\partial^2 \phi_a}{\partial x^2} + \nabla_2^2 \phi_a = 0 \tag{D34}$$

and

$$\nabla_2^2 \Phi_v = 0 \tag{D35}$$

The form of equation (D35) is based on the fact that the cross-flow derivatives of Φ_v are dominant. The complex potential which satisfies equation (D35) is

$$W_v = -i\gamma_v(x) \log_e \left[\frac{Y(x,X) - Y_v(x)}{Y(x,X) + Y_v^*(x)} \right] \tag{D36}$$

where X, Y, and Y_v are given by equations (C2), (C4), and (C20), respectively, and where $\gamma_v(x)$ is the strength of the vortex core.

The complex velocity associated with the attached-flow portion of the linear lift potential is

$$V_a = \frac{\partial \phi_a}{\partial y} - i\frac{\partial \phi_a}{\partial z} \tag{D37}$$

The boundary conditions which are used to determine the strength and location of the vortex core for a separated-leading-edge flow are the leading-edge Kutta condition and the no-force condition on the system composed of the vortex core and the vorticity feeding sheet. These conditions are expressed as

$$\left(V_a + \frac{dW_v}{dX}\right)_{X=y_2} = 0 \tag{D38}$$

and

$$\frac{d\gamma_v}{dx}\left(X_v - y_2\right) = \gamma_v(x)\left[\lim_{X\to X_v}\left(V_a^* + \frac{dW_v^*}{dX^*} + \frac{\gamma_v}{i}\frac{1}{X^* - X_v^*}\right) - \frac{dX_v}{dx}\right] \tag{D39}$$

For the problem of a strake-generated vortex, equation (D38) is not enforced.

The same general procedure is used to evaluate the derivatives $\partial \phi_a / \partial y$ and $\partial \phi_a / \partial z$ for subsonic and supersonic flow. It is assumed that the variation of ϕ_a in the cross-flow plane is the same as that of slender-wing theory. Consequently, the potential ϕ_a is written as

$$\phi_a = R_1 \, \text{Re}\left\{i\left[\overline{X} - Y(x,X)\right]\right\} \tag{D40}$$

where X and Y are given by equations (C2) and (C4), respectively, and where R_1 is a function to be determined. With equations (D24), (D25), and (D40), it can be shown that R_1 has the value

$$R_1(x) = \frac{2g(x)}{\pi \eta_2^2(x)} \tag{D41}$$

Thus, for subsonic and supersonic flow the complex velocity V_a is

$$V_a = i\,\frac{2g(x)}{\pi \eta_2^2(x)}\left[1 - \frac{\partial Y}{\partial X}(x,X)\right]$$

The solution procedure used to find the vortex core strength and location is given in appendix G.

90

APPENDIX E

APPROXIMATE FORM OF FAR-FIELD LIFT POTENTIAL
FOR SUPERSONIC FLOW

Heaslet and Lomax (ref. 48) show that the linear lift potential for supersonic flow past a wing can be written in integral form as

$$\varphi(x,y,z) = \frac{\sin \alpha}{2\pi} z \int_{s=0}^{s=x-\beta r} (x - s) \, ds \int_{t=-y_2(x)}^{t=y_2(x)} \frac{1}{(y - t)^2 + z^2} \frac{\Delta u_\alpha(s,t)}{R} \, dt$$

where Δu_α is the jump in the x-derivative of the lift potential ϕ_α across the wing and where

$$R = \sqrt{(x - s)^2 - \beta^2 \left[(y - t)^2 + z^2\right]} \tag{E1}$$

For large values of r the potential $\varphi_1(x,r)$ in the outer expansion (eq. (10)) can be written as

$$\varphi_1(x,r) = \frac{\varphi(x,r,\omega)}{\sin \alpha \sin \omega} = \frac{1}{r} \int_{s=0}^{s=x-\beta r} \frac{(x - s) \, f'(s)}{\sqrt{(x - s)^2 - \beta^2 r^2}} \, ds \tag{E2}$$

where

$$f'(x) = \frac{1}{2\pi} \int_{t=-y_2(x)}^{t=y_2(x)} \Delta u_\alpha(x,t) \, dt$$

If $f'(0) = 0$, equation (E2) can be integrated by parts to yield

$$\varphi_1(x,r) = \frac{1}{r} \int_{s=0}^{s=x-\beta r} \sqrt{(x - s)^2 - \beta^2 r^2} \, f''(s) \, ds \tag{E3}$$

If the flow is attached at the leading edge, $f(x)$ is given by the equation

$$f(x) = \frac{1}{2} y_2^2(x) \tag{E4}$$

From the results of appendix C it is seen that equation (E4) is also a reasonable approximation for separated-leading-edge flow for the angle-of-attack range considered in this report. For wings for which the derivative $y_2'(x)$ is either constant or a slowly varying function of x, equation (E3) can be integrated to yield

$$\varphi_1(x,r) = \frac{\left[y_2'(x)\right]^2}{2r} \left\{ x\sqrt{x^2 - \beta^2 r^2} + \beta^2 r^2 \left[\log_e \beta r - \log_e\left(x + \sqrt{x^2 - \beta^2 r^2}\right)\right] \right\}$$

(E5)

Since y_2' can be approximated as

$$y_2'(x) \approx \frac{y_2(x)}{x} = \frac{y_2(x - \beta r)}{x - \beta r}$$

equation (E5) can be written in the form

$$\varphi_1(x,r) = \frac{f(x - \beta r)}{r\left(1 - \frac{\beta r}{x}\right)^2} \left[\sqrt{1 - \frac{\beta^2 r^2}{x^2}} + \left(\frac{\beta r}{x}\right)^2 \log_e\left(\frac{\frac{\beta r}{x}}{1 + \sqrt{1 - \frac{\beta^2 r^2}{x^2}}}\right) \right]$$

APPENDIX F

NUMERICAL METHOD

In this report, the method of successive line overrelaxation is used to solve equations (42) and (55). Equation (42), which governs the flow at the points $r > y_2(x)$, is used in the form shown at the points $r > r_a(x)$, where $r_a(x)$ is slightly larger than $y_2(x)$. Equation (55), which governs the flow at the points $r < y_2(x)$, is used in the form given. In the region $y_2(x) < r < r_a(x)$, it is assumed that the outer expansion (eq. (10)) is applicable and that the terms proportional to $\sin \omega$ and $\cos 2\omega$ are governed by equations of the form of equation (8) if ϕ_α is obtained from slender-wing theory and by equations of the form of equation (9) if ϕ_α is obtained from the theory of Lawrence and Flax or from quasiconical theory. Consequently, the equation which governs φ_0 for $y_2(x) < r < r_a(x)$ is

$$\Lambda \frac{\partial^2 \varphi_0}{\partial x^2} + \frac{1}{r} \frac{\partial}{\partial r}\left(r \frac{\partial \varphi_0}{\partial r}\right) = M_\infty^2 \sin^2\alpha \left(\frac{\gamma + 1}{2} \frac{f'f''}{r^2} + \frac{2ff'}{r^4}\right)$$
$$- \lambda\left[\sin \alpha \frac{f''}{r} \sin \omega + \sin^2\alpha \left(\frac{\gamma + 1}{2} \frac{f'f''}{r^2} - \frac{2ff'}{r^4}\right)'' \cos 2\omega\right] \tag{F1}$$

where

$$\Lambda = 1 - M_\infty^2 - (\gamma + 1)M_\infty^2\left[\varphi_0' + \sin \alpha \frac{f'}{r} \sin \omega + \sin^2\alpha \left(\frac{\gamma + 1}{2} \frac{f'f''}{r^2} - \frac{2ff'}{r^4}\right) \cos 2\omega\right]$$

The function λ is related to Λ by equation (49) or (50).

Equations (42), (F1), and (55) can be written as

$$\Lambda \frac{\partial^2 \psi}{\partial x^2} + \frac{1}{r} \frac{\partial}{\partial r}\left(r \frac{\partial \psi}{\partial r}\right) = F(x,r,\omega) \tag{F2}$$

where

$$\Lambda = 1 - M_\infty^2 - (\gamma + 1)M_\infty^2\left[\frac{\partial \psi}{\partial x} + G(x,r,\omega)\right] \tag{F3}$$

93

APPENDIX F

The function ψ is equal to φ for $r > r_a$ and to φ_0 for $r \leqq r_a$, and the functions F and G are the appropriate known analytical expressions. The grid system used is virtually the same as that used by Bailey (ref. 28). In the radial direction the transformation

$$r = r_0 + \frac{\eta}{b - a\eta}$$

is used so that r varies from r_0 to r_{max} as y varies from 0 to 1. The effect of the transformation is to concentrate points near the axis. The constants b and a must be appropriately chosen to give the desired point distribution. Note that if $b = a$, the outer boundary is at infinity. In the vicinity of the body a uniform grid is used for the x-coordinate. For $M_\infty \leqq 1$, the x-grid is stretched downstream and upstream of this region in the manner used in reference 28. This stretching continues the x-grid to the finite values x_{min} and x_{max}. For $M_\infty > 1$ the x-grid spacing is uniform throughout.

For $M_\infty \leqq 1$, the boundary condition which is applied at x_{min} and x_{max} and at the outer radial boundary if that boundary is at infinity is $\varphi = 0$. For $M_\infty > 1$, this condition is applied only at x_{min} since no downstream boundary condition is required and since the outer boundary is located at a finite value of r if the free stream is supersonic. The boundary condition which is applied at the inner boundary is given by equation (58), and the one which is used at the outer boundary if that boundary is to represent a tunnel wall is given by equation (28) if the wall is solid, by equation (32) if it is slotted, and by equation (33) if it is porous.

The partial derivatives with respect to x are approximated with central finite-difference expressions if the local Mach number $M < 1$ and backward expressions if $M > 1$. Let the indices for the x- and r-coordinates be j and k, respectively, and let

$$\left.\begin{aligned}
\Delta x_1 &= x_{j-1} - x_{j-2} \\[6pt]
\Delta x_2 &= x_j - x_{j-1} \\[6pt]
\Delta x_3 &= x_{j+1} - x_j
\end{aligned}\right\} \tag{F4}$$

The central-difference expressions are

$$\left(\frac{\partial \psi}{\partial x}\right)_c = \frac{\Delta x_2}{\Delta x_3 \left(\Delta x_2 + \Delta x_3\right)} \psi_{j+1,k} + \frac{\Delta x_3 - \Delta x_2}{\Delta x_2 \, \Delta x_3} \psi_{j,k} - \frac{\Delta x_3}{\Delta x_2 \left(\Delta x_2 + \Delta x_3\right)} \psi_{j-1,k} \tag{F5}$$

94

$$\left(\frac{\partial^2 \psi}{\partial x^2}\right)_c = \frac{2}{\Delta x_3 \left(\Delta x_2 + \Delta x_3\right)} \psi_{j+1,k} - \frac{2}{\Delta x_2 \, \Delta x_3} \psi_{j,k} + \frac{2}{\Delta x_2 \left(\Delta x_2 + \Delta x_3\right)} \psi_{j-1,k} \qquad (F6)$$

and the backward expressions are

$$\left(\frac{\partial \psi}{\partial x}\right)_b = \frac{1}{\Delta x_2} \left(\psi_{j,k} - \psi_{j-1,k}\right)$$

$$\left(\frac{\partial^2 \psi}{\partial x^2}\right)_b = \frac{2}{\Delta x_2 \left(\Delta x_1 + \Delta x_2\right)} \psi_{j,k} - \frac{2}{\Delta x_1 \, \Delta x_2} \psi_{j-1,k} + \frac{2}{\Delta x_1 \left(\Delta x_1 + \Delta x_2\right)} \psi_{j-2,k}$$

At strong shock waves the nonlinear term $\Lambda \dfrac{\partial^2 \psi}{\partial x^2}$ in equation (F2) is replaced by the Murman shock operator (ref. 29) which is written as

$$\left(\Lambda \frac{\partial^2 \psi}{\partial x^2}\right)_s = \Lambda_b \left(\frac{\partial^2 \psi}{\partial x^2}\right)_b + \Lambda_c \left(\frac{\partial^2 \psi}{\partial x^2}\right)_c$$

The partial derivatives with respect to the radial coordinate are written as

$$\frac{1}{r} \frac{\partial}{\partial r}\left(r \frac{\partial \psi}{\partial r}\right) = A_k \psi_{j,k-1} - B_k \psi_{j,k} + C_k \psi_{j,k+1} \qquad (F7)$$

where

$$A_k = \frac{\left(b - a\eta_k\right)^3}{b^2 (\Delta\eta)^2} \left\{ b - a\eta_k - \frac{\Delta\eta}{2}\left[\frac{b}{\eta_k + \left(b - a\eta_k\right)r_0} - 2a\right] \right\} \qquad (F8a)$$

$$B_k = \frac{2\left(b - a\eta_k\right)^4}{b^2 (\Delta\eta)^2} \qquad (F8b)$$

$$C_k = \frac{\left(b - a\eta_k\right)^3}{b^2 (\Delta\eta)^2} \left\{ b - a\eta_k + \frac{\Delta\eta}{2}\left[\frac{b}{\eta_k + \left(b - a\eta_k\right)r_0} - 2a\right] \right\} \qquad (F8c)$$

except at points on the boundaries. At the inner boundary the radial difference expression is written as

$$\frac{1}{r}\frac{\partial}{\partial r}\left(r\frac{\partial \psi}{\partial r}\right) = \frac{1}{r_1 \, \Delta r}\left(r_{3/2}\frac{\psi_{j,2} - \psi_{j,1}}{\Delta r} - r_b\frac{dr_b}{dx}\right)$$

and at the outer boundary as

$$\frac{1}{r}\frac{\partial}{\partial r}\left(r\frac{\partial \psi}{\partial r}\right) = \frac{1}{r_{km} \, \Delta r}\left[r_{km+\frac{1}{2}}\left(\frac{\partial \psi}{\partial r}\right)_{j,km+\frac{1}{2}} - r_{km-\frac{1}{2}}\frac{\psi_{j,km} - \psi_{j,km-1}}{\Delta r}\right]$$

where the derivative $\left(\dfrac{\partial \psi}{\partial r}\right)_{j,km+\frac{1}{2}}$ is obtained from equation (28), (32), or (33).

When the computational plane is the horizontal plane ($\omega = 0$), the velocity potential is calculated both above and beneath the wing for $r < y_2(x)$. Modifications to the finite-difference formulas need to be made at several points neighboring the wing. If the point j,k lies just ahead or just outside of the leading edge, then the value of $\psi_{j+1,k}$ in equations (F5) and (F6) or the value of $\psi_{j,k-1}$ in equation (F7), respectively, must be the average of the values above and beneath the wing. If the point j,k lies at the trailing edge of the wing and the flow at this point is subsonic, the potential jump across the vortex sheet at the point j+1,k is set equal to that across the wing at the point j-1,k in order to satisfy the Kutta condition.

The line relaxation process used here is the same as that used by Murman and Cole (ref. 8), Bailey (ref. 28), and others. A relaxation factor of 1 is used at all points where the flow is supersonic. At points where the flow is subsonic, the value of the relaxation factor is between 1 and 2.

APPENDIX G

SOLUTION PROCEDURE FOR GENERALIZED BROWN AND MICHAEL
SEPARATED-FLOW MODEL FOR WING-BODY COMBINATIONS

It appears that a computer program for the Brown and Michael model for separated flow past a general nonconical wing-body configuration has not been set up previously. Smith (ref. 49) has set up a computer program for nonconical wings, and Wei, Levinsky, and Su (ref. 31) have set up a program which uses the more complicated model of Mangler and Smith to calculate the flow over nonconical wing bodies. However, the wing bodies which can be treated by the method of reference 31 must have conical wing-body noses.

The equations for the Mach number dependent Brown and Michael model for separated flow past a general nonconical wing-body configuration are

$$\eta = \frac{\sqrt{2}}{2}\sqrt{1 + \lambda_v{}^2 - \tau_v{}^2 + \sqrt{\left(1 + \lambda_v{}^2 - \tau_v{}^2\right)^2 + 4\lambda_v{}^2\tau_v{}^2}}$$

$$\xi = \frac{\lambda_v\tau_v}{\eta}$$

$$h = y_2(x) + \frac{r_b{}^2(x)}{y_2(x)}$$

$$y_v = \frac{1}{2}\left\{\eta h + \sqrt{\eta^2 h^2 + \frac{1}{2}\left(\sqrt{\left[h^2\left(\eta^2 + \xi^2\right) + 4r_b{}^2\right]^2 - 16\eta^2 h^2 r_b{}^2} - \left[h^2\left(\xi^2 + \eta^2\right) + 4r_b{}^2\right]\right)}\right\}$$

$$z_v = \frac{\xi h y_v}{2y_v - \eta h}$$

$$A_y = \frac{y_v\lambda_v + z_v\tau_v}{h\left(\lambda_v{}^2 + \tau_v{}^2\right)}$$

$$A_z = \frac{y_v\tau_v - z_v\lambda_v}{h\left(\lambda_v{}^2 + \tau_v{}^2\right)}$$

$$B_y = \left(y_v{}^2 - z_v{}^2\right)^2 - 4y_v{}^2 z_v{}^2$$

$$B_z = 4y_v z_v \left(y_v{}^2 - z_v{}^2\right)$$

$$B_{y0} = 1 - \frac{r_b{}^4 B_y}{B_y{}^2 + B_z{}^2}$$

$$B_{z0} = -\frac{r_b{}^4 B_z}{B_y{}^2 + B_z{}^2}$$

$$C_y = A_y B_{z0} + A_z B_{y0}$$

$$C_z = A_y B_{y0} - A_z B_{z0}$$

$$D_y = \left(A_y{}^2 - A_z{}^2\right) B_{y0} - 2A_y A_z B_{z0}$$

$$D_z = 2A_y A_z B_{y0} + \left(A_y{}^2 - A_z{}^2\right) B_{z0}$$

$$D_{y0} = 1 + \frac{3r_b{}^2 \left(y_v{}^2 - z_v{}^2\right)}{\left(y_v{}^2 + z_v{}^2\right)^2}$$

$$D_{z0} = \frac{6y_v z_v r_b{}^2}{\left(y_v{}^2 + z_v{}^2\right)^2}$$

$$E_y = \frac{B_{y0} D_{y0} + B_{z0} D_{z0}}{B_{y0}{}^2 + B_{z0}{}^2}$$

$$E_z = \frac{B_{y0}D_{z0} - B_{z0}D_{y0}}{B_{y0}^2 + B_{z0}^2}$$

$$F_y = \frac{y_v\left(E_z - D_z\right) + z_v\left(E_y - D_y\right)}{y_v^2 + z_v^2}$$

$$F_z = -\frac{y_v\left(E_y - D_y\right) + z_v\left(E_z - D_z\right)}{y_v^2 + z_v^2}$$

For separated-leading-edge flow,

$$\gamma_v = \frac{1}{2}h\left(\lambda_v + \frac{\tau_v^2}{\lambda_v}\right)R_1$$

$$M_y = \frac{\left(y_v - y_2\right)h\tau_v R_1}{2\gamma_v}\left(1 - \frac{\lambda_v^2}{\tau_v^2}\right)$$

$$M_z = \frac{z_v h R_1}{2\gamma_v}\left(1 - \frac{\lambda_v^2}{\tau_v^2}\right)$$

$$N_y = \frac{\left(y_v - y_2\right)h\tau_v R_1}{\gamma_v\lambda_v}$$

$$N_z = \frac{z_v h \tau_v R_1}{\gamma_v\lambda_v}$$

$$O_y = \frac{y_v - y_2}{h}$$

$$O_z = \frac{z_v}{h}$$

$$P_y = \frac{y_v - y_2}{R_1}$$

$$P_z = \frac{z_v}{R_1}$$

For a strake-generated vortex γ_v is constant and M_y, M_z, N_y, N_z, O_y, O_z, P_y, and P_z vanish.

$$Q_y = \frac{B_{y0}h}{\left(y_v^2 + z_v^2\right)\left(B_{y0}^2 + B_{z0}^2\right)}$$

$$Q_z = \frac{B_{z0}h}{\left(y_v^2 + z_v^2\right)\left(B_{y0}^2 + B_{z0}^2\right)}$$

$$R_y = Q_y\left(y_v\lambda_v + z_v\tau_v\right) - Q_z\left(y_v\tau_v - z_v\lambda_v\right)$$

$$R_z = Q_y\left(y_v\tau_v - z_v\lambda_v\right) + Q_z\left(y_v\lambda_v + z_v\tau_v\right)$$

$$G_{y0} = \frac{r_b^2\left(y_v^2 - z_v^2\right)}{\left(y_v^2 + z_v^2\right)^2}$$

$$G_{z0} = -\frac{2y_v z_v r_b^2}{\left(y_v^2 + z_v^2\right)^2}$$

$$G_y = \frac{y_v\left(1 - G_{y0}\right) + z_v G_{z0}}{\left(y_v^2 + z_v^2\right)\left[\left(1 - G_{y0}\right)^2 + G_{z0}^2\right]}$$

$$G_z = \frac{y_v G_{z0} - z_v\left(1 - G_{y0}\right)}{\left(y_v^2 + z_v^2\right)\left[\left(1 - G_{y0}\right)^2 + G_{z0}^2\right]}$$

$$\overline{G}_y = \frac{y_v B_{y0} + z_v B_{z0}}{\left(y_v^2 + z_v^2\right)\left(B_{y0}^2 + B_{z0}^2\right)}$$

$$\overline{G}_z = \frac{y_v B_{z0} - z_v B_{y0}}{\left(y_v^2 + z_v^2\right)\left(B_{y0}^2 + B_{z0}^2\right)}$$

$$H_{11} = hR_y + M_y$$

$$H_{12} = -hR_z + N_y$$

$$H_{21} = hR_z + M_z$$

$$H_{22} = hR_y + N_z$$

$$H_1 = -\sin \alpha \left[C_y - \frac{\gamma_v}{2}\left(\frac{C_y}{\lambda_v h} - F_y\right)\right] + \left(\frac{y_v}{y_v^2 + z_v^2} + 2G_y\right)r_b \frac{dr_b}{dx}$$

$$- \left(R_y \lambda_v - R_z \tau_v + O_y + h\overline{G}_y\right)\frac{dh}{dx} - P_y \frac{dR_1}{dx}$$

$$H_2 = \sin \alpha \left[C_z - \frac{\gamma_v}{2}\left(\frac{C_z}{\lambda_v h} + F_z\right)\right] + \left(\frac{z_v}{y_v^2 + z_v^2} + 2G_z\right)r_b \frac{dr_b}{dx}$$

$$- \left(R_y \tau_v + R_z \lambda_v + O_z + h\overline{G}_z\right)\frac{dh}{dx} - P_z \frac{dR_1}{dx}$$

$$\frac{d\lambda_v}{dx} = \frac{H_1 H_{22} - H_2 H_{12}}{H_{11} H_{22} - H_{21} H_{12}}$$

$$\frac{d\tau_v}{dx} = \frac{H_2 H_{11} - H_1 H_{21}}{H_{11} H_{22} - H_{21} H_{12}}$$

These equations are solved by fourth-order Runge-Kutta integration. The function R_1 has a value of 1 if the attached-flow solution is obtained from slender-wing theory. If the approximate subsonic or supersonic attached-flow solutions are used, the function R_1 is evaluated with equation (D41). Note that it is only through equation (D41) that the Mach number influences the solution.

In order to start the solution at a point just downstream of where the leading edge of the wing emerges from the body surface, the configuration in the vicinity of the junction is approximated by a slender wing with the semispan $y_2 - r_b \ll r_b$ at an angle of attack of 2α. This approximation is depicted in figure 40.
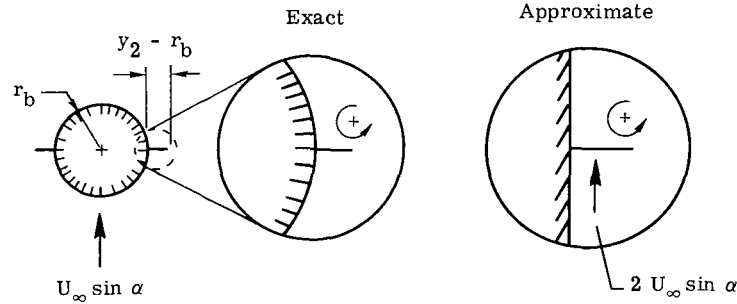

Figure 40.- Approximation used to start calculation.

The empirical formulation of Jobe (ref. 50) is used to determine initial values for y_v and z_v. The starting equations are

$$\tilde{z}_0 = -0.00451 + 0.56114 \left(\frac{R_1 \sin \alpha}{y_2' - r_b'} \right) - 0.12152 \left(\frac{R_1 \sin \alpha}{y_2' - r_b'} \right)^2$$

$$y_v = r_b + \left(y_2 - r_b \right) \left(0.99031 - 0.98407 \tilde{z}_0 + 2.29981 \tilde{z}_0^2 - 1.78322 \tilde{z}_0^3 \right)$$

$$z_v = \left(y_2 - r_b \right) \tilde{z}_0$$

$$\eta = 1 + \frac{1}{2r_b^2} \left[\left(y_v - r_b \right)^2 - \left(y_2 - r_b \right)^2 - z_v^2 \right]$$

$$\xi = \frac{z_v \left(y_v - r_b\right)}{r_b{}^2}$$

$$\lambda_v = \frac{\sqrt{2}}{2r_b} \sqrt{\left(y_v - r_b\right)^2 - \left(y_2 - r_b\right)^2 - z_v{}^2 + \sqrt{\left[\left(y_v - r_b\right)^2 - \left(y_2 - r_b\right)^2 - z_v{}^2\right]^2 + 4\eta^2 \xi^2 r_b{}^4}}$$

$$\tau_v = \frac{\eta \xi}{\lambda_v}$$

REFERENCES

1. Stahara, Stephen S.; and Spreiter, John R.: Calculative Techniques for Transonic Flows About Certain Classes of Wing-Body Combinations. NASA CR-2103, 1972. Phase II. NASA CR-2157, 1972.

2. Heaslet, Max A.; and Spreiter, John R.: Three-Dimensional Transonic Flow Theory Applied to Slender Wings and Bodies. NACA Rep. 1318, 1957. (Supersedes NACA TN 3717.)

3. Oswatitsch, Klaus; and Keune, Friedrich (K. W. Mangler, transl.): A Theorem of Equivalence for Wings of Small Aspect Ratio at Zero Incidence in Transonic Flow. Lib. Transl. No. 545, Brit. R.A.E., Aug. 1955.

4. Whitcomb, Richard T.: A Study of the Zero-Lift Drag-Rise Characteristics of Wing-Body Combinations Near the Speed of Sound. NACA Rep. 1273, 1956. (Supersedes NACA RM L52H08.)

5. Jones, Robert T.: Properties of Low-Aspect-Ratio Pointed Wings at Speeds Below and Above the Speed of Sound. NACA Rep. 835, 1946. (Supersedes NACA TN 1032.)

6. Spreiter, John R.: The Aerodynamic Forces on Slender Plane- and Cruciform-Wing and Body Combinations. NACA Rep. 962, 1950. (Supersedes NACA TN's 1897 and 1662.)

7. Ward, G. N.: Supersonic Flow Past Slender Pointed Bodies. Quart. J. Mech. Appl. Math., vol. II, pt. 1, Mar. 1949, pp. 75-97.

8. Murman, Earll M.; and Cole, Julian D.: Calculation of Plane Steady Transonic Flows. AIAA J., vol. 9, no. 1, Jan. 1971, pp. 114-121.

9. Bailey, Frank R.; and Ballhaus, William F.: Relaxation Methods for Transonic Flow About Wing-Cylinder Combinations and Lifting Swept Wings. Proceedings of the Third International Conference on Numerical Methods in Fluid Mechanics, Volume II. Volume 19 of Lecture Notes in Physics, Henri Cabannes and Roger Temam, eds., Springer-Verlag, 1973, pp. 2-9.

10. Schmidt, W.; Rohlfs, S.; and Vanino, R.: Some Results Using Relaxation Methods for Two- and Three-Dimensional Transonic Flows. Proceedings of the Fourth International Conference on Numerical Methods in Fluid Dynamics. Volume 35 of Lecture Notes in Physics, Robert D. Richtmyer, ed., Springer-Verlag, 1975, pp. 364-372.

11. Klunker, E. B.; and Newman, P. A.: Computation of Transonic Flow About Lifting Wing-Cylinder Combinations. J. Aircraft, vol. 11, no. 4, Apr. 1974, pp. 254-256.

12. Barnwell, R. W.: Transonic Flow About Lifting Configurations. AIAA J., vol. 11, no. 5, May 1973, pp. 764-766.

13. Barnwell, Richard W.: Analysis of Transonic Flow About Lifting Wing-Body Configurations. NASA TR R-440, 1975.

14. Cheng, H. K.; and Hafez, M. M.: Equivalence Rule and Transonic Flow Theory Involving Lift. AIAA J., vol. 11, no. 8, Aug. 1973, pp. 1210-1212.

15. Cheng, H. K.; and Hafez, Mohamed M.: Equivalence Rule and Transonic Flows Involving Lift. USCAE 124, Univ. of Southern California, Apr. 1973.

16. Barnwell, R. W.: Transonic Flow About Lifting Wing-Body Combinations. AIAA Paper No. 74-185, Jan.-Feb. 1974.

17. Barnwell, Richard W.: Approximate Method for Calculating Transonic Flow About Lifting Wing-Body Combinations. Aerodynamic Analyses Requiring Advanced Computers, Part II, NASA SP-347, 1975, pp. 1281-1303.

18. Barnwell, Richard W.; and Davis, Ruby M.: Approximate Method for Calculating Transonic Flow About Lifting Wing-Body Configurations: Computer Program and User's Manual. NASA TM X-72758, 1975.

19. Liepman, H. W.; and Roshko, A.: Elements of Gasdynamics. John Wiley & Sons, Inc., c.1957.

20. Brown, Clinton E.; and Michael, William H., Jr.: On Slender Delta Wings With Leading-Edge Separation. NACA TN 3430, 1955.

21. Lawrence, H. R.; and Flax, A. H.: Wing-Body Interference at Subsonic and Supersonic Speeds – Survey and New Developments. J. Aeron. Sci., vol. 21, no. 5, May 1954, pp. 289-324.

22. Carafoli, Elie; Mateescu, Dan; and Nastase, Adriana: Wing Theory in Supersonic Flow. Pergamon Press, Ltd., c.1969.

23. Klunker, E. B.: Contribution to Methods for Calculating the Flow About Thin Lifting Wings at Transonic Speeds – Analytic Expressions for the Far Field. NASA TN D-6530, 1971.

24. Mangler, K. W.: Calculation of the Pressure Distribution Over a Wing at Sonic Speeds. R. & M. No. 2888, Brit. A.R.C., 1955.

25. Lawrence, H. R.: The Lift Distribution on Low Aspect Ratio Wings at Subsonic Speeds. J. Aeron. Sci., vol. 18, no. 10, Oct. 1951, pp. 683-695.

26. Baldwin, Barrett S., Jr.; Turner, John B.; and Knechtel, Earl D.: Wall Interference in Wind Tunnels With Slotted and Porous Boundaries at Subsonic Speeds. NACA TN 3176, 1954.

27. Chen, C. F.; and Mears, J. W.: Experimental and Theoretical Study of Mean Boundary Conditions at Perforated and Longitudinally Slotted Wind Tunnel Walls. AEDC-TR-57-20, DDC Doc. No. AD 144 320, U.S. Air Force, Dec. 1957.

28. Bailey, Frank R.: Numerical Calculation of Transonic Flow About Slender Bodies of Revolution. NASA TN D-6582, 1971.

29. Murman, Earll M.: Analysis of Embedded Shock Waves Calculated by Relaxation Methods. AIAA J., vol. 12, no. 5, May 1974, pp. 626-633.

30. Munk, Max M.: The Aerodynamic Forces on Airship Hulls. NACA Rep. 184, 1924.

31. Wei, M. H. Y.; Levinsky, E. S.; and Su, F. Y.: Nonconical Theory of Flow Past Slender Wing-Bodies With Leading-Edge Separation. NASA CR-73446, [1969].

32. Mirels, Harold: Aerodynamics of Slender Wings and Wing-Body Combinations Having Swept Trailing Edges. NACA TN 3105, 1954.

33. Adams, Mac C.; and Sears, W. R.: Slender-Body Theory — Review and Extension. J. Aeron. Sci., vol. 20, no. 2, Feb. 1953, pp. 85-98.

34. Taylor, Robert A.: Pressure Distributions at Transonic Speeds for Bumpy and Indented Midsections of a Basic Parabolic-Arc Body. NASA MEMO 1-22-59A, 1959.

35. South, Jerry C., Jr.; and Jameson, Antony: Relaxation Solutions for Inviscid Axisymmetric Transonic Flow Over Blunt or Pointed Bodies. AIAA Computational Fluid Dynamics Conference, July 1973, pp. 8-17.

36. Taylor, Robert A.; and McDevitt, John B.: Pressure Distributions at Transonic Speeds for Parabolic-Arc Bodies of Revolution Having Fineness Ratios of 10, 12, and 14. NACA TN 4234, 1958.

37. Woodward, Frank A.: Analysis and Design of Wing-Body Combinations at Subsonic and Supersonic Speeds. J. Aircraft, vol. 5, no. 6, Nov.-Dec. 1968, pp. 528-534.

38. Peckham, D. H.: Low-Speed Wind-Tunnel Tests on a Series of Uncambered Slender Pointed Wings With Sharp Edges. R. & M. No. 3186, Brit. A.R.C., 1961.

39. Smith, J. H. B.: Improved Calculations of Leading-Edge Separation From Slender Delta Wings. Tech. Rep. No. 66070, Brit. R.A.E., Mar. 1966.

40. Polhamus, Edward C.: A Concept of the Vortex Lift of Sharp-Edge Delta Wings Based on a Leading-Edge-Suction Analogy. NASA TN D-3767, 1966.

41. Hill, William A., Jr.: Experimental Lift of Low-Aspect-Ratio Triangular Wings at Large Angles of Attack and Supersonic Speeds. NACA RM A57I17, 1957.

42. Polhamus, Edward C.: Predictions of Vortex-Lift Characteristics by a Leading-Edge Suction Analogy. J. Aircraft, vol. 8, no. 4, Apr. 1971, pp. 193-199.

43. McDevitt, John B.; and Taylor, Robert A.: Pressure Distributions at Transonic Speeds for Slender Bodies Having Various Axial Locations of Maximum Diameter. NACA TN 4280, 1958.

44. Grabau, Martin: A Method of Forming Continuous Empirical Equations for the Thermodynamic Properties of Air From Ambient Temperatures to 15,000° K, With Applications. AGARD Rep. 333, Sept. 1959.

45. Reissner, Eric: On the General Theory of Thin Airfoils for Nonuniform Motion. NACA TN 946, 1944.

46. Lamb, Horace: Hydrodynamics. Sixth ed., Dover Publ., Inc., 1945.

47. Sacks, Alvin H.; Lundberg, Raymond E.; and Hanson, Charles W.: A Theoretical Investigation of the Aerodynamics of Slender Wing-Body Combinations Exhibiting Leading-Edge Separation. NASA CR-719, 1967.

48. Heaslet, Max. A.; and Lomax, Harvard: Supersonic and Transonic Small Perturbation Theory. General Theory of High Speed Aerodynamics, W. R. Sears, ed., Princeton Univ. Press, 1954, pp. 122-344.

49. Smith, J. H. B.: A Theory of the Separated Flow From the Curved Leading Edge of a Slender Wing. R. & M. No. 3116, Brit. A.R.C., 1959.

50. Jobe, C. E.: An Aerodynamic Theory of Slender Wings With Leading Edge Separation. M. S. Thesis, Ohio State Univ., 1966.

"The aeronautical and space activities of the United States shall be
conducted so as to contribute . . . to the expansion of human knowl-
edge of phenomena in the atmosphere and space. The Administration
shall provide for the widest practicable and appropriate dissemination
of information concerning its activities and the results thereof."
—NATIONAL AERONAUTICS AND SPACE ACT OF 1958

NASA SCIENTIFIC AND TECHNICAL PUBLICATIONS

TECHNICAL REPORTS: Scientific and
technical information considered important,
complete, and a lasting contribution to existing
knowledge.

TECHNICAL NOTES: Information less broad
in scope but nevertheless of importance as a
contribution to existing knowledge.

TECHNICAL MEMORANDUMS:
Information receiving limited distribution
because of preliminary data, security classifica-
tion, or other reasons. Also includes conference
proceedings with either limited or unlimited
distribution.

CONTRACTOR REPORTS: Scientific and
technical information generated under a NASA
contract or grant and considered an important
contribution to existing knowledge.

TECHNICAL TRANSLATIONS: Information
published in a foreign language considered
to merit NASA distribution in English.

SPECIAL PUBLICATIONS: Information
derived from or of value to NASA activities.
Publications include final reports of major
projects, monographs, data compilations,
handbooks, sourcebooks, and special
bibliographies.

TECHNOLOGY UTILIZATION
PUBLICATIONS: Information on technology
used by NASA that may be of particular
interest in commercial and other non-aerospace
applications. Publications include Tech Briefs,
Technology Utilization Reports and
Technology Surveys.

Details on the availability of these publications may be obtained from:

SCIENTIFIC AND TECHNICAL INFORMATION OFFICE

NATIONAL AERONAUTICS AND SPACE ADMINISTRATION

Washington, D.C. 20546